# PERMEABILITY PREDICTION AND DRAINAGE CAPILLARY PRESSURE SIMULATION IN SANDSTONE RESERVOIRS

A Dissertation

by

TAO WU

Submitted to the Office of Graduate Studies of
Texas A&M University
in partial fulfillment of the requirements for the degree of

DOCTOR OF PHILOSOPHY

December 2004

Major Subject: Geology

# PERMEABILITY PREDICTION AND DRAINAGE CAPILLARY PRESSURE SIMULATION IN SANDSTONE RESERVOIRS

A Dissertation

by

TAO WU

Submitted to Texas A&M University
in partial fulfillment of the requirements
for the degree of

DOCTOR OF PHILOSOPHY

Approved as to style and content by:

| | |
|---|---|
| Robert R. Berg<br>(Chair of Committee) | Wayne M. Ahr<br>(Member) |
| Brian J. Willis<br>(Member) | Joel S. Watkins<br>(Member) |
| Thomas A. Blasingame<br>(Member) | Richard L. Carlson<br>(Head of Department) |

December 2004

Major Subject: Geology

# ABSTRACT

Permeability Prediction and Drainage Capillary Pressure Simulation in Sandstone Reservoirs. (December 2004)

Tao Wu, B.S., Jianghan Petroleum Institute, Jinzhou, P. R. China;

M.S., China University of Geosciences, Beijing, P. R. China;

Chair of Advisory Committee: Dr. Robert R. Berg

Knowledge of reservoir porosity, permeability, and capillary pressure is essential to exploration and production of hydrocarbons. Although porosity can be interpreted fairly accurately from well logs, permeability and capillary pressure must be measured from core. Estimating permeability and capillary pressure from well logs would be valuable where cores are unavailable.

This study is to correlate permeability with porosity to predict permeability and capillary pressures. Relationships between permeability to porosity can be complicated by diagenetic processes like compaction, cementation, dissolution, and occurrence of clay minerals. These diagenetic alterations can reduce total porosity, and more importantly, reduce effective porosity available for fluid flow. To better predict permeability, effective porosity needs to be estimated. A general equation is proposed to estimate effective porosity. Permeability is predicted from effective porosity by empirical and theoretical equations.

A new capillary pressure model is proposed. It is based on previous study, and largely empirical. It is tested with over 200 samples covering a wide range of lithology

(clean sandstone, shaly sandstone, and carbonates dominated by intergranular pores). Parameters in this model include: interfacial tension, contact angle, shape factor, porosity, permeability, irreducible water saturation, and displacement pressure. These parameters can be measured from routine core analysis, estimated from well log, and assumed. An empirical equation is proposed to calculate displacement pressure from porosity and permeability. The new capillary-pressure model is applied to evaluate sealing capacity of seals, calculate transition zone thickness and saturation above free water level in reservoirs. Good results are achieved through integration of well log data, production data, core, and geological concepts.

# DEDICATION

To my parents and parents-in-law, my wife, Hui Shao, my daughter, Yuting, and my son, Yuchen (Daniel), for their love, patience, and support all these years.

# ACKNOWLEDGEMENTS

I wish to express my deep appreciation to Dr. Robert R. Berg, Chair of my committee, for his endless support, encouragement, and patience.

I wish to thank Dr. Wayne M. Ahr, Dr. Brian J. Willis, Dr. Joel S. Watkins, and Dr. Thomas A. Blasingame for serving as committee members, and Dr. Frank E. Gilstrap for serving as graduate council representative. I would like to acknowledge their helpful comments and suggestions.

I would like to thank Dr. John C. Calhoun, Olav Walderhaug, and John W. Neasham for providing part of the data used in this study. I wish to thank Dr. William R. Bryant, Dr. Jerry L. Jensen, Dr. Ramon G. Bentsen, Lee T. Billingsley, Robert B. Truman, and Dan Georgi for their helpful discussions and suggestions. I also wish to thank Charles R. Berg for interpreting part of the well logs used in this study.

I would like to thank AAPG Grants-in-Aid for financial support for this study.

Finally, I thank Texas A&M University and its Geology & Geophysics Department for receiving me as a graduate student.

# TABLE OF CONTENTS

Page

ABSTRACT ……iii

DEDICATION……... v

ACKNOWLEDGEMENTS……vi

TABLE OF CONTENTS …….vii

LIST OF FIGURES…… x

LIST OF TABLES……... xv

CHAPTER

I INTRODUCTION……1

II BACKGROUND……..3

2.1 Permeability……3
2.2 Capillary Pressure…….. 4

III PERMEABILITY MODELS ……..8

3.1 Theoretical Models ……8
3.1.1 Capillary-tube based models……8
3.1.2 Models based on sphere packing …… 13
3.2 Empirical Models ……17
3.2.1 Models based on pore-throat size…… 19
3.2.2 Models based on surface area ……..21
3.3 Summary …… ……21

IV PREDICTING PERMEABILITY FROM EFFECTIVE POROSITY……..23

4.1 The Concept of Effective Porosity …….. 23
4.2 Estimation of Effective Porosity……..27
4.2.1 Microporosity of clay minerals…… 27
4.2.2 Dissolution porosity …… 35

CHAPTER Page

4.2.3 Effective porosity from mineralogy analysis……37
4.2.4 Effective porosity from capillary pressure analysis …… 39
4.3 Permeability Models Based on Effective Porosity …… 40
4.3.1 Kozeny-Carman model and its derivatives…….. 40
4.3.2 Regression models……45
4.4 An Example of Permeability Prediction ……..47
4.5 Summary ……..52

V DRAINAGE CAPILLARY PRESSURE MODELS ……..53

5.1 Introduction …… 53
5.2 Capillary-Tube Models……54
5.3 Models Based on Curve-Fitting ……..56
5.4 Pore-Throat Size Distribution ……61
5.4.1 Brooks and Corey's λ (1966) ……61
5.4.2 Thomeer's Fg (1960, 1983)…… ……65
5.4.3 Correlation between permeability and pore-throat distribution …… 67
5.5 Summary……..70

VI A REVISED CAPILLARY PRESSURE MODEL……72

6.1 A Revised Capillary Pressure Model……....72
6.2 Testing the Revised Model ……..73
6.2.1 Interfacial tension and contact angle……73
6.2.2 Displacement pressure……...74
6.2.3 Shape factor, β……...76
6.2.4 Results……...76
6.3 Summary ……83

VII UPSCALING CAPILLARY PRESSURES …… 84

7.1 Introduction…….. 84
7.2 Statistical Correlation……84
7.3 Leverett's (1941) J-Function…… 88
7.4 Reservoir Zonation……91
7.5 Summary……96

VIII APPLICATION OF CAPILLARY PRESSURE MODELS…… 98

8.1 Introduction…….. 98

CHAPTER Page

8.2 Sealing Capacity Evaluation…….99
8.2.1 Wilcox sandstone, Milbur Field, Texas…… 99
8.2.2 Vicksburg sandstone, East McCook Field, Texas…….. 103
8.3 Height Above the Free Water Level…….. 108
8.3.1 Wilcox unconsolidated sandstone, Texas …….. 108
8.3.2 Pennsylvanian Dolomite, West Texas…… 110
8.4 Calculating Relative Permeability……..112

IX DISCUSSION……. 116

9.1 Porosity……...116
9.2 Permeability……....116
9.3 Irreducible Water Saturation…….. 119
9.4 Displacement Pressure……122
9.5 Interfacial Tension and Contact Angle……123

X CONCLUSIONS…… 126

NOMENCLATURE……130

REFERENCES CITED……132

APPENDIX A: LITERATURE SURVEY OF PERMEABILITY AND CAPILLARY PRESSURE MODELS……142

APPENDIX B: ESTIMATES OF EFFECTIVE POROSITY…… 146

APPENDIX C: MEASURED PETROGRAPHIC ANALYSIS ……149

APPENDIX D: MEASURED CAPILLARY PRESSURES ……..155

APPENDIX E: MEASURED AND CAPILLARY-PRESSURE DERIVED PETROPHYSICAL PROPERTIES……...161

APPENDIX F: RELATIVE PERMEABILITIES ……..165

VITA……168

# LIST OF FIGURES

FIGURE Page

2.1 A diagram showing basic capillary pressure concepts.……4

2.2 A schematic diagram showing a typical mercury-injection capillary pressure curve …….. 6

3.1 Comparison between calculated (kc) and measured (km) permeability ……...11

3.2 Relationship among permeability, median grain size (diameter), and sorting…...14

3.3 An illustration of the largest rectilinear pores through unit cells in systematic packings of uniform spheres ……..…..15

3.4 Comparison between calculated and measured permeability for unconsolidated sands ……18

3.5 An idealized capillary pressure curve showing measures used by different authors for determination of characteristic pore dimension ……...19

3.6 Comparison between calculated and measured permeability ……20

4.1 Depiction of the models used to define core, log, and engineering “effective porosity” ……26

4.2 Classification of nonfracture porosity in sandstones summarizing the influence of porosity type on reservoir quality……27

4.3 Effects of clay on permeability-porosity relationships.…… 28

4.4 Classification of the morphology of authigenic clays ……...30

4.5 Cross plots of air permeability vs. total porosity .……30

4.6 Correlation between permeability and clay content ……..31

4.7 Cross plot of permeability and effective porosity for shaly sandstones ……33

4.8 Cross plot of permeability and median pore-throat diameter for shaly sandstones ……. 34

FIGURE Page

4.9 Correlation of median pore-throat diameter (MPD) with total porosity (a), and effective porosity (b)……. 35

4.10 Correlation between permeability with total and effective porosity …….. 36

4.11 Comparison of calculated permeability (kc) with measured permeability (km) for the Yowlumne sandstone, Kern County, California ……..…38

4.12 (a) Manner of defining Swanson's parameter (Swanson, 1981); (b) Pittman's (1992) approach to determine Swanson's Apex parameter……39

4.13 Cross plot of calculated (kc) and measured (km) permeabilities from the Kozeny-Carman model ……..43

4.14 Comparison between calculated (kc) and measured permeability (km) …….44

4.15 Cross plot of measured air permeability and effective porosity …… 46

4.16 Comparison between calculated (kc) and measured (km) permeability…….47

4.17 Regional map of the southern San Joaquin basin ……...48

4.18 QFR ternary diagram showing the framework grain compositions of the sandstones in North Belridge, Rio Viejo, and Yowlumne fields ……50

4.19 Comparison of calculated and measured permeabilities of arkosic sandstones, from Rio Viejo and Yowlumne Fields, San Joaquin Basin, California …… 51

4.20 Comparison of calculated and measured permeabilities …… 52

5.1 A family of capillary pressure curves showing Thomeer's three parameters: $P_d$, $S_{b\infty}$, and $F_g$……..58

5.2 Comparison between calculated and measured capillary pressures……..60

5.3 Correlations of $\lambda$ with permeability and $S_{wir}$ ……62

5.4 (a) MICP curves showing distinctive pore-throat distribution (b) Brooks and Corey's method of determining $\lambda$ ……63

5.5 Cross plot Se and Pc/Pd. Two fit lines are obtained …… 64

5.6 Correlation between $\lambda 1$ with $\sqrt{k/\phi}$ and $S_{wir}$ ..……...64

FIGURE Page

5.7 Correlation between λ2 with $\sqrt{k/\phi}$ and $S_{wir}$ ...…….65

5.8 A cross plot of Log (Pc/Pd) vs. –1/ln(1-Se) showing a linear relationship ……..66

5.9 Correlation between Fg with $\sqrt{k/\phi}$ and $S_{wir}$ ……. 66

5.10 Comparison between calculated (kc) and measured permeability ……..68

5.11 Comparison between calculated (kc) and measured permeability (km) …….70

6.1 (a) Correlation between Pd (air-mercury) and $\sqrt{k/\phi}$;
(b) Comparison between calculated and measured Pd ……...75

6.2 Comparison between calculated and measured capillary pressures of shaly sandstones……78

6.3 Comparison between calculated and measured capillary pressures……..80

6.4 Comparison between calculated and measured air-mercury capillary pressures…… 81

6.5 Comparison between measured and calculated centrifugal air-water capillary pressures……82

7.1 Correlation between permeability and water saturation……... 85

7.2 Correlation between permeability and water saturation (logarithm) ……..…86

7.3 Leverett's (1941) J-function as a function of water saturation (triangles), Sw, and as a function of effective water saturation (dots), Se, respectively…… 89

7.4 Measured capillary pressures, and calculated average capillary-pressure curve from equation 6-4 and equation 7-10 , respectively…… 91

7.5 Cross plot of permeability and porosity ……93

7.6 Measured and calculated capillary pressures of four flow units in Yowlumne Field…… 95

7.7 Effect of reservoir heterogeneity on fluid contacts and distribution……..96

FIGURE Page

8.1 Well log and core-measured saturation, Lower Wilcox Formation, well Clark Cotton 1, Milbur Field, Burleson County, Texas …… 100

8.2 Synthetic capillary-pressure curves of the seal and reservoir, and production profile of the reservoir, Lower Wilcox Formation, well Clark Cotton 1, Milbur Field, Burleson County, Texas …… 102

8.3 A schematic diagram showing depositional environment and stratigraphic trap in the Milbur Field, Burleson County, Texas ……103

8.4 Diagrammatic cross sections and dip logs through a normal-faulted section of sandstones (stippled) and shales (blank)……..105

8.5 Well logs through a section of Vicksburg sandstone and shale in the Davis 3 well, East McCook field ……106

8.6 Synthetic capillary-pressure curve of the sheared zone, Davis 3 well, East McCook field ……..107

8.7 Well log, log interpretation, and capillary pressure of the Eocene Wilcox sandstone in well Cashco Hicks 1, Martens Prairie Field, Grimes County, TX ……109

8.8 Measured permeability, porosity, and capillary-pressure derived water saturation and water cut, Pennsylvanian Dolomite ……...110

8.9 A conceptual saturation model showing effects of reservoir heterogeneity on fluid distribution ……..111

8.10 Measured capillary pressures and synthetic average capillary-pressure curve, Stevens Sandstone, T27X-34, Yowlumne Field, Kern County, California ……115

8.11 Measured relative permeabilities and calculated relative permeability curves, Stevens Sandstone, T27X-34, Yowlumne Field, Kern County, California …… 115

9.1 Comparison between core porosity and well log (density) porosity of three different wells…….117

9.2 Comparison between measured core permeability (km) and calculated permeability (kc) of the same data sets in Figure 9.1 ……118

FIGURE Page

9.3 Configuration of pendular rings forming at spherical grain contacts……..119

9.4 Capillary pressure curves showing (a) zero $S_{wir}$, for high-pressure mercury injection test; and (b) no definite $S_{wir}$ for air-water centrifugal test……...121

9.5 A air-water plate capillary pressure curve showing no definitive $S_{wir}$ and $P_d$ …… 123

9.6 Surface tensions between water and pure compounds correlated with reduced temperature (Tr) showing the range of values for dry gas (methane) in the subsurface…….. 124

9.7 Surface tensions between water and reservoir oils showing values for a wide range of oil-water density difference……125

# LIST OF TABLES

TABLE Page

4.1 Properties of authigenic clay minerals…….. 32

4.2 Sandstone properties in Paloma, Yowlumne, Rio Viejo, and North Belridge Fields …… 49

5.1 Measured rock properties and parameters obtained from mercury injection capillary pressure curves…… 62

6.1 Commonly used contact angle and interfacial tension values ……...74

6.2 Empirical values of β as a function of lithology, pore type, and permeability…… 76

6.3 Parameters used in synthesizing capillary pressure curves …….. 77

7.1 Correlation equations between permeability and water saturation at different capillary pressures ……. 87

7.2 Average petrophysical properties of flow units in Yowlumne Field……. 93

8.1 Basic data and oil-column calculations for selected fields ……..100

9.1 Average properties from core plug and well logs…… 118

9.2 Irreducible water saturation of different sphere packing ……..120

# CHAPTER I

# INTRODUCTION

Permeability and capillary pressures are important petrophysical properties. Permeability determines the fluid flow capacity in reservoir rocks. It is one of the most important parameters for reservoir management and development. Capillary pressure data have been widely used in evaluating reservoir rock, sealing capacity, transition zone thickness, pay versus nonpay, and absolute and relative permeability.

Permeability and capillary pressure can be measured on cores. Two different types of approaches are used to predict permeability and capillary pressure where cores are unavailable. The first, theoretical approaches, are based on mathematical models of simplified porous systems (e.g., a bundle of capillary tubes). Although such approaches offer insight into physical processes controlling permeability, simplification reduces accuracy where porous media are complicated by geological processes like compaction, cementation, and dissolution that are not incorporated into the mathematical description. Theoretical models also usually contain adjustable variables that are difficult to constrain from laboratory measurements.

---

This dissertation follows the style of the American Association of Petroleum Geologists Bulletin.

The second type of approach is based on empirical correlations of permeability and capillary pressure to well logs. For instance, permeability has been correlated with porosity estimated from well logs. Capillary pressure has been correlated with permeability and/or porosity estimates. Accuracy of the correlations can be improved by adding more variables, such as grain size and sorting, specific surface area, and irreducible water saturation.

This study combines theoretical and empirical models to improve predictions of permeability and capillary pressure from well logs. A model is developed starting with a simple capillary tube model, which is valid for unconsolidated sandstones and artificially packed spheres. The model is extended to describe consolidated sandstones containing dissolution porosity and shaly sandstones containing microporosity by incorporating effective porosity. Effective porosity has been estimated from mineralogical and petrographic analysis, and capillary pressure measurements. This study correlates permeability with a wide range of effective porosity. An empirical model is proposed based on the simple relationship between permeability and estimates of porosity from well logs.

A modified empirical model is proposed to correlate capillary pressure with porosity and permeability. Drainage capillary pressure curves are then generated from porosity and permeability estimates. Improvements are achieved by incorporating irreducible water saturation, and a “pore distribution factor” that accounts for the complexity of real porous systems. The model is tested with a large number of samples of different lithology and a wide range of porosity and permeability. Application of the model is also presented.

# CHAPTER II

# BACKGROUND

## 2.1 Permeability

Permeability is defined as a measure of a porous medium's capacity to transmit fluids (API Code 27) or fluid conductivity of porous media.

Permeability can be measured from core samples extracted from a formation or by in-place testing (Bass, 1992). It is defined by Darcy's law (1856):

$$q = kA\frac{\Delta p}{\mu L} \qquad (2\text{-}1)$$

where $q$ is volume rate of flow, $k$ is permeability, $A$ is cross-sectional area, $\mu$ is viscosity of the fluid, L is length of the column, $\Delta p$ is pressure loss over length $L$. Permeability has dimensions of length squared and units of *darcy* (D) and *millidarcy* (md).

Liquid or gas can be used to measure permeability of core samples in the laboratory. Gas permeability is determined most frequently because sample preparation is simpler and analytical procedures fairly rapid (Ohen and Kersey, 1993). When gas (usually Helium) is used at low mean pressure, resistance to flow from drag is very low, resulting in "slippage" effects. Because of this effect, permeability calculated directly from Darcy's law are too high, and are generally corrected using the Klinkenberg (1941) model. Such permeability measurements corrected for gas slippage are called "equivalent liquid" or "Klinkenberg" permeability. Although accuracy of measured permeabilities declines at low and high values, they are usually within ±5% (Keelan, 1972).

## 2.2 Capillary Pressure

When a capillary pressure tube is placed in a wetting fluid, pressure difference exists across the interface between wetting phase and nonwetting phase in the capillary tube. This pressure difference is called "capillary pressure" (Leverett, 1941, Brooks and Corey, 1966, Dullien, 1992, Vavra et al., 1992). The wetting phase rises until adhesive and gravitational forces balance (Figure 2.1).

$$P_c = (\rho_w - \rho_{nw})gh \qquad (2\text{-}2)$$

Where subscripts w and nw denote wetting phase and nonwetting phases, respectively, $\rho_w$ and $\rho_{nw}$ are densities of the respective phases, $g$ is the gravitational constant, and h is height above the free water level.

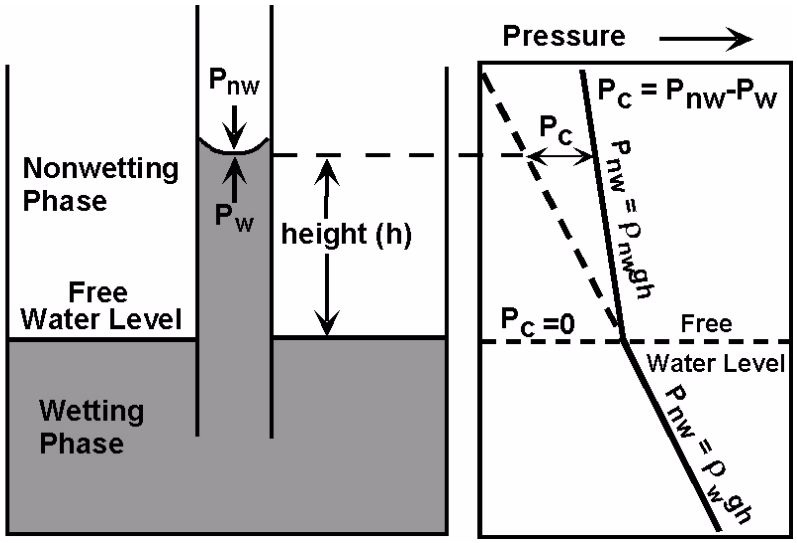


**Figure 2.1 A diagram showing basic capillary pressure concepts. $P_{nw}$ and $P_w$ are the surface pressures of the non-wetting phase and the wetting phase. Capillary pressure is defined as the difference between $P_{nw}$ and $P_w$. This pressure difference results in a rise (h) of wetting phase above free water level (from Vavra et al., 1992).**

Vavra et al. (1992) summarize three laboratory methods of measuring capillary pressures: 1) porous plate, 2) centrifuge, and 3) mercury-injection. Porous plate and centrifuge methods use the actual or simulated hydrocarbon/brine system of the reservoir to approximate the wetting phase. In the mercury injection method, mercury is the non-wetting phase. The volume of mercury injected at each pressure determines the non-wetting phase saturation. The procedure is continued until the sample is filled with mercury or the injection pressure reaches some predetermined value.

The mercury injection is favored because it is simple, cheaper, and less time consuming than porous plate and centrifuge methods. Mercury injection also significantly increases the range of pressure investigation, can be conducted on cuttings or sidewall samples, and measurements can easily be converted to reservoir system. Disadvantages of mercury-injection method are the difference in wetting properties and permanent loss of the sample (Vavra et al., 1992). A typical mercury injection capillary pressure curve is shown in Figure 2.2.

A drainage capillary-pressure curve typically consists of two parts: a gentle plateau in the lower capillary pressure range, and a steep slope in the higher capillary pressure range (Figure 2.2). The inflection point of these two parts is called “Apex” (Swanson, 1981, 1985). The plateau is inferred to record injection of mercury into macropores, while the steep slope records injection into micropores. A gentle plateau suggests constant pore-throat sizes, while a steep plateau suggests variable pore-throat sizes. As pore-throat sizes become extremely variable, the two parts of the curve will merge, suggesting an even distribution of pore-throat sizes between macro and micro scales.

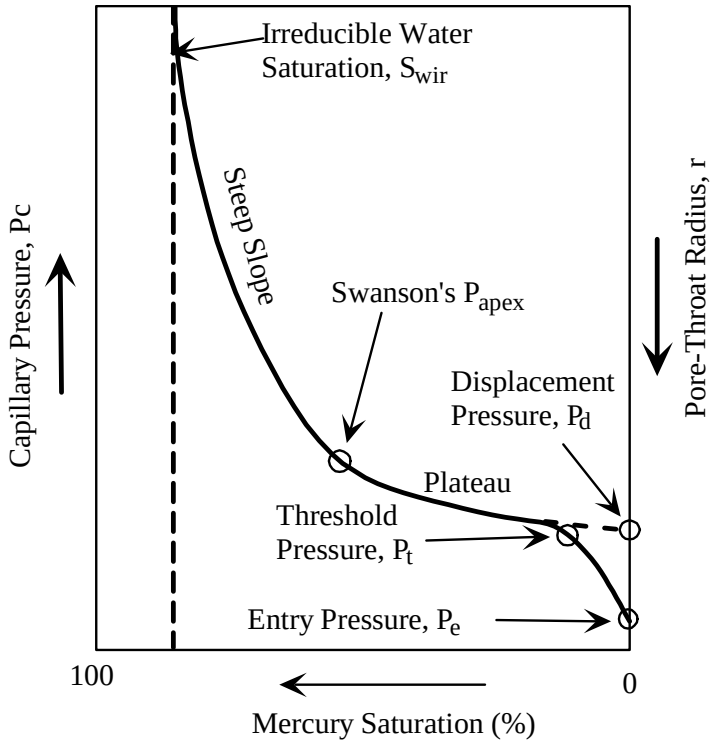


**Figure 2.2 A schematic diagram showing a typical mercury-injection capillary pressure curve (modified from Jennings, 1987).**

Several critical parameters can be defined from a capillary pressure curve. The entry pressure, $P_e$, is "the pressure at which the sample first accepts mercury into the pore system" (Jenning, 1987). According to Jennings, "$P_e$ is of limited importance and is primarily a function of the mercury conforming to irregularities on the surface of the sample plug". Displacement pressure, $P_d$, is (Schowalter, 1979): "that pressure required to form a continuous filament of non-wetting fluid through the largest connected pore throats of the rock". Following Jennings, 1987, displacement pressure in this study is estimated by extending the plateau to the right side of the graph (Figure 2.2) to define the extrapolated displacement pressure of Thomeer (1960).

Threshold pressure is defined by Katz and Thompson (1986) as the pressure at which mercury forms a connected pathway across the sample. This is estimated from the inflection point of a graph like that in Figure 2.2. Threshold pressure is graphically similar to displacement pressure.

Irreducible water saturation, $S_{wir}$, is the percentage of the pore space that the mercury could not enter at infinite pressure (Jennings, 1987).

# CHAPTER III

# PERMEABILITY MODELS

## 3.1 Theoretical Models

Theoretical permeability models generally have the following characteristics: 1) they use some simplified descriptions of the real pore structure; 2) they have physical basis (such as Darcy's Law); and 3) they are dimensionally correct. Theoretical models provide insight into physical properties that control permeability and provide a starting point for empirical models.

### 3.1.1 Capillary-tube based models

Poiseuille (1840) conducted experiments on steady-state flow of fluids through capillaries and determined an equation relating fluid properties and conduit characteristics to fluid velocity. Poiseuille's law for viscous (laminar) flow through a tube of circular cross-section is:

$$v = \frac{q}{A} = \frac{d^2 \Delta p}{32 \mu L} \qquad (3\text{-}1)$$

where v is average velocity inside the tube, $q$ is flow rate, $A$ is cross-section area of the tube, $d$ and $L$ are diameter and length of the tube, respectively, $\mu$ is fluid viscosity. Written in terms of flow rate, equation 3-1 becomes:

$$q = \frac{\pi r^4 \Delta p}{8 \mu L} \qquad (3\text{-}2)$$

where $r$ is the radius of the tube. The total flow rate for a bundle of identical capillary tubes is:

$$q = n\frac{\pi r^4 \Delta p}{8\mu L} \qquad (3\text{-}3)$$

where $n$ is the number of capillary tubes. The porosity of a cubic box of length $L$ filled with $n$ identical capillary tubes, and space between tubes filled with solid matrix can be expressed as:

$$\phi = \frac{n\pi r^2}{L^2} \qquad (3\text{-}4)$$

According to Darcy's law (equation 2-1), the flow rate through the box is:

$$q = k\frac{L^2 \Delta p}{\mu L} \qquad (3\text{-}5)$$

Combining equations 3-3, 3-4, and 3-5 yields:

$$k = \frac{\phi r^2}{8} \qquad (3\text{-}6)$$

If capillary tubes are tortuous rather than straight, the above equation is written:

$$k = \frac{\phi r^2}{8\tau} \qquad (3\text{-}7)$$

where $\tau$ is tortuosity factor defined as the square of the ratio of the actual flow path length to the apparent flow path length (Cornell and Katz, 1953, Carman, 1956):

$$\tau = \left(\frac{L_e}{L}\right)^2 \qquad (3\text{-}8)$$

where $L$ is the direct distance between the ends of the tube and $L_e$ is the length of the tortuous tube. Tortuosity can be calculated from electrical properties:

$$\tau = F\phi \qquad (3\text{-}9)$$

where $F$ is the formation resistivity factor (Archie, 1942). Substituting equation 3-9 into equation 3-7 yields:

$$k = \frac{r^2}{8F} \qquad (3\text{-}10)$$

where $F$ is expressed as:

$$F = \phi^{-m} \qquad (3\text{-}11)$$

The "cementation factor" ($m$) usually ranges from 1 to 3, and has an average value of 2 for clean sandstones. Equation 3-7 or 3-10 is usually called the "Kozeny-Carman" equation, and has been widely used as the starting point for many other permeability models.

The following example illustrates the application of Kozeny-Carman equationin real reservoir sandstones where pore-throats are well-sorted. The data set comes from Hodgkins and Howard (1999). Porosity and permeability were made on 14 sandstone samples from an oil-productive well in the Gulf of Mexico. The sandstones are interpreted as turbidite channel deposits. Quartz is the predominant framework constituent (over 74%). Sand grains are well-sorted. Median grain diameters range from 15 to 114 μm. Porosities range from 24.7 to 35%, and permeabilities range from 26 to 1280 md. Mercury-injection capillary pressures were measured. Pore-throat radii at 45% mercury saturation ($r_{45}$) is used as an approximate of the representative pore-throat radius. Permeabilities are calculated with equation 3-10 (assume $m$=1.8). A good

agreement between calculated and measured permeability is observed (Figure 3.1), with a coefficient of correlation ($R^2$) value of 0.9996.

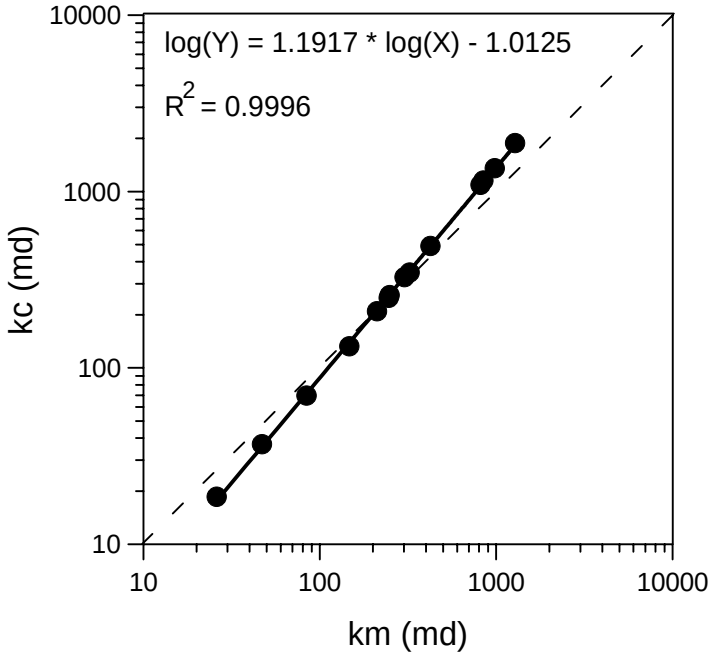


**Figure 3.1 Comparison between calculated (kc) and measured (km) permeability. Permeability is calculated with equation 3-10. Dash line denotes 1:1 correlation (data from Hodgkins and Howard, 1999).**

The *r* in equation 3-10 is related to specific surface:

$$r = \frac{2}{S_p} = \frac{2\phi}{S_g(1-\phi)} \qquad (3\text{-}12)$$

where $S_p$ and $S_g$ are the internal surface area per unit pore volume and grain (solid) volume, respectively. Substituting equation 3-12 into equation 3-7 yields:

$$k = \frac{\phi}{2\tau S_p^{\,2}} = \frac{\phi^3}{2\tau(1-\phi)S_g^{\,2}} \qquad (3\text{-}13)$$

The constant 2 in equation 3-13 is often replaced by a shape factor, $k_0$, to account for the differences between actual pore cross-section shapes and the modeled idealized conduits. Shape factors are commonly between 2 and 3 (Carman, 1956). Thus, equation 3-13 is written as:

$$k = \frac{\phi}{k_0 \tau S_p^{\ 2}} = \frac{\phi^3}{k_0 \tau (1-\phi) S_g^{\ 2}} \qquad (3\text{-}14)$$

Equation 3-14 is a form of the Kozeny-Carman equation. The combined constant $k_0 \tau$ is the Kozeny constant, it found empirically to be about 5 (Carman, 1956).

The Kozeny-Carman equation assumes pore spaces are composed of a bundle of identical capillary tubes; clearly a simplified description of natural porous media. Purcell (1949) derived a permeability equation by approximating the pore structure as a bundle of capillary tubes of different size. The distribution of capillary radii can be obtained from mercury injection capillary pressure (MICP) data. The equation is:

$$k = 10.66(\sigma \cos\theta)^2 \phi f \int_0^1 \frac{dS_{nw}}{P_c^{\ 2}} \qquad (3\text{-}15)$$

where $f$ is the "lithology factor", introduced to account for differences between the model and natural pore structure. An empirically value of 0.216 was found for clean sandstones.

Katz and Thompson (1986) proposed a theoretical equation to predict permeability based on percolation theory:

$$k = 226 \frac{l_c^{\ 2}}{F} \qquad (3\text{-}16)$$

where $l_c$ is diameter of the "critical" pore-throat size that controls permeability. This pore size is inferred to correspond to the inflection point on a MICP curve or a diameter

corresponding to displacement pressure (Katz and Thompson, 1986). Dullien (1992) suggested the coefficient in equation 3-16 varies from sample to sample.

### 3.1.2 Models based on sphere packing

Porosity and permeability are known to correlate with grain size and sorting (Graton and Fraser, 1935, Krumbein and Monk, 1942, Berg, 1970, 1975, Beard and Weyl, 1973, Gangi, 1985). Permeability generally increases with grain size and sorting (Figure 3.2). Generally speaking, permeability increases with grain size and sorting. The correlation is poored for more poorly-sorted sandstones.

Hubbert (1940) determined theoretically that permeability is proportional to grain diameter square:

$$k = Nd^2 \qquad (3\text{-}17)$$

where $d$ is the grain diameter and N is a dimensionless factor that depends on pore shape.

Graton and Fraser (1935) developed models for the packing of spherical grains (Figure 3.3). Geometric arrangements were visualized with the unit cell, a polygon formed by connecting the centers of each of eight regularly packed spheres. Each unit cell contains one sphere volume, and associated pore volume changes depending on sphere arrangement. Pore size and porosity decrease from cubic to rhombohedral packing.

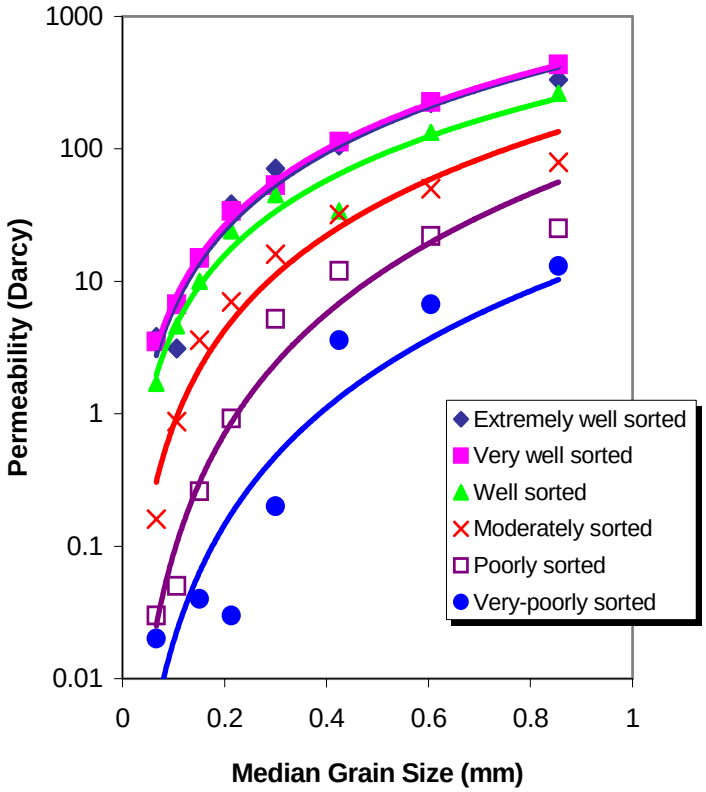


**Figure 3.2 Relationship among permeability, median grain size (diameter), and sorting (data from Beard and Weyl, 1973)**

Berg (1970) derived the following equation for permeability based on sphere packing:

$$k = 5.1\times10^{-3}\phi^{5.1}d^{2} \qquad (3\text{-}18)$$

where $d$ is the diameter of spheres in millimeters. Equation 3-18 is based on uniform sphere packing in several regular ways with porosities in the range 26% to 47.6%. In reality, we have to find what particle size must replace $d$ for particles neither spherical

nor uniform in size. Berg (1975) suggested that ninetieth percentile grain size controls the permeability in well-sorted quartzose sandstones, and modified equation 3-18 to:

$$k = 5.3 \times 10^{-3} \phi^{5.1} (P_{90})^2 \qquad (3\text{-}19)$$

where $P_{90}$ is the ninetieth-percentile grain size in millimeters as determined by cumulative weight-percent analysis.

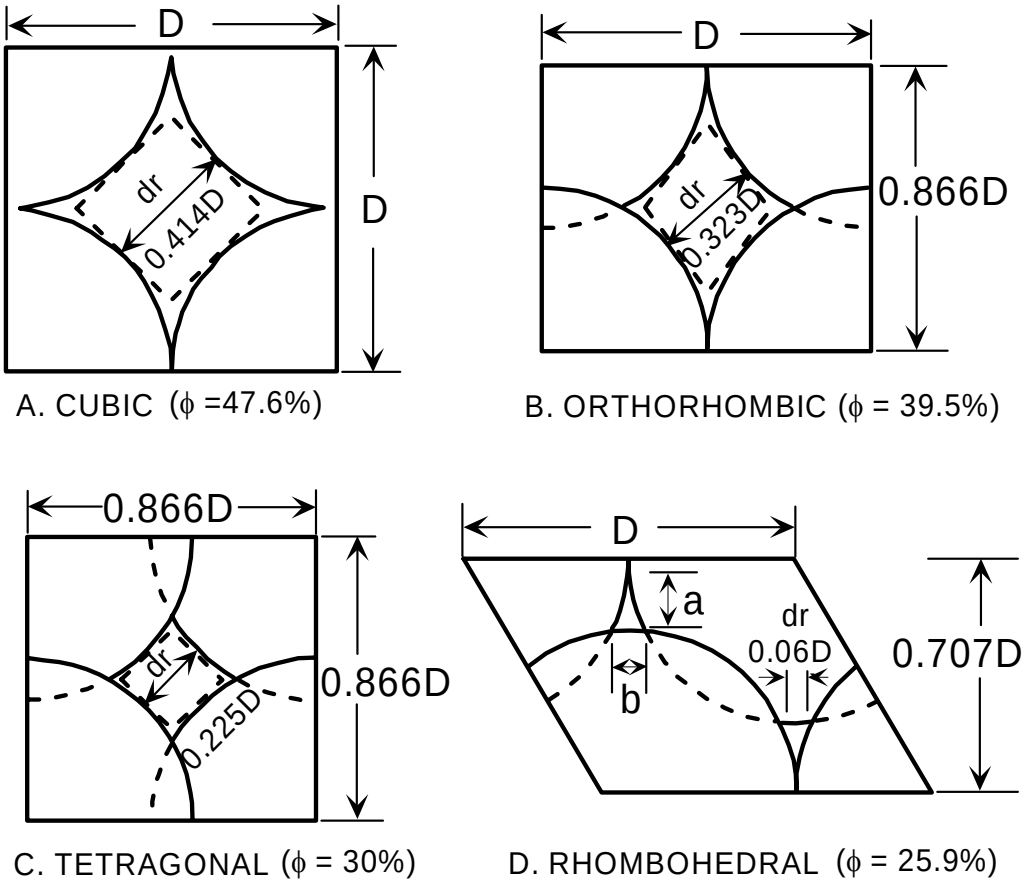


**Figure 3.3 An illustration of the largest rectilinear pores through unit cells in systematic packings of uniform spheres (modified from Berg, 1970)**

Krumbein and Monk (1942) developed an empirical relationship between median grain size and permeability:

$$k = 760 d_w^{\,2} e^{-1.36\sigma_\phi} \qquad (3\text{-}20)$$

where $d_w$ is the median grain diameter by weight, obtained by sieving analysis; $\sigma_\phi$ is the standard deviation in phi ($\Phi$) units, where $d_w = 2^{-\Phi}$.

Gangi (1985) reanalyzed Krumbein and Monk's data, and pointed out that the grain size term should be replaced by the mean diameter by number of grains. The mean diameter by weight for a sample of two grain sizes, places equal importance on a large size $d_1$ and a small size $d_2$. However, for the same weight of $d_1$ and $d_2$, $d_2$ will have a greater number of grains. Therefore, the smaller grains will determine the dominant pore size of the sample. Berg (1975) pointed out that the 90$^{th}$ percentile by weight ($P_{90}$) is approximately equal to the median grain size by number. The median grain size by number can be obtained from thin-section by counting the numbers of grains of different size.

The Kozeny-Carman model can also be expressed in terms of grain size and porosity. For uniform spheres:

$$S_g = 6/d \qquad (3\text{-}21)$$

substituting equation 3-21 into equation 3-14, we have

$$k = \frac{d^2 \phi^3}{36 k_0 \tau (1-\phi)} \qquad (3\text{-}22)$$

Assuming $k_0\tau$=5, equation 3-22 can be rewritten as:

$$k = \frac{d^2 \phi^3}{180(1-\phi)} \qquad (3\text{-}23)$$

A data set from Beard and Weyl (1973) is illustrated here to show the influence of grain size and sorting on permeability. Porosity, permeability, and grain size/sorting were measured on 48 unconsolidated sand samples from two Texas rivers. Berg's model (equation 3-18) and Kozeny-Carman model (equation 3-23) are used to calculate permeability (Figure 3.4). The two models display similar results: they predict permeability well for well-sorted samples, and poorly for poorly-sorted samples. The error increases as sorting becomes poor, and reaches 2-3 orders of magnitude.

### 3.2 Empirical Models

Empirical models based on statistical relationships between permeability and parameters that have direct or indirect influence on permeability are more commonly used. Such parameters include pore-throat radius, grain size and sorting, specific surface area, irreducible water saturation, and cation exchange capacity. Here, two widely used kinds of empirical models are discussed, i.e., those based on pore-throat size and those based on surface area.

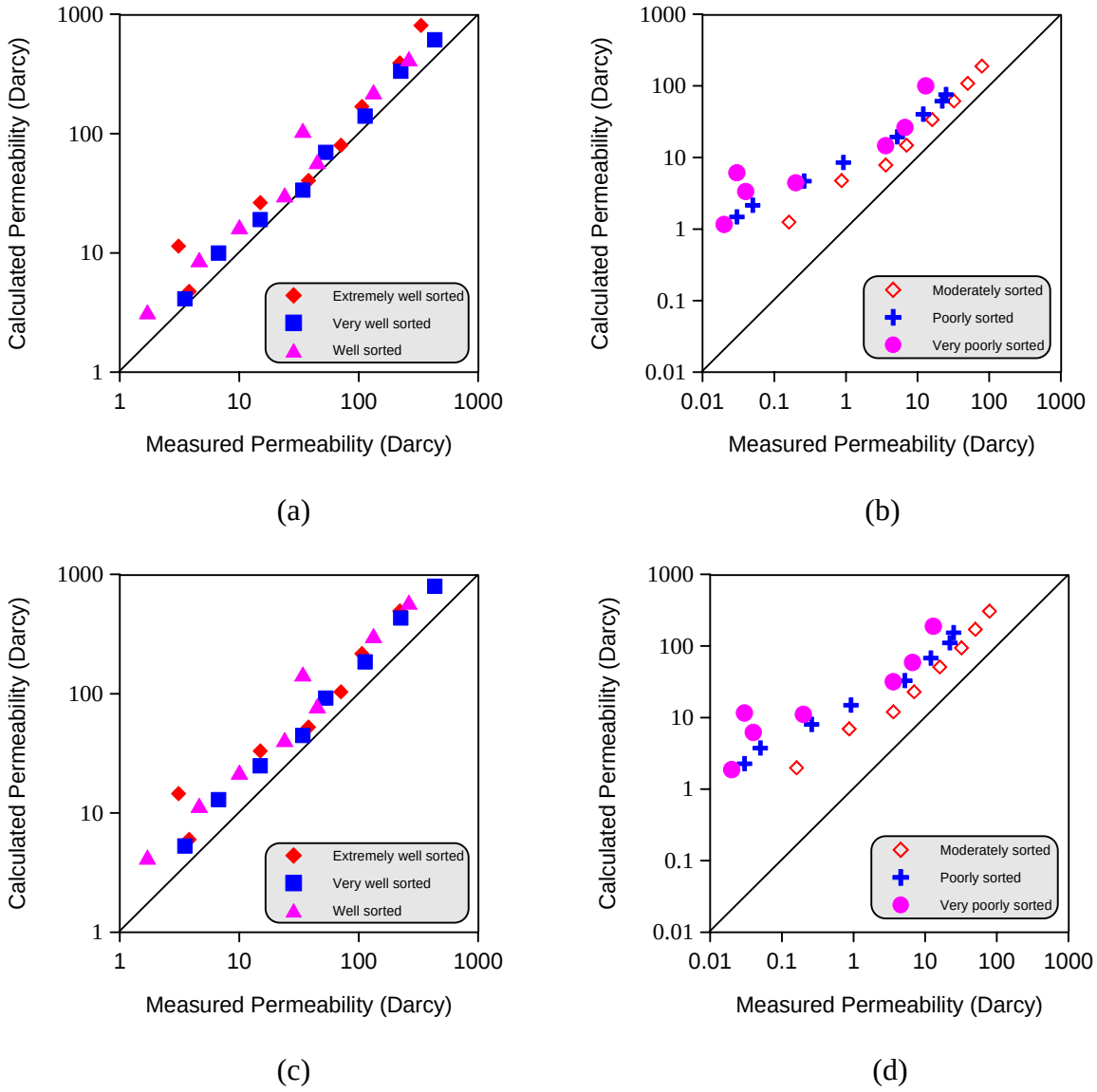


**Figure 3.4 Comparison between calculated and measured permeability for unconsolidated sands. In (a) and (b), permeabilities are calculated with equation 3-18; in (c) and (d), permeabilities are calculated with the equation 3-23. The diagonal line denotes a 1:1 correlation (data from Beard and Weyl, 1973).**

### 3.2.1 Models based on pore-throat size

The Kozeny-Carman equation (equation 3-10) indicates that pore-throat radius controls permeability. Pore-throat information obtained from capillary-pressure measurements has long been used to correlate with porosity and permeability (Figure 3.5). Winland (published by Kolodzie, 1980) used $r_{35}$ (pore-throat radius at 35% mercury saturation). Swanson (1981) used $r_{apex}$ (radius at the point of the maximum rate of mercury intrusion). Basan et al. (1997), Pape et al. (1999), and Sigal (2002) used $r_{50}$ (median pore-throat radius). Hagiwara (1984) used average pore throat radius.

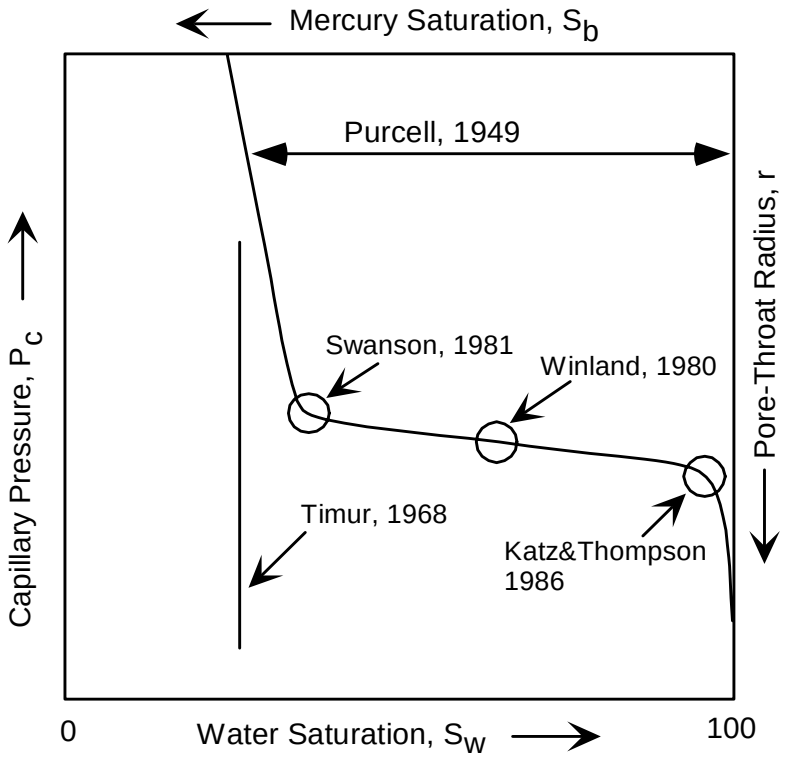


**Figure 3.5 An idealized capillary pressure curve showing measures used by different authors for determination of characteristic pore dimension (modified from Nelson, 1994).**

The most widely used empirical model is perhaps Swanson's model (1981, 1985):

$$k = 399\left(\frac{S_b}{P_c}\right)_{\max}^{1.691} \qquad (3\text{-}24)$$

where $S_b$ is the bulk volume of mercury saturation. Although it is empirical, Swanson's model usually give good estimation of permeability (Figure 3.6). Very low permeability (<0.1 md) samples may be exceptions.

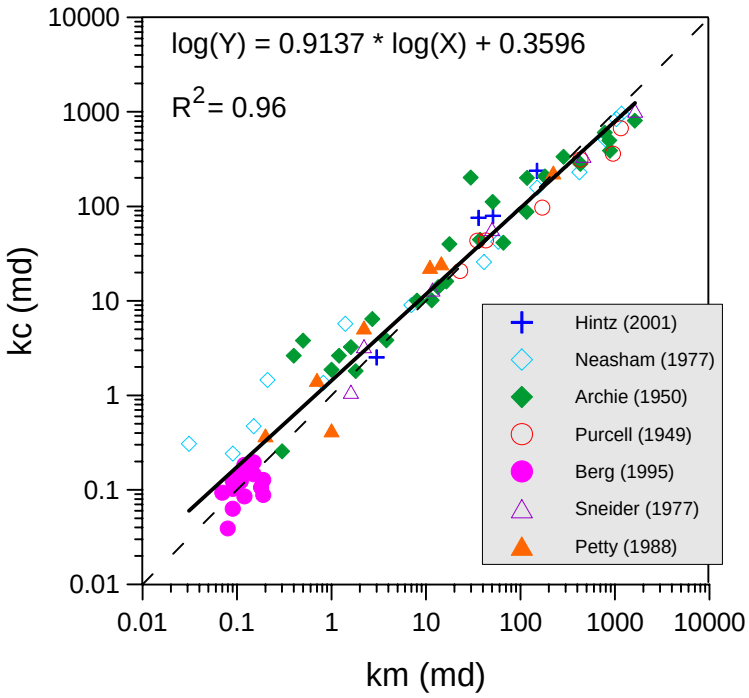


**Figure 3.6 Comparison between calculated and measured permeability. Permeability is calculated with Swanson's (1981) model (equation 3-24). Dash line denotes 1:1 correlation.**

### 3.2.2 Models based on surface area

The Kozeny-Carman model (equation 3-13) suggests that permeability depends on a power of porosity and on the inverse square of surface area. It has been found that irreducible water saturation $S_{wir}$ is proportional to specific surface area $S_g$ (Nelson, 1994). Several models based on this assumption have been proposed (Morris and Biggs, 1967, Timur, 1968, Coates et al., 1991). The limitation of this type of models is that $S_{wir}$ usually derives from capillary pressure data, which is rare.

Other measures of specific surface area, such as cation exchange capacity, $Q_v$, nuclear magnetic resonance decay time, $T_1$ or $T_2$, can also be correlated with permeability (Kenyon, 1988, Sen et al., 1990, Coates et al., 1991). These equations have the same limitation as other empirical correlations, i.e., the correlation can not be extended outside the range of original data.

## 3.3 Summary

Theoretical models offer insight into physical processes controlling permeability. They are a compromise between the feasibility of mathematics and the reality (Kwon and Pickett, 1975). Although a three-dimensional network is more realistic than a one dimensional capillary tube model, the benefit might be offset by tremendously increased computation and measurement expense. Although the bundle of capillaries model is somewhat simplified, the results are acceptable if the assumptions are met.

Pore-throat size has the most significant influence on permeability. Other parameters, such as grain size and sorting, specific surface area, irreducible water

saturation, are secondary to permeability prediction. Thus, models based on pore-throat size, either theoretical or empirical, have the best accuracy.

Empirical models based on statistical relationships between permeability and affecting variables are fast and easy to use. To be statistically meaningful, however, a large number of measurements have to be made. Coefficients derived from one data set may not fit another data set.

The permeability models discussed above and other commonly used models are listed in Appendix A.

# CHAPTER IV

# PREDICTING PERMEABILITY FROM EFFECTIVE POROSITY

## 4.1 The Concept of Effective Porosity

Porosity is frequently measured in the laboratory by the gas expansion method. Gas at a specified pressure is admitted to an evacuated core plug. This is a measure of total porosity because it includes pores of all sizes (Spain, 1992). However, not all pores contribute to fluid flow. Many studies have shown that permeability is a function of the abundance of intergranular macroporosity (Pittman, 1979, Ehrenberg, 1990, Ehrlich et al., 1991, Spain, 1992, Anguy et al., 1994, Nelson, 1994, 2000, Worthington, 1998, Hearst et al., 2000). Anguy et al. (1994) reported that most sandstones have one or two pore types (mostly intergranular pores) that account for over 80% of the permeability, whereas other pore types (i.e., grain dissolution or intragranular pores) are unrelated to permeability. Because small pores (micro pores) are “invisible” in thin sections, Ehrlich et al (1991) proposed that “optical porosity” (or Spain’s, 1992, “visual porosity”) represent the portion of porosity controlling permeability.

Nelson (2000) used the terms “contributing porosity” and “noncontributing porosity” to distinguish portions of porosity contributing and not contributing to flow, respectively. Contributing porosity consists of the interconnected pore space, usually composed of large pores with connecting throats, whereas noncontributing porosity consists of micropores and isolated pores.

Another widely used pair of terms are “primary porosity” and “secondary

porosity". Primary porosity refers to pore space formed during deposition, whereas secondary porosity refers to pore space formed after deposition, usually by dissolution. Because pore space formed during deposition is dominantly intergranular, the primary porosity is usually equated with intergranular porosity (Milliken, 2001).

Although "effective porosity" is perhaps the most widely used term, it has no rigorous definition. Core analysts define effective porosity as a measure of connected voids. It is derived from either the difference between bulk and apparent grain, or by a direct measurement of the connected void space. Measured volumes of connected void space may vary with sample preparation and analytical method. (API RP-40, 1998)

Log analysts have a different view of this term. Hearst et al. (2000) stated, "Log analysts often use the term *effective porosity*, $\phi_e$, referring to the pore space from which fluids can be produced. Often $\phi_e$ is referred to interconnected porosity. Some authors include clay-bound water within $\phi_e$, others do not. Thus, effective porosity has no generally accepted, rigorous definition. The remaining pore fraction (*noneffective porosity*) contains fluid in isolated vugs, or else retained by surface and capillary forces. Noneffective porosity occupies the small end of the pore size distribution; it may be intragranular porosity, or it may be porosity in the silt-size and clay-size fractions. Very often noneffective porosity is referred to as microporosity."

Schlumberger (2003) defines effective porosity as: "The interconnected pore volume or void space in a rock that contributes to fluid flow or permeability in a reservoir. Effective porosity excludes isolated pores and pore volume occupied by water adsorbed on clay minerals or other grains."

The "effective porosity" of log analysts can be expressed as:

$$\phi_e = \phi_t - \phi_{cl} \qquad (4\text{-}1)$$

where $\phi_{cl}$ is the clay porosity (the volume of clay-bound water), and written as:

$$\phi_{cl} = V_{cl} \times \phi_m \qquad (4\text{-}2)$$

where $\phi_m$ is the microporosity of 100% clay minerals, $V_{cl}$ is the clay volume.

Petroleum engineers define this term as (Bass, 1992) "the ratio of the interconnected void space in the rock to the bulk volume (BV) of the rock. From the reservoir-engineering standpoint, effective porosity is the desired quantitative value because it represents the space that is occupied by mobile fluids."

The "effective porosity" of petroleum engineers can be expressed as:

$$\phi_e = \phi_t (1 - S_{wir}) \qquad (4\text{-}3)$$

where $\phi_t$ is the total porosity, and $S_{wir}$ is the irreducible water saturation, which includes both clay-bound water and capillary bound water.

Figure 4.1 illustrates the models used by core analysts, log interpreters, and petroleum engineers to define "effective porosity". For core analysts, the effective porosity depends on the method in which cores are dried. Log analysts include capillary bound water. Petroleum engineers do not include either capillary bound or clay bound water.

Pittman (1979) divided porosity into four categories: (1) primary intergranular porosity, (2) microporosity associated with clay minerals or other very fine mineral constitutes, (3) dissolution porosity, and (4) fracture porosity. Proportions of the first three can be displayed on a ternary diagram (Figure 4.2). Based on the discussion above, "intergranular porosity", "visual porosity", and "primary porosity" from petrographic image analysis are approximates of the "effective porosity".

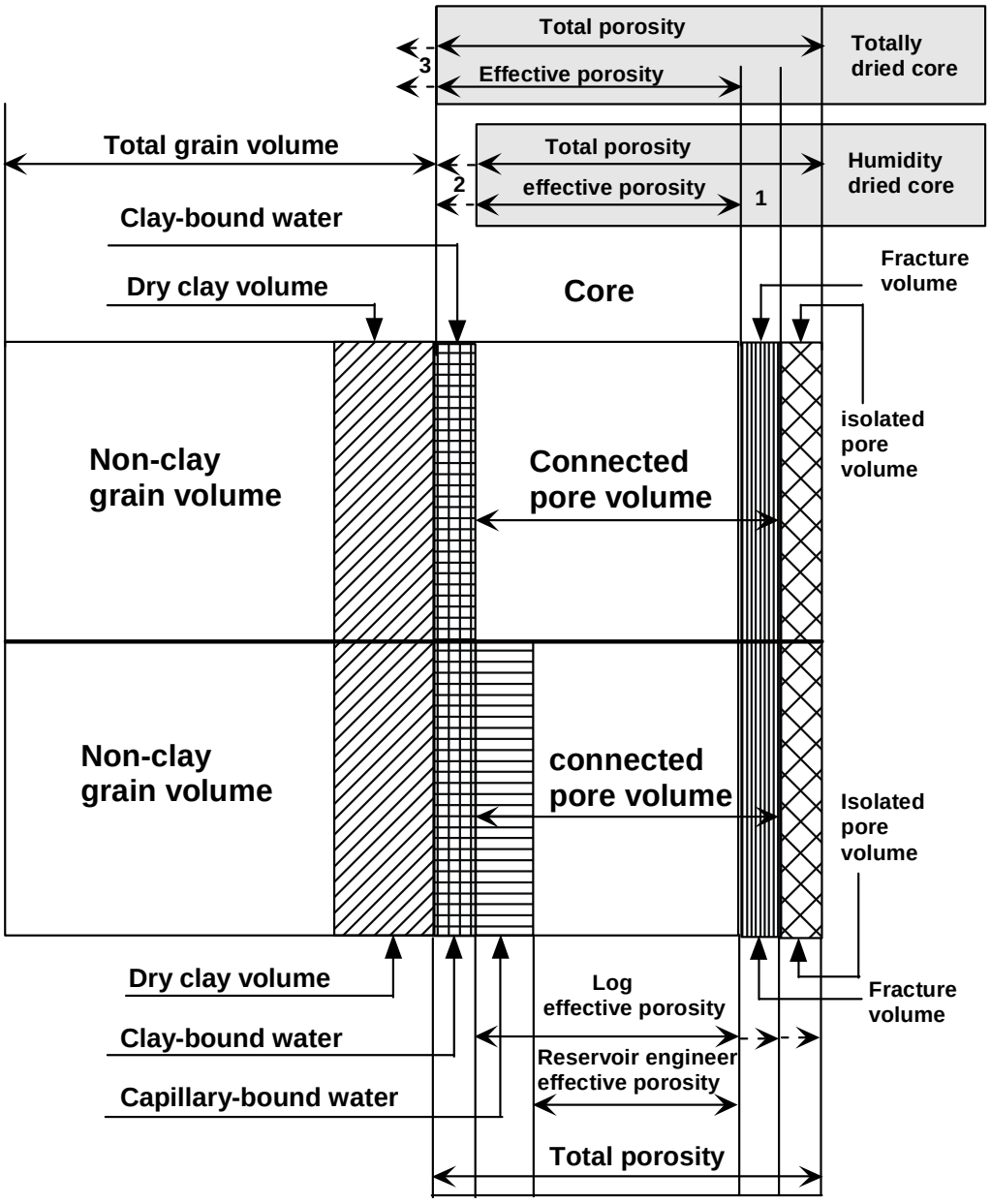


**Figure 4.1 Depiction of the models used to define core, log, and engineering "effective porosity". Note: 1. fracture and isolated porosities will be excluded only if they have been measured by core or log analysis; 2. total and effective porosity of humidity-dried cores intend to, but may not, exclude all clay-bound water; 3. drying cores at 250°C may alter mineralogy, which could result in total and effective porosity being overestimated (modified from Schlumberger, 2003)**

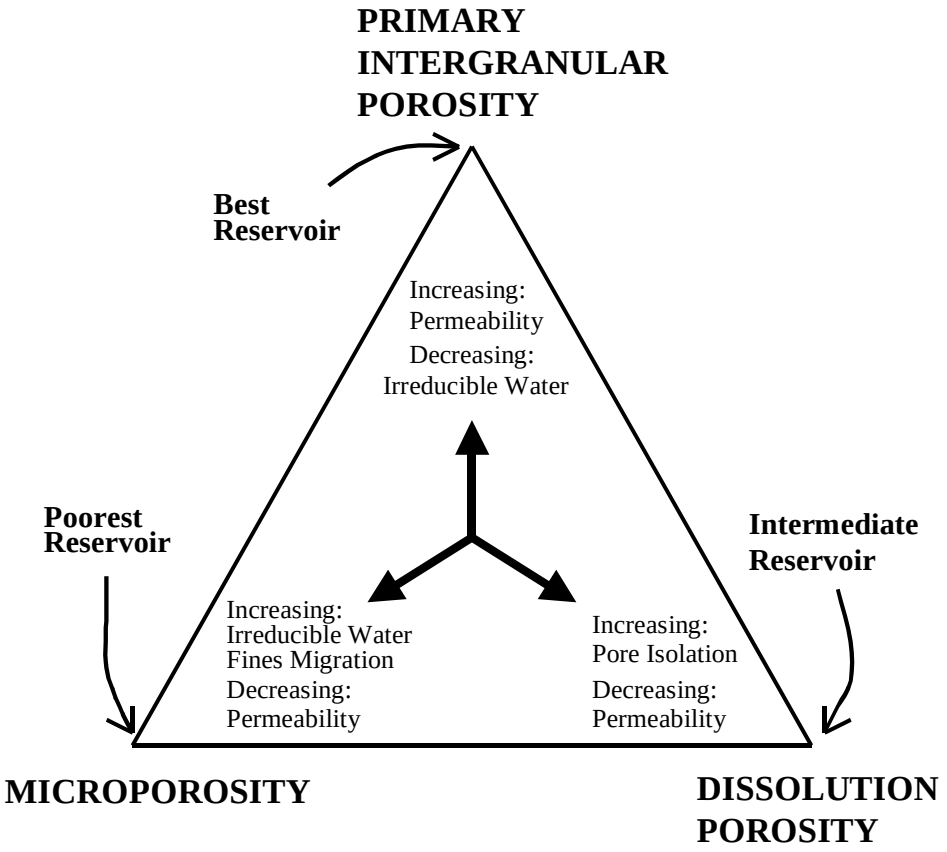


**Figure 4.2 Classification of nonfracture porosity in sandstones summarizing the influence of porosity type on reservoir quality (after Houseknecht, 1992, modified from Pittman, 1979).**

## 4.2 Estimation of Effective Porosity

### 4.2.1 Microporosity of clay minerals

The presence of clays has two effects on petroleum reservoir rocks: 1) reducing a reservoir's storage capacity by reducing effective porosity, and 2) reducing a reservoir's productivity by reducing permeability (Asquith, 1990). As clay particles fill pore space, they reduce pore and pore-throat size, and create micropores within clay particles. As

shown in Figure 4.3, to achieve the same permeability, shaly sandstones must have much greater porosities than quartzose sandstones because the microporosities associated with clays don't contribute to permeability.

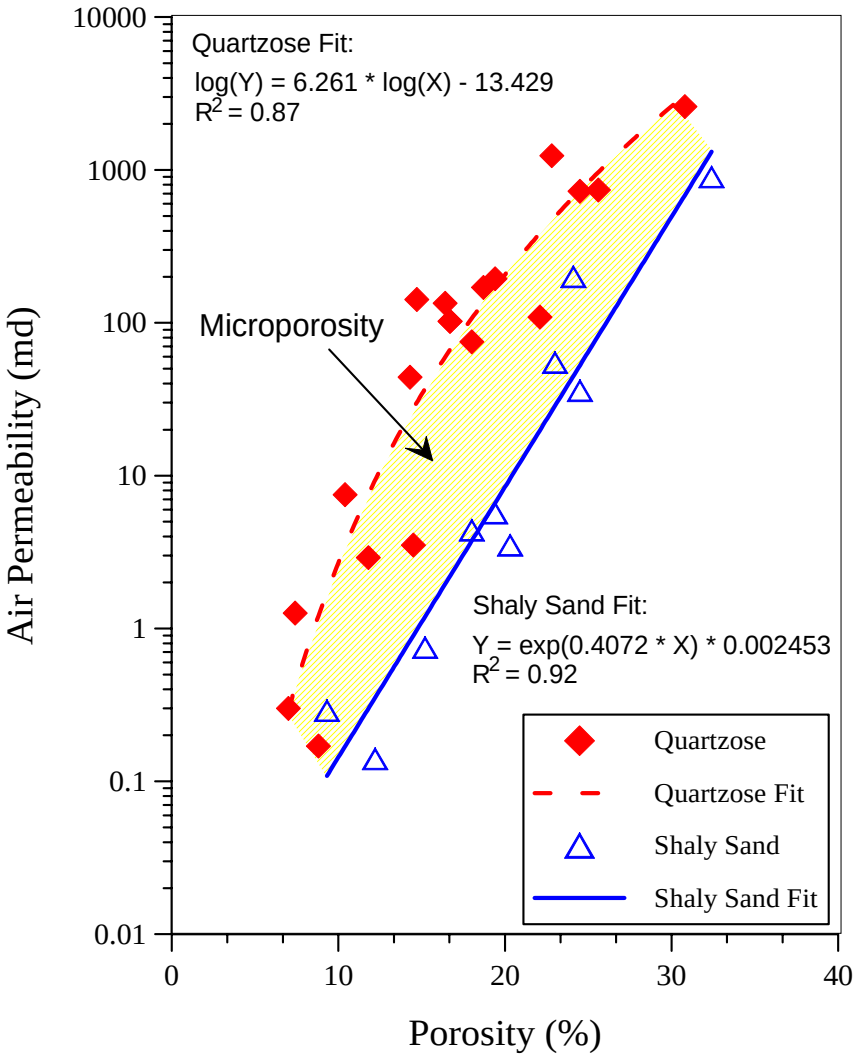


**Figure 4.3 Effects of clay on permeability-porosity relationships. Porosity and permeabilities are average values of core measurements from 28 wells in Texas. Shaded area denotes microporosity (data from Berg, 2003 personal communication, Appendix C).**

Clay minerals exist in three morphologies: dispersed clay, structural clay, and laminated clay (Asquith, 1990). In this study, only the dispersed, authigenic clays formed in the diagenetic process are discussed because this type of clay is very common and damaging in petroleum reservoirs. Structural clays can be treated as grains, and usually have little effect on permeability. Laminated shale usually affects permeability anisotropy. Asquith (1990) suggested that average permeability and porosity of interlaminated sand/shale sequences is reduced in proportion to shale volume.

Neasham (1977) divided authigenic clays into three morphologic groups (Figure 4.4). Groups of pore-bridging, pore-lining and discrete particles of clay are commonly associated with illite, chlorite and smectite, and kaolinite, respectively. These three groups define regions on a porosity-permeability cross-plot (Figure 4.5). Pore-bridging clays reduce the porosity only slightly but can greatly reduce sandstone permeability, whereas discrete particle clays only slightly lower both porosity and permeability. Although there is no general relationship between porosity and permeability for all samples, a relationship exists within each group (with the exception of pore-bridging clay).

Clay content, $V_{cl}$, usually shows an inverse relationship with permeability (Figure 4.6) and has been used in permeability prediction (Xu and White, 1998). The relationship is between $V_{cl}$ and k is weak. For instance, at constant 10% clay volume, permeability changes by two orders of magnitude (Figure 4.6). This range is usually attributed to the effects of clay morphology.

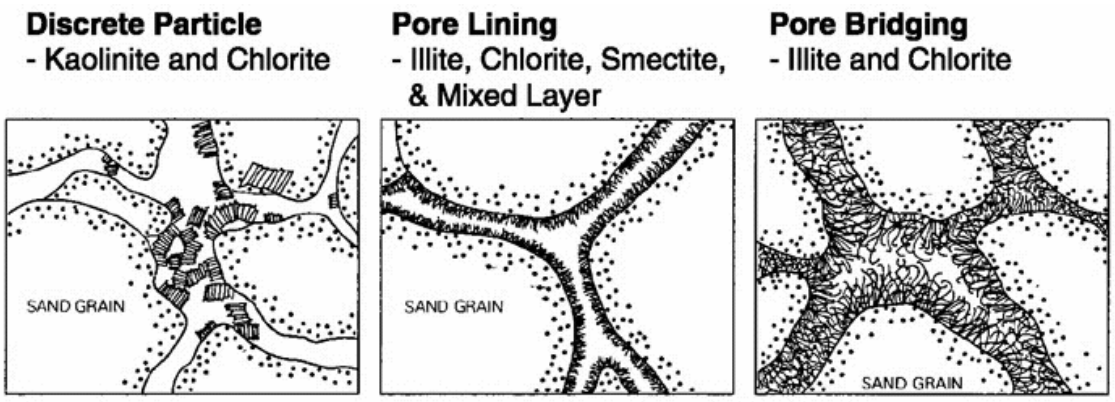


**Figure 4.4 Classification of the morphology of authigenic clays (after Neasham, 1977)**

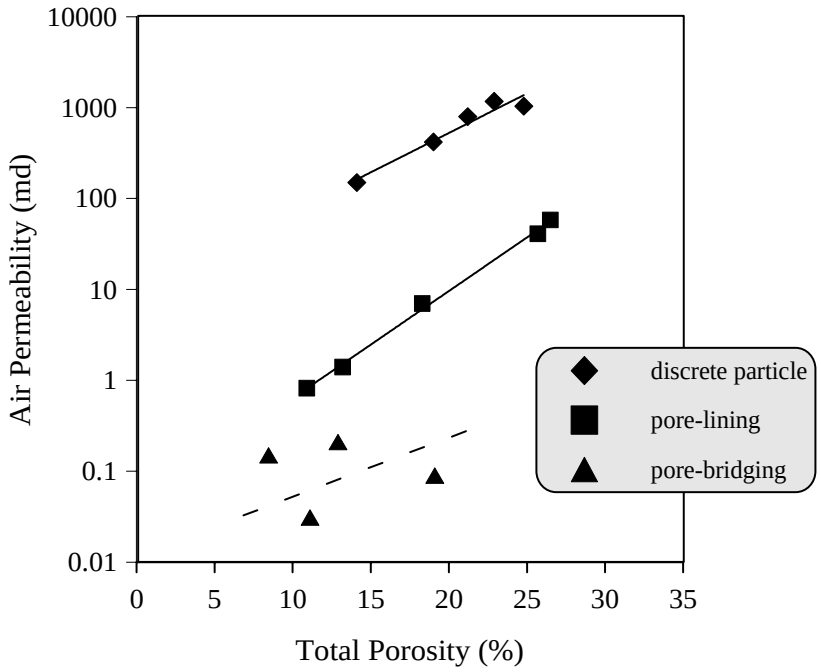


**Figure 4.5 Cross plots of air permeability vs. total porosity. Solid lines denote best fits of the data, and dashed line denotes conjectural fit line (data from Neasham, 1977, figure modified from Wu and Berg, 2003).**

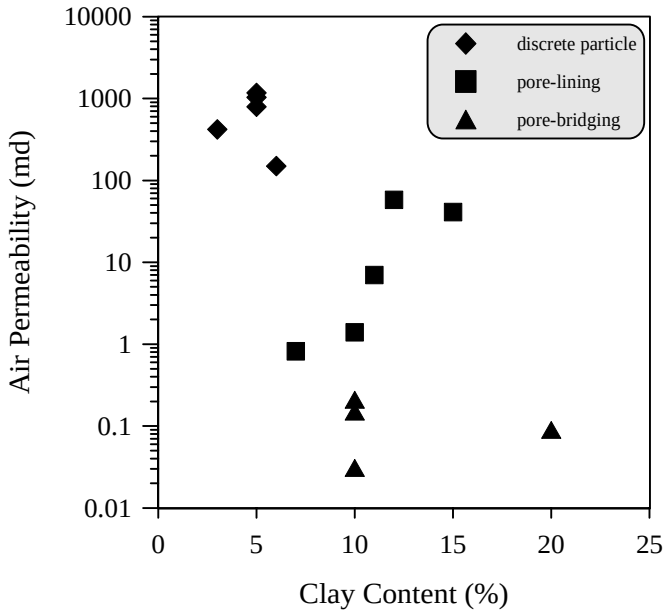


**Figure 4.6 Correlation between permeability and clay content (data from Neasham, 1977, figure modified from Wu and Berg, 2003)**

For shaly sandstone, the major problem is clay micropores, with pore-aperture radii less than 0.5 μm (Pittman, 1979), which are pores generally associated with clay minerals (Hurst and Nadeau, 1995). Although Neasham's classification has been widely used to evaluate qualitatively clay microporosity, only recently have efforts been made to quantitatively estimate clay-microporosity with the aid of Back Scattered Electron (BSE) analysis or SEM (Nadeau and Hurst, 1991, Hurst and Nadeau, 1995, Basan et al., 1997). Based on BSE and SEM analysis, Hurst and Nadeau (1995) proposed average microporosity values of 43%, 51%, and 63% for diagenetic kaolinite, chlorite, and fibrous illite, respectively (Table 4.1), and 10% for detrital clays independent of mineralogy. Because fibrous illitic clays are difficult to characterize by the X-ray method (BSE), more reliable analyses were conducted by stereo-pair micrographs from scanning-electron microscopy, which revealed that illite commonly has microporosity of

approximately 90% (Hurst and Nadeau, 1995). These values are subject to change because they are based on a relatively small data set (52 samples for kaolinite, 10 for chlorite, and 5 for illite).

**Table 4.1 Properties of authigenic clay minerals (from Wu and Berg, 2003)**

| Clay minerals | Clay morphology * | Qv (meq/ ml)* | Specific surface area ($m^2$/gm)** | Microporosity Range + | Average microporosity + | Average microporosity used in this study |
|---|---|---|---|---|---|---|
| Kaolinite | Discrete particles | 0.034 | 23 | 15 – 61 | 43 | 20 |
| Chlorite | Pore-lining | 0.222 | 42 | 44 – 58 | 51 | 70 |
| Illite | Pore-bridging | 0.313 | 113 | 47 – 76 | 63 (90) + | 90 |

* from Neasham, 1977. $Q_v$ is cation exchange capacity per unit pore volume (meq/ml). The values are average values.
** from Asquith, 1991
+ from Hurst and Nadeau, 1995. 90% was obtained by the analysis of stereo-air micrographs from scanning-electron microscopy.

In this study, 20%, 70%, and 90% are assumed to be average microporosity values for diagenetic kaolinite, chlorite, and illite respectively (Table 4.1). These values are close to, but differ somewhat from, those of Hurst and Nadeau (1995), and are used here because they provide a better fit between effective porosity and permeability. A 20% microporosity for kaolinite was supported by experimental results (Robert B. Truman, 2003, personal communication). A chlorite microporosity of 70% is used because chlorite has similar cation exchange capability to illite (Table 4.1). Since micro porosity mostly occurs in diagenetic clay minerals, it is critical to separate diagenetic from detrital (structural) clays. Otherwise, microporosity might be overestimated, and negative effective porosity values might be obtained.

Here, a data set from Neasham (1977) is used to illustrate the estimation of

effective porosity. The data set consists of 14 samples (Appendix B) from a larger sample population of 44 petroleum reservoir sandstones. These samples cover a porosity and air permeability range of 8.5 to 26.5% and 0.031 to 1173 md, respectively. Effective porosities are calculated with equation 4-1 and 4-2. The cross plot of permeability against effective porosity is shown in Figure 4.7. Instead of three separate trends for the three clay morphologies, a single trend is obtained for all the three groups. The best fit curve is expressed as:

$$\ln k = -3.307 + 1.043(\ln \phi_e)^2 \qquad (4\text{-}4)$$

where $k$ is air permeability in millidarcy. The coefficient of determination ($R^2$) value is 0.95. Figure 4.8 shows the correlation between permeability and median pore-throat diameter is independent of clay morphology.

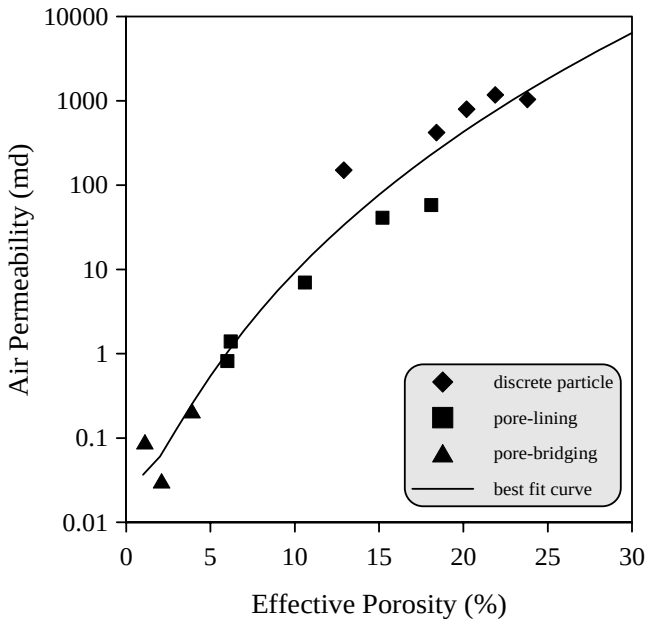


**Figure 4.7 Cross plot of permeability and effective porosity for shaly sandstones (data from Neasham, 1977, figure modified from Wu and Berg, 2003).**

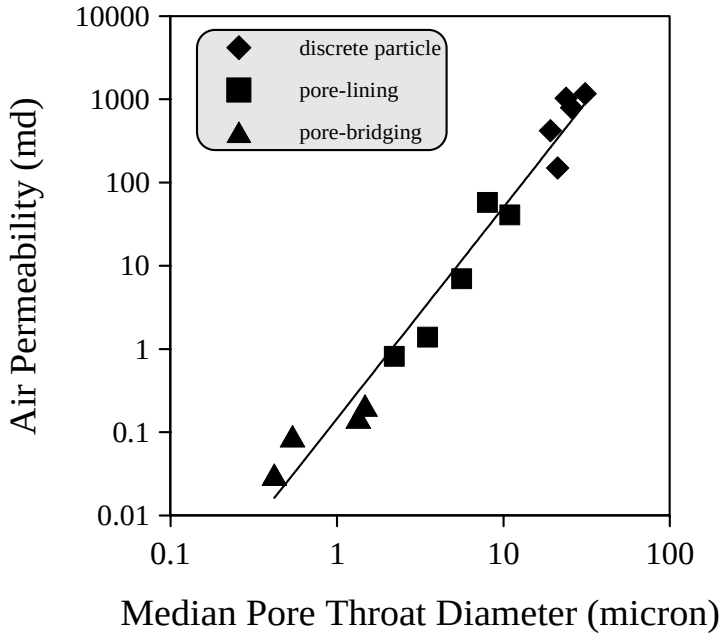


**Figure 4.8 Cross plot of permeability and median pore-throat diameter for shaly sandstones (data from Neasham, 1977, figure modified from Wu and Berg, 2003).**

Figure 4.9 shows the correlation between median pore-throat diameter (MPD) and total porosity and effective porosity, respectively. A weak relationship between MPD and total porosity is observed (Figure 4.9a). A strong relationship between MPD and effective porosity is observed (Figure 4.9b), which may account for the strong correlation between permeability and effective porosity in Figure 4.7.

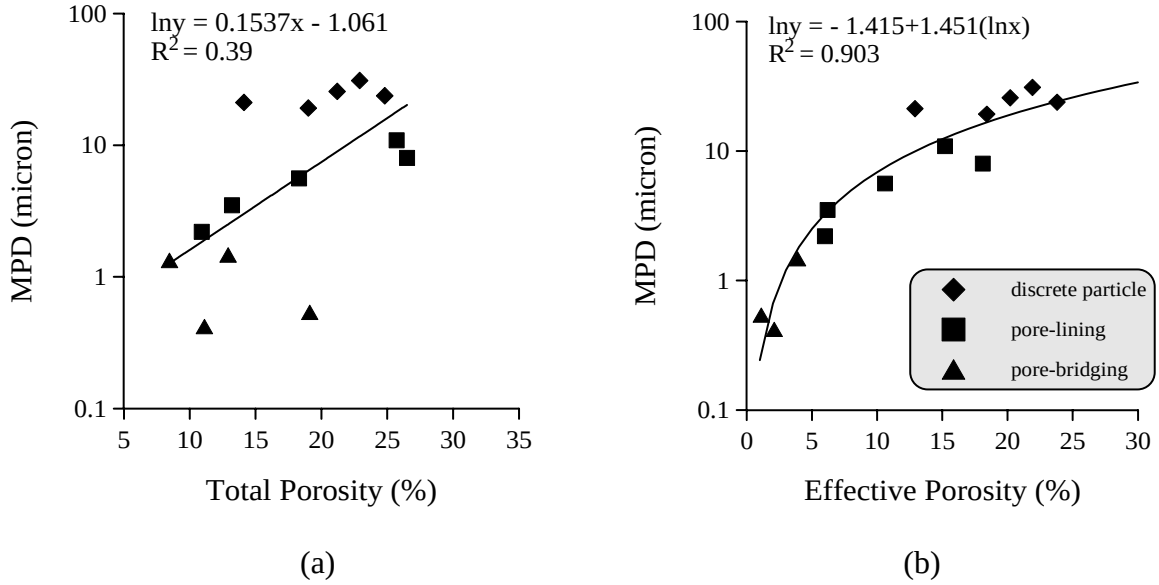


**Figure 4.9 Correlation of median pore-throat diameter (MPD) with total porosity (a), and effective porosity (b). (data from Neasham, 1977, figure modified from Wu and Berg, 2003).**

### 4.2.2 Dissolution porosity

Dissolution pores result from removal of carbonates, feldspar, sulfate, or other soluble materials (Pittman, 1979). Ehrenberg (1990) reported two types of dissolution pores (intragranular macropores and intragranular micropores) and concluded that both types contribute little to fluid flow. The former are commonly isolated and the latter are commonly too small. Thus, in most cases, dissolution porosity falls into the noneffective porosity class (Nelson, 2000).

A data set from Walderhaug (2000) is used as an example to show the affects of dissolution. The data set comes from Middle Jurassic, Brent Group sandstones from the Norwegian sector of the North Sea. Quartz overgrowths are the dominant cement and range from less than 1 to 29% of sample volumes. A large proportion of the porosity is

secondary pores formed by feldspar dissolution. The dissolution porosities range from 0 to 7.7%, with an average of 4.3%. As shown in Figure 4.10, dissolution porosity contributes little to permeability. For instance, 10 md permeability corresponds to 17.5% total porosity and 11.2% effective porosity. The difference, 6.3% porosity (dissolution porosity) does not increase permeability.

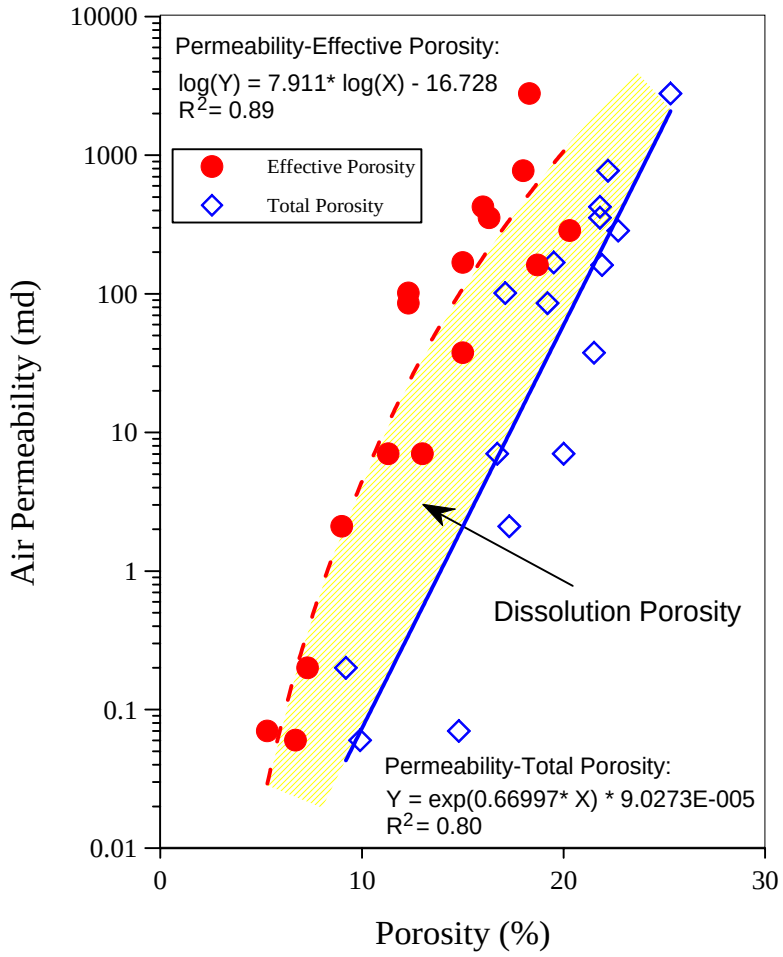


**Figure 4.10 Correlation between permeability with total and effective porosity. The dash line denotes the best fit for permeability and effective porosity; the solid line denotes the best fit for permeability and total porosity. Shaded area denotes dissolution porosity (data from Walderhaug, 2000, Appendix C, figure modified from Wu and Berg, 2003).**

As the total porosity increases to high values (>25%) and decreases to low values (<5%), effective porosity tends to be approximately equal to total porosity (Figure 4.10). At high porosities, the pores are predominately macropores, and at low porosities, the pores are predominately micropores. Based on above discussion, a general equation for effective porosity can be written as:

$$\phi_e = \phi_t - \phi_{cl} - \phi_d \qquad (4\text{-}5)$$

where $\phi_d$ is the dissolution porosity.

Equation 4.5 can be used for both clean sandstones and shaly sandstones. For clean sandstones, $\phi_{cl}$ might be negligible (the above example) since $\phi_d$ is the predominant noneffective porosity. For shaly sandstone, if $\phi_d$ is negligible, then equation 4-5 is the same as equation 4-1.

### 4.2.3 Effective porosity from mineralogy analysis

If several clay minerals exist in a shaly sandstone, then equation 4-5 can be written as:

$$\phi_e = \phi_t - \sum_j V_{clj}\phi_{mj} - \phi_d \qquad (4\text{-}6)$$

where $\phi_{cl} = \sum_j V_{clj}\phi_{mj}$, $V_{clj}$ is the volume of clay mineral j, $\phi_{mj}$ is the average microporosity of 100% clay mineral j; and $\phi_d$ is the dissolution porosity.

Relative volume content of each clay mineral can be obtained from X-ray diffraction analysis. A data set (Pike, 1981) from Yowlumne sandstone, Kern County, California, is used to illustrate this method (Appendix B). X-ray diffraction analysis reveals the relative weight percent of clay minerals, while the petrograhic analysis

provides clay volume. The weight percentages are first converted to volume percentage, effective porosity values are then estimated with equation 4-6. Permeabilities are calculated with equation 4-4. A better prediction was achieved when the estimated effective porosities were applied (Figure 4.11). Most of the predicted permeability values fall into the range 0.25<kc/km<4, where kc and km are calculated and measured permeabilities, respectively. This range is considered acceptable because Bradley et al. (1972) pointed out that closely spaced permeability measurements in core analysis can vary up to four times and still be considered accurate estimates.

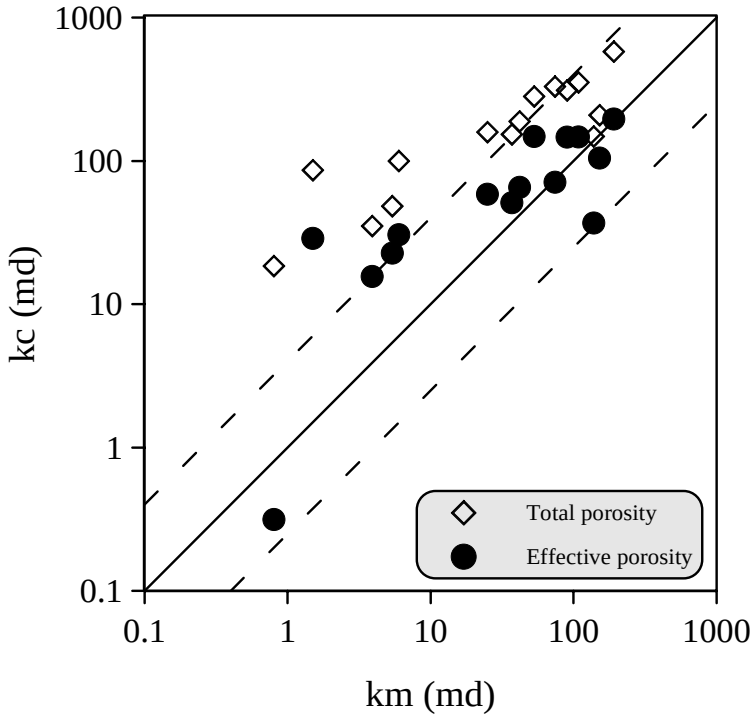


**Figure 4.11 Comparison of calculated permeability (kc) with measured permeability (km) for the Yowlumne sandstone, Kern County, California. The solid line denotes 1:1 correlation. The upper and lower dashed lines denote the range of 0.25< kc/km <4 (data from Pike, 1981, figure modified from Wu and Berg, 2003)**

### 4.2.4 Effective porosity from capillary pressure analysis

Pore-size distribution is commonly obtained from mercury-injection capillary pressure curves. Injection into larger intergranular pores is recorded by the gentle plateau of a curve, while that into small pores usually is recorded by remaining steep section of a curve. Pittman (1979) proposed a pore-throat radius of 0.5 μm as a cutoff between effective and noneffective porosity. Swanson (1981, 1985) determined the point on the mercury injection curve that represents a continuous, interconnected pore system through the rock. Swanson (1977, p.2498) mentioned that at this point, "the mercury saturation expressed as percent of bulk volume is indicative of that portion of the space effectively contributing to fluid flow." Thus, this point can be used as the cutoff between microporosity (non-effective) and macroporosity (effective). He determined that on a mercury injection curve, this point corresponds to the apex of the hyperbola of a log-log plot of $P_c$ vs. $S_b$. Pittman (1992) proposed a convenient method to locate the apex by plotting $S_b/P_c$ versus $S_b$, the peak (maximum $S_b/P_c$) is the apex point (Figure 4.12).

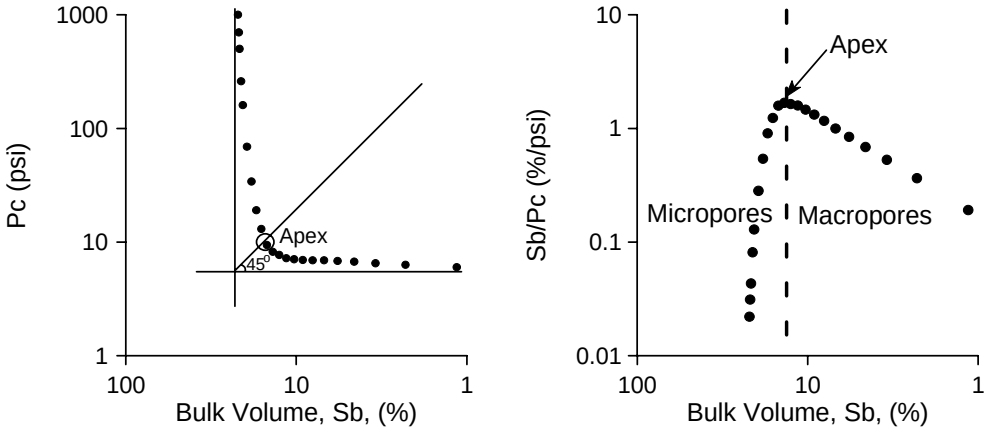


**Figure 4.12 (a) Manner of defining Swanson's parameter (Swanson, 1981); (b) Pittman's (1992) approach to determine Swanson's Apex parameter.**

## 4.3 Permeability Models Based on Effective Porosity

### 4.3.1 Kozeny-Carman model and its derivatives

The Kozeny-Carman equation has been successfully applied in glass beads, unconsolidated sands, and consolidated clean sandstones. It has been less successful in predicting permeability of shaly sandstones, as the presence of clay complicates the pore structure. It also poorly predicts k in rocks with low porosities where permeability decreases much more rapidly with decreasing porosity (Dullien, 1992, Korvin, 1992, Nelson, 1994, Mavko and Nur, 1997, Revil and Cathles, 1999).

Some investigators attribute the failure of the Kozeny-Carman equation in shaly sandstones to the enormous specific area of clay minerals (Patchett, 1975, Sen et al., 1990, and Korvin, 1992). Korvin (1992) studied 229 kaolinite-bearing sandstones, and concluded that the dramatic decrease of permeability below some critical clay-volume fraction is due to the divergence of tortuosity ($\tau \to \infty$) in the Kozeny-Carman equation. For this reason, the tortuosity (or Kozeny constant), $\tau$ ($K_z$), is interpreted by Dullien (1992, p.257) as a "fudge factor", i.e. $\tau(K_z) \equiv k_{\mathrm{mod}\,el} / k_{measured}$. Dullien (1992) stated " The frequent claim that the main reason for disagreement between permeabilities predicted by the Carman-Kozeny equation and experimental values lies in (anomalously) high sample tortuosities is unfounded."

Revil and Cathles (1999) suggested that a major deficiency of the Kozeny-Carman equation is that it does not distinguish effective from total porosity. They pointed out that sandstones commonly consist of larger, isolated pores that are connected by much smaller throats. The pore throats control the permeability but contribute little to the total porosity used in the calculation of permeability. Taking this into account, the

Kozeny-Carman equation can be modified as:

$$k = \frac{(\phi_e)^3}{k_0 \tau (1-\phi_e) S_g{}^2} \qquad (4\text{-}7)$$

or

$$k = \frac{(\phi_e)^3 d^2}{180(1-\phi_e)} \qquad (4\text{-}8)$$

The data set from Neasham (1977) (Appendix B) can be used to show the improvement in permeability prediction by the modified Kozeny-Carman equation. The specific surface area, $S_g$, can be estimated from an empirical equation derived from Sen et al's. (1990) data set (Wu and Berg, 2003):

$$S_g = 61.316 Q_v^{0.8304} \qquad (4\text{-}9)$$

where $S_g$ is specific surface area in 1/100μm, $Q_v$ is cation exchange capability in meq/ml.

Permeabilities from the original Kozeny-Carman model (equation 3-14) are shown in Figure 4.13. The discrepancy between prediction and measurement increases with decreasing permeability, and may reach three orders of magnitude. Although tuning the constant, $K_z$ ($k_0\tau$), can shift the graph downward, it will not change the scatter. Xu and White (1998) claimed that the constant $K_z$ is a function of clay content and porosity, and varies from sample to sample. Although it is true that $K_z$ varies, much data in the literature show that it changes in a very small range. Thus the influence on permeability prediction is limited. For instance, Hagiwara (1984) published a data set including porosity, permeability, formation resistivity factor, and mercury injection capillary pressure measurements. The permeability of the data set ranges from 1 to 4133 md, which means four orders of magnitude of variance, while the tortuosity varies from 2 to

7.2, with an average value of 4.2. Obviously, the variance of tortuosity is insufficient to explain the variance of permeability. Using the average value of tortuosity will not significantly affect the results.

Since permeability is sensitive to the third power of porosity (equation 4-9), substituting effective porosity for the porosity term, instead of tuning the "fudge factor", $K_z$, should reduce the discrepancy. Permeabilities from the modified Kozeny-Carman model (equation 4-10) are also shown in Figure 4.13. Although the Kozeny constant, $k_0\tau$, is kept constant at 5, the calculated permeabilities from effective porosities agree well with the measurements.

Revil and Cathles (1999) developed a modified Kozeny-Carman model based on electrical parameters that separate pore throat from total porosity. Their equation for clean sandstone is expressed as:

$$k = \frac{1013 \times 10^6 \times d^2 \times \phi^{3m}}{24} \qquad (4\text{-}10)$$

where $d$ is the grain diameter (in mm), m is the cementation exponent for clean sands ($1.5 \leq m \leq 2$, usually 1.7 or 1.8), and 1013 is unit conversion factor ($1\mu m^2 = 1013$ md). If m is assigned 3, then the exponent of porosity would be the same as that proposed by Berg (1970).

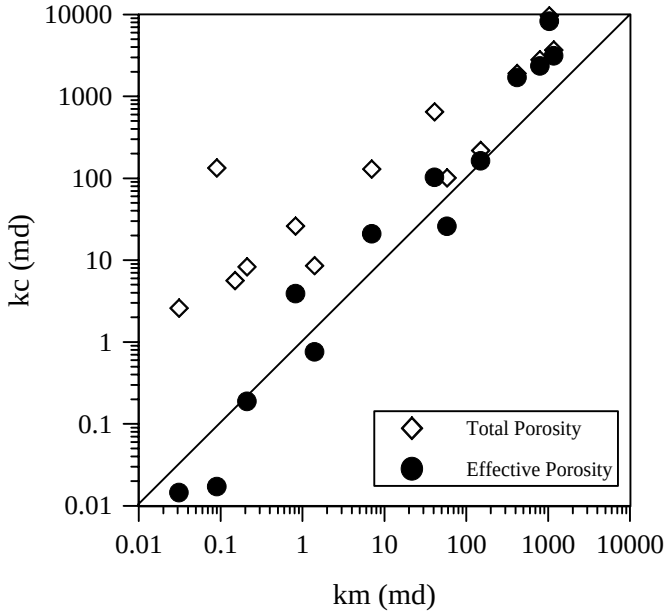


**Figure 4.13 Cross plot of calculated (kc) and measured (km) permeabilities from the Kozeny-Carman model. Diamonds denote the prediction with total porosity (equation 3-14). Dots denote the prediction with effective porosity (equation 4-10) (data from Neasham, 1977, figure modified from Wu and Berg, 2003)**

For illustration, a data set from Garn Formation, North Sea (Ehrenberg, 1990) is selected. The Garn sandstones are subarkosic arenites. Median grain size ranges from 0.1 to 1.0 mm, but is mostly on the order of 0.3 to 0.5 mm. Most samples are well to very well sorted. The porosity ranges from 8% to 33.2%, with an average value of 16.8%. The permeability ranges from 0.5 md to 8043 md, with an average value of 1227 md. In all samples, grain dissolution provides the only type of secondary porosity. “Macroporosity” from thin-sections refers to pores that are entirely free of clay and cement, and have diameters larger than approximately 20 um, and are interpreted as effective porosity (Ehrenberg, 1990).

Permeabilities calculated from the Kozeny-Carman equation (equation 3-23) has only a fair accuracy at the high permeability range (>1000 md). The discrepancy increases with decreasing permeability, and reaches over three orders of magnitude at about 1 md (Figure 4.14). Permeabilities calculated from Revil and Cathles (1999)'s model (equation 4-12) shows some improvement at permeabilities less than 1000 md, but only fair accuracy at permeabilities lower than 100 md. Substituting effective porosity for the porosity term in equation 4-12 significantly improves the accuracy at moderate to low permeability range (1 ~ 100 md) (Figure 4.14).

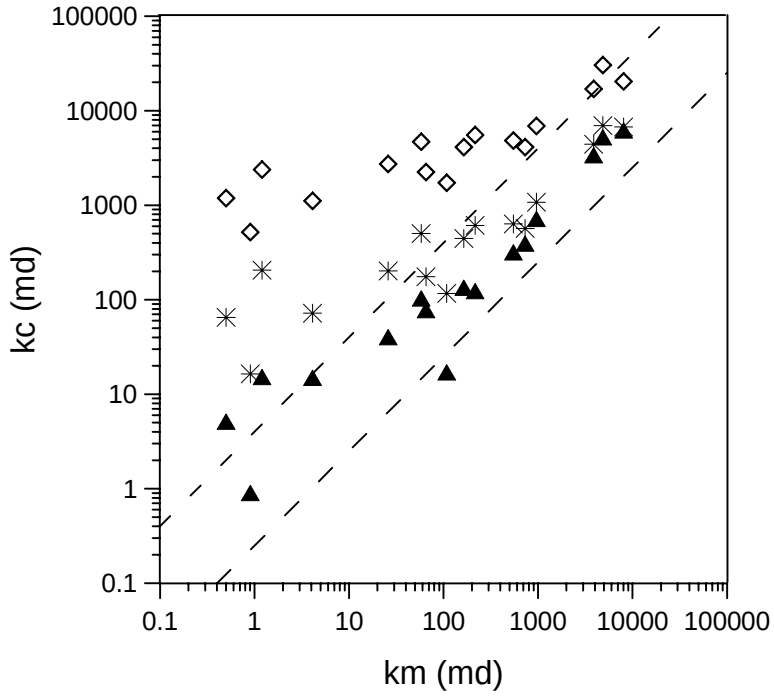


**Figure 4.14 Comparison between calculated (kc) and measured permeability (km). Diamonds denote the calculation from the Kozeny-Carman equation (equation 3-23) with total porosity; asterisks and triangles denote the calculation from Revil and Cathles (1999) equation with total porosity and effective porosity, respectively. The dashed lines represent the range of 0.25 < kc/km <4 (data from Ehrenberg, 1990).**

### 4.3.2 Regression models

Linear regression techniques have become popular for predicting permeabilities from other variables (Nelson, 1994). The techniques are based on correlations with measurements that have plausible connections to permeability without investigating the physics behind the equations (Xu and White, 1998). Many theoretical models, such as the Kozeny-Carman model, can be expressed in linear regression format. However, the limitation of regression models is that they are only valid within the range of variables from which the relationships are derived. To get a more general empirical equation, a analysis of relatively large and diverse data set is needed.

Five published data sets (Neahsam, 1977, Ehrenberg, 1990, Ehrlich et al., 1991, Walderhaug, 2000, Milliken, 2001) and one unpublished data set are selected in our investigation. The data sets include 109 sandstone and shaly sandstone samples of different texture and diagenetic styles. Porosity ranges from 3.9% to 33.2%, and permeability ranges from 0.031 md to 8043 md. This porosity-permeability range covers most reservoir sandstones. Since all the samples have petrographic or mineralogic analysis, effective porosity can be estimated with the methods discussed above. A linear relationship is found between ln(k) and effective porosity (Figure 4.15).

An improved relationship is found as:

$$\ln k = 21.42 + 11.425 \ln \phi_e + 1.327 (\ln \phi_e)^2 \qquad (4\text{-}11)$$

The coefficient of correlation ($R^2$) is 0.88. The cross plot of predicted and measured values is shown in Figure 4.16. Most samples fall into the acceptable range, $0.25<(k_c/k_m)<4$.

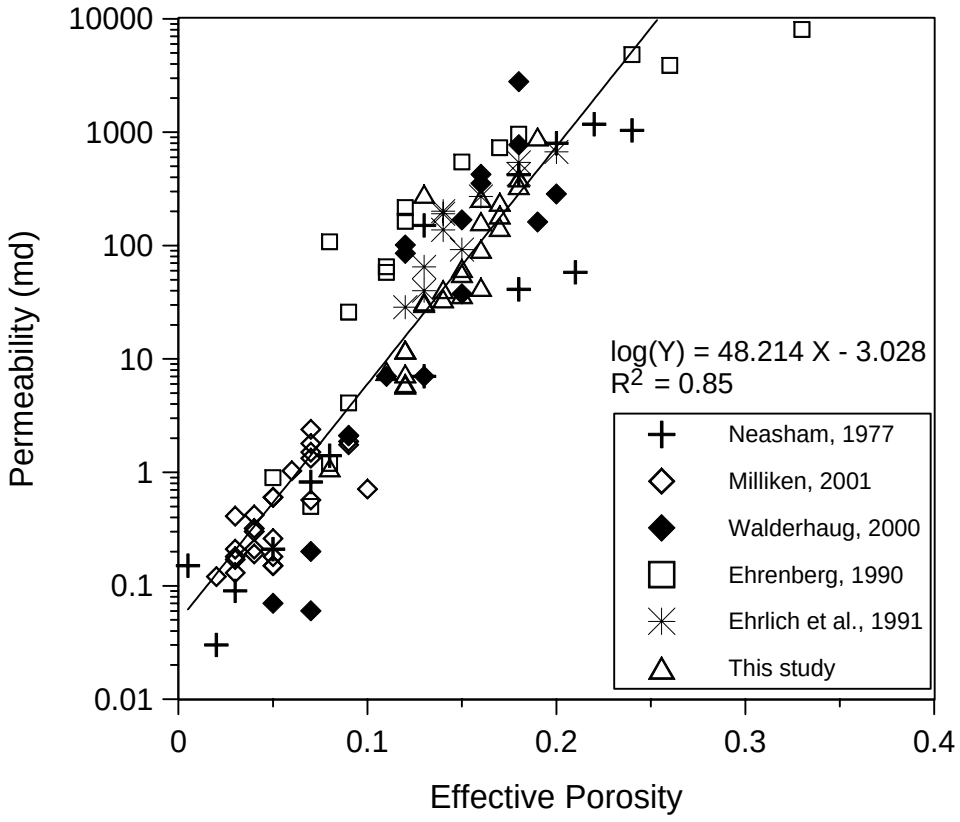


**Figure 4.15 Cross plot of measured air permeability and effective porosity. The data set "this study" is from Dakota sandstone, Coyote Creek field, Wyoming (see Appendix C) (modified from Wu and Berg, 2003).**

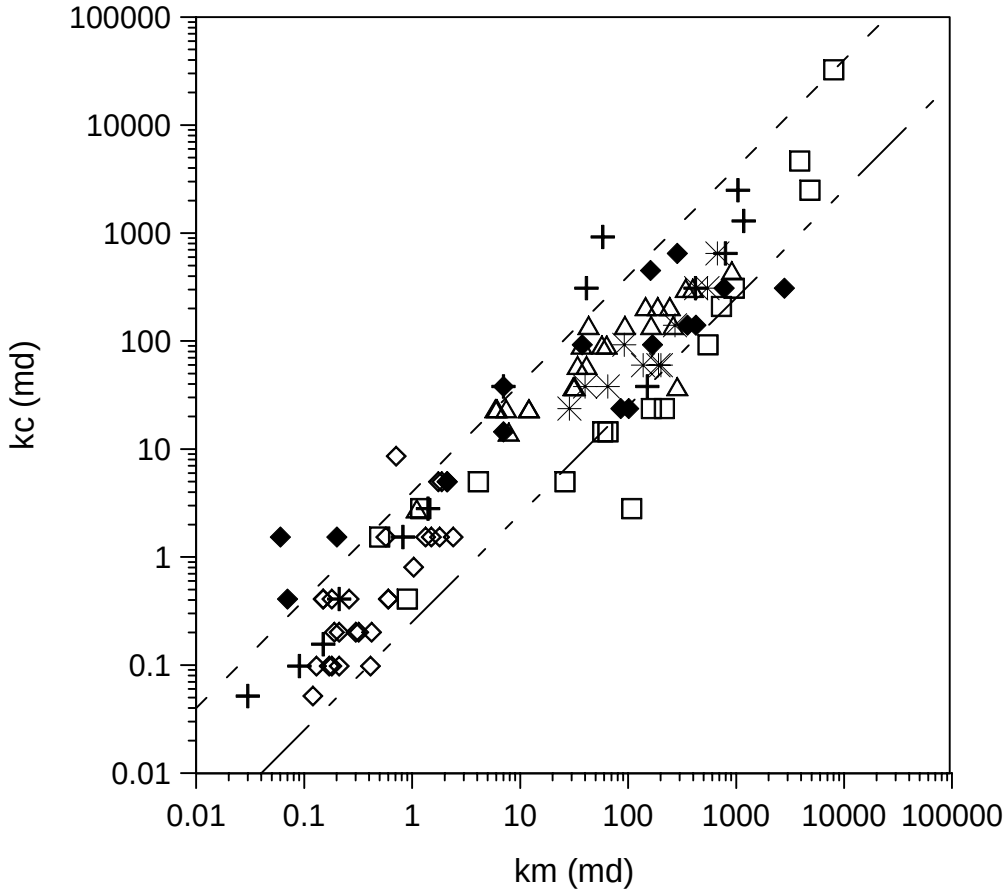


**Figure 4.16 Comparison between calculated (kc) and measured (km) permeability. The upper and lower dashed lines represent the range of 0.25 < kc/km < 4. Symbols are the same as Figure 4.15 (modified from Wu and Berg, 2003)**

### 4.4 An Example of Permeability Prediction

A data set from the San Joaquin basin, California, is used to show the estimation of effective porosity, and prediction of permeability from effective porosity. The Miocene Stevens sandstones, have two prominent facies based on composition: (1) a lithic facies that contains abundant volcanic glass, and (2) an arkosic facies rich in orthoclase feldspar. The lithic sediment was derived from the Sierra Nevada uplift to the east, and

the arkosic sediment was derived from the south and west where granites were exposed along the San Andreas fault (Figure 4.17) (Tieh, et al., 1986). These differences are illustrated by the properties of selected cores (Table 4.2).

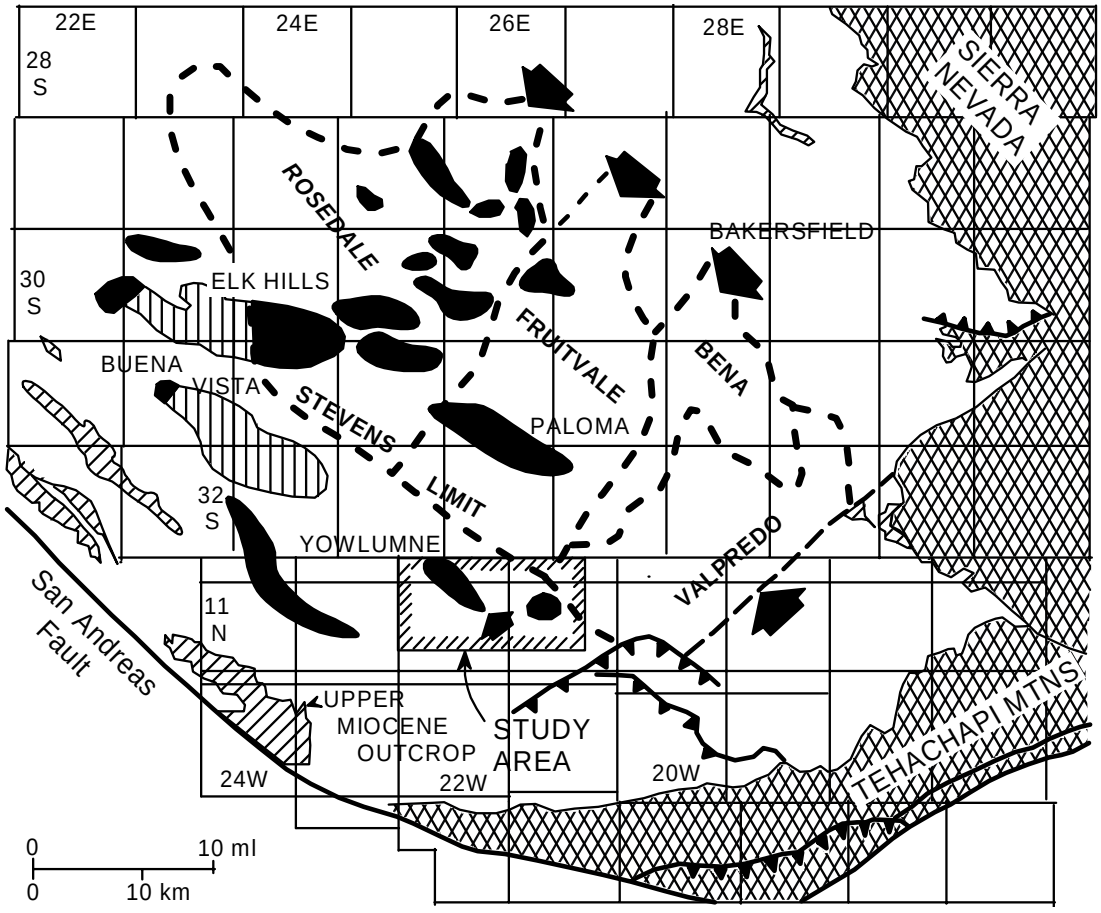


**Figure 4.17 Regional map of the southern San Joaquin basin. The main body of Steven sandstones is bounded by the dashed lines. Oil fields are black. Reservoirs beyond the limit of the Stevens are isolated channels; and reservoirs in fractured Monterey Shale are vertical lines (modified from Tieh, et al., 1986)**

**Table 4.2 Sandstone properties in Paloma, Yowlumne, Rio Viejo, and North Belridge Fields**

| Field | Wells | Sand Type | Depth (ft) | No. of Samples | Dm (mm) | Qz (%) | F (%) | R (%) | MX (%) | CMT (%) | km (md) | ϕ |
|---|---|---|---|---|---|---|---|---|---|---|---|---|
| Paloma | 72-10 | Lithic | 11850 | 21 | 0.29 | 43 | N/A | 55 | N/A | 2 | 2.4 | 0.166 |
| Yowlumne | 66-11 | Arkose | 11200 | 22 | 0.29 | 49 | 28 | 11 | N/A | 12 | 194 | 0.194 |
| Yowlumne | 67-11 | Arkose | 11302 | 19 | 0.32 | 44 | 36 | 5 | 10 | 5 | 129 | 0.197 |
| Yowlumne | 12X-11 | Arkose | 11363 | 27 | 0.3 | 43 | 37 | 6 | 8 | 6 | 82 | 0.188 |
| Yowlumne | 54X-4 | Arkose | 11540 | 33 | 0.29 | 45 | 35 | 5 | 10 | 6 | 75 | 0.18 |
| Yowlumne | 27X-34 | Arkose | 12302 | 23 | 0.38 | 57 | 32 | 3 | 4 | 4 | 58 | 0.163 |
| Yowlumne | 55X-34 | Arkose | 13021 | 33 | 0.36 | 62 | 21 | 2 | 11 | 4 | 13 | 0.148 |
| Rio Viejo | 22X-34 | Arkose | 14190 | 24 | 0.3 | 55 | 27 | 4 | 12 | 3 | 32 | 0.155 |
| North Belridge | N/A | Arkose | 8472-8773 | 43 | N/A | 44 | 26 | 6.4 | 4.9 | 7.5 | 34.6 | 0.138 |

Dm= median grain diameter, Qz= Quartz, F= Feldspar, R= Rock fragments, MX= matrix, CMT= Cement, km= measured air permeability, ϕ= porosity, N/A=not available

The diagenetic effects of the compositional differences are shown in cores from two fields: the Paloma field in the east part of the basin, and the Yowlumne field in the southwest part of the basin (Berg and Royo, 1990). The reservoir sandstones are arkosic at Yowlumne and lithic at Paloma field. The Yowlumne sandstones show abundant, partial or complete dissolution of feldspar grains. The average porosity is 17%, and average permeability is 80 md. The Paloma field shows extensive devitrification of volcanic glass to masses of smectite, vermiculite, and chlorite (Tieh, et al., 1986), and average porosity is 16.6% and average permeability is 2.4 md. Detailed petrograhic image analysis is unavailable in this area, but quantative petrographic analysis is available in the Oligocene, arkosic sandstones at North Belridge field, located about 20 miles north of Yowlumne. The sandstone in North Belridge shows the same composition as the Stevens sandstones in Rio Viejo and Yowlumne (Figure 4.18).

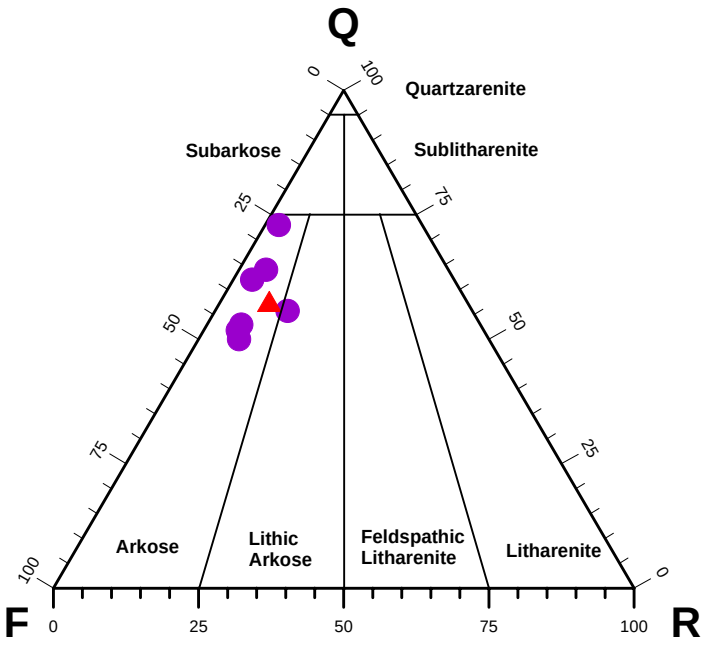


**Figure 4.18 QFR ternary diagram showing the framework grain compositions of the sandstones in North Belridge (triangle), Rio Viejo, and Yowlumne (dots) fields. The sandstones in the three fields are classified as arkoses (after Folk, 1974)**

Feldspar dissolution is also common in the Oligocene, arkosic sandstones at North Belridge field. The dissolution porosity ranges from 1 % to 5.6 %, with a mean of 3 % of bulk volume (Taylor and Soule, 1993). The 3 % dissolution porosity is interpreted to be non-effective porosity (does not contribute to permeability). Assuming the same value for the arkosic sandstones in Rio Viejo and Yowlumne fields, effective porosities are calculated by subtracting 3 % from the total porosity. The calculated permeabilities from equation 4-13 agree well with the measurements (Figure 4.19).

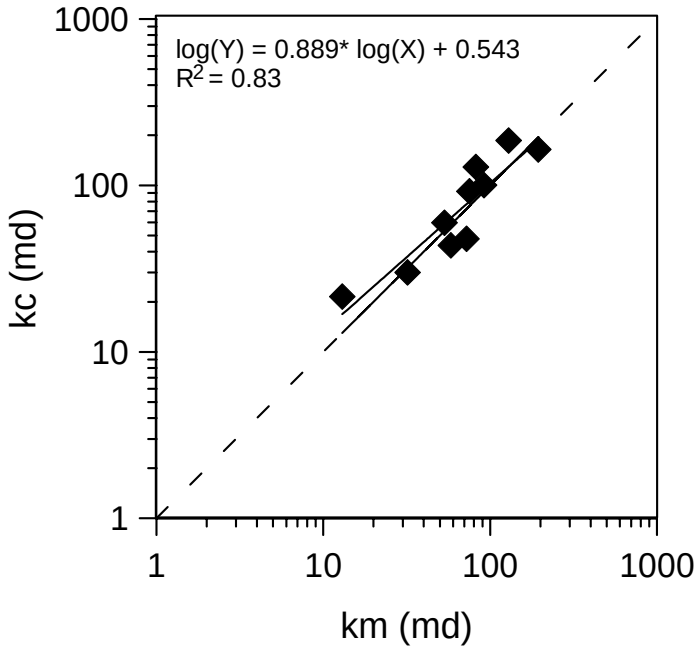


**Figure 4.19 Comparison of calculated and measured permeabilities of the arkosic sandstones, Rio Viejo field and Yowlumne fields, San Joaquin basin, California. Dashed line represents 1:1 correlation.**

A limited number of air-brine centrifugal capillary pressures were made on cores from three wells in the Yowlumne field (T67X-11, T55X-34, and T27X-34), and one well from the Paloma field (T58-3) (Appendix D). If we take $\phi S_{wir}$ as an approximation of non-effective porosity, then the non-effective of the three wells ranges from 1.73 to 5.81%, with an average value of 3.46%, which is close to the assumed dissolution porosity of 3%. Figure 4.20 shows the results of permeability calculation from capillary pressure measurements. The calculated permeabilities agree well with measurements.

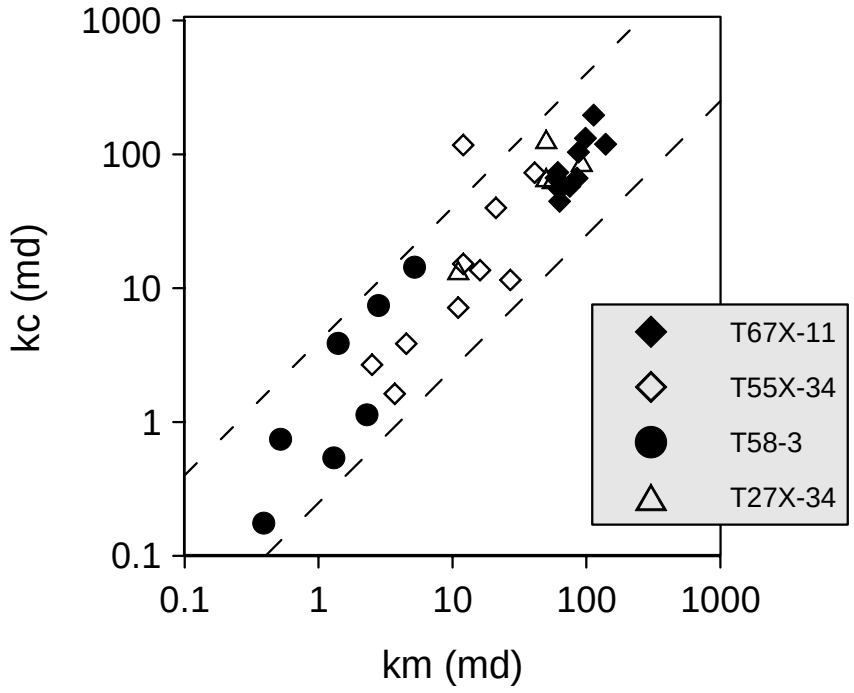


**Figure 4.20 Comparison of calculated and measured permeabilities. Permeabilities are calculated with equation 4-13, and effective porosities are approximated as $\phi(1-S_{wir})$. Dashed lines represent the acceptable range of 0.25<kc/km<4.**

### 4.5 Summary

A detailed review of effective porosity and its relationship with permeability is presented in this chapter. Dissolution porosity and clay-related microporosity are non-effective porosity, and should be excluded in attempts to correlate permeability with porosity. Empirical relationships between permeability and effective porosity can be established. Theoretical models, such as Kozeny-Carman model, can be improved by using effective porosity. Direct measurement of effective porosity is difficult. Effective porosity is generally estimated from mineralogical analysis, thin-section analysis, and capillary pressure.

# CHAPTER V

# DRAINAGE CAPILLARY PRESSURE MODELS

## 5.1 Introduction

Capillary pressure data are expensive and require core. Drainage capillary-pressure models can be used to generate drainage capillary-pressure curves from porosity and permeability. Most capillary pressure models start from the capillary tube model, in which the pore system of a rock is modeled as a bundle of different size capillary tubes. Capillary pressure for a single tube can be calculated from the Washburn (1921) equation:

$$P_c = \frac{2\sigma \cos\theta}{r} \qquad (5\text{-}1)$$

where $P_c$ is the capillary pressure in dyne/cm$^2$, $\sigma$ is the surface tension in dyne/cm, $\theta$ is the contact angle, and $r$ is the radius of a capillary tube.

If pore-throat distribution is known, it would be easy to generate a capillary pressure curve from equation 5-1. Efforts have been made to obtain pore-throat distribution from thin-sections (Thomeer, 1983, Ehrlich et al., 1991), but it is difficult to distinguish pore-throats from pores in thin-sections, especially when the pore-system is dominated by small pores. More often, capillary pressures are correlated with other pore-throat related parameters, like grain size, permeability and/or porosity, and saturation (Guthrie and Greenburger, 1955, Thomeer, 1960, 1983, Brooks and Corey, 1966, Heseldin, 1974, Berg, 1975, Kwon and Pickett, 1975, Bentsen, 1976, 1984, Winland,

1980, Johnson, 1987, Alger et al., 1989, Pittman, 1992, Hawkins, et al., 1993, Wu and Berg, 2003) (Table A-2, Appendix A). If such correlations are strong, then drainage capillary-pressures can be estimated.

Another approach is to use networks to simulate pore systems (Fatt, 1956, Chatzis and Dullien, 1977, and Dullien, 1992, McDougall et al., 2002). Pore networks are composed of large pore bodies that are interconnected by small pore-throats. The numbers of pore-throats connecting each pore is called the coordination number. Both the physical features of the network (coordination number, pore size/pore-throat size) and the choice of rules for displacement in the network affect the calculated capillary pressure curve. Although 2D or 3D networks are more realistic than one dimensional capillary tubes, wide application of these models are limited because of heavily increased calculation, cost, and extra measurements (e.g. pore-size information from photomicrography analysis), and adjustable variables. A detailed discussion of empirical drainage capillary-pressure models is presented in the following. These are capillary-tube and curve-fitting models.

## 5.2 Capillary-Tube Models

Capillary pressures are correlated with permeability and porosity. The physics behind these relationships are defined by the Washburn equation (equation 5-1) and the Kozeny-Carman equation (equation 3-6). Thomas et al. (1968) derived the following theoretical equation to calculate displacement pressure based on the bundle of capillary-tube model:

$$P_d = \frac{0.1461\sigma\cos\theta}{\sqrt{k_0}F}\sqrt{\frac{1000}{\phi k}} \qquad (5\text{-}2)$$

where $P_d$ is displacement pressure in psi; $k_0$ is a dimensionless shape factor, which falls between 2 and 3; $F$ is formation resistivity factor (Archie, 1942).

Schowalter (1979) proposed that the capillary pressure at 10% mercury saturation is an approximation of displacement pressure. An empirical relationship among the pore-throat radius corresponding to Schowalter's displacement pressure ($r_{pd}$ in μm), air permeability, and porosity, was proposed by Pittman (1992):

$$\log r_{pd} = 0.459 + 0.5\log k - 0.385\log\phi \qquad (5\text{-}3)$$

Winland (published by Kolodzie, 1980) correlated pore-throats at different saturations with porosity and permeability, and found that the best correlation occurs at 35% mercury saturation. The Winland equation is written as:

$$\log r_{35} = 0.732 + 0.588\log k - 0.864\log(100\phi) \qquad (5\text{-}4)$$

where $r_{35}$ is the pore-throat radius at 35% mercury saturation.

Pittman (1992) found that most pay zones have $r_{35}$ values greater than 0.5μm, while most non-pay zones have $r_{35}$ values less than 0.5um. He also extended the Winland equation by correlating pore-throat radius with porosity and permeability at different mercury saturations ranging from 10% to 75% by 5% increments. The best correlations occur at 20%-30% mercury saturation, and the accuracy decreases as saturation of mercury increases. Kwon and Pickett (1975), however, may have been the first to make such correlations. They analyzed 2500 rock samples from 30 formations from North America, and found that for fixed mercury saturations in the range from 10% to 70%, a general relation between capillary pressure and $k/\phi$ exists:

$$P_c = A\left(\frac{k}{100\phi}\right)^{-B} \qquad (5\text{-}5)$$

where A and B are coefficients. Equation 5-5 would be identical to equation 5-3 or 5-4 if we take the logarithm on both sides and convert $P_c$ to pore-throat radius. The values of B are approximately equal to 0.45. The values of A can be calculated with the following equation (Aguilera, 2002):

$$A = 19.5 S_w^{-1.7} \qquad (5\text{-}6)$$

where $S_w$ is the wetting-phase saturation (in fraction).

Pittman (1992) and Kwon and Pickett (1975) models are empirical. The disagreement between calculation and measurements increases with increasing mercury saturation. They offer only a fair fit in low to medium saturation ranges (usually less than 50%). The accuracy also decreases as porosity and permeability decrease.

**5.3 Models Based on Curve-Fitting**

The second group of empirical correlations uses mathematical models to fit capillary pressure curves. Usually, a parameter is included to depict the shape of a pore-throat distribution. Among the most popular are Brooks and Corey (1966) and Thomeer (1960, 1983) models, and their derivatives.

Brooks and Corey (1966) found that drainage capillary-pressure curves can be approximated by a power-law relationship:

$$S_e = \left(\frac{P_c}{P_d}\right)^{-\lambda} \quad \text{for } P_c \geq P_d \qquad (5\text{-}7)$$

where $S_e$ is normalized, wetting-phase saturation, called “effective saturation”, which is expressed as:

$$S_e = \frac{S_w - S_{wir}}{1 - S_{wir}} \qquad (5\text{-}8)$$

where $S_{wir}$ is irreducible water saturation.

The λ in equation 5-7 is called “pore-size distribution index”. It controls the slope of a capillary pressure curve. Larger λ values usually have gentle curves, while smaller λ values usually have steeper curves. The λ typically is obtained by fitting the experimental data with the least-squares technique. It is the negative slope of the points on a log-log plot of $S_e$ vs. $P_c/P_d$.

To synthesize capillary pressure curves with equation 5-7, λ must be estimated. But λ usually shows poor relationship with porosity and permeability, which makes it hard to predict and thus, restricts the application of equation 5-7.

Thomeer (1960) analyzed 279 samples, and found that capillary pressure curves can be fitted by the following hyperbolic model:

$$\frac{S_b}{S_{b\infty}} = e^{-Fg/(\log Pc/Pd)} \qquad (5\text{-}9)$$

where $S_b$ is the fractional bulk volume occupied by mercury at pressure $P_c$, $S_{b\infty}$ is the fractional bulk volume occupied at infinite pressure (assumed equal to total porosity), $F_g$ is a dimensionless factor called “pore geometrical factor”. Since $S_b/S_{b\infty}$ is equal to the non-wetting phase saturation (assume $S_{b\infty} = \phi$), $S_{nw}$, equation 5-9 can be written as:

$$\log P_c = -F_g / \ln(1 - S_w) + \log P_d \qquad (5\text{-}10)$$

A capillary-pressure curve is defined by the three parameters: $P_d$, $S_{b\infty}$, and $F_g$. The former two parameters control the location of the curve, i.e., the start and end points, $F_g$ controls the shape of the curve. Greater $F_g$ values indicate broader pore-size distributions, and lower $F_g$ values indicate narrower pore-size distributions. The relationship among these three parameters is illustrated in Figure 5.1.

Thomeer (1983) proposed an empirical equation to correlate permeability with these three parameters:

$$k = 3.8068 F_g^{-1.3334} (100\phi / P_d)^{2.0} \qquad (5\text{-}11)$$

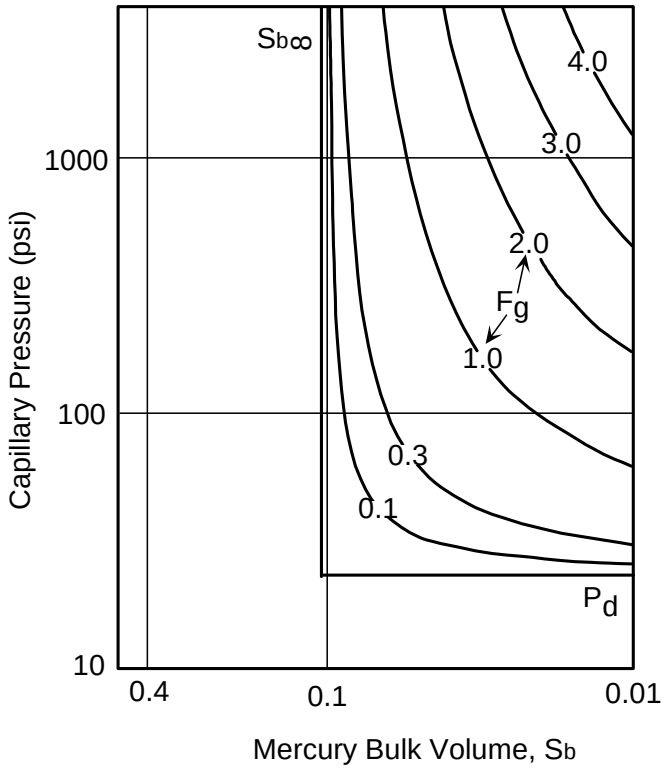


**Figure 5.1 A family of capillary pressure curves showing Thomeer's three parameters: $P_d$, $S_{b\infty}$, and $F_g$. Note the greater the $F_g$ value, the steeper the curve (modified from Thomeer, 1960).**

*Fg* can be estimated by overlying capillary pressure curves on a nomograph proposed by Thomeer (1960). It can be more conveniently estimated by rewriting equation 5-11 as:

$$F_g = e^{[1.3368+2\ln(100\phi/P_d)-\ln k]/1.3334} \qquad (5\text{-}12)$$

The assumption in equation 5-10 that $S_{b\infty}=\phi$ is not always valid, especially for shaly sandstones. Wu and Berg (2003) improved Thomeer's model by incorporating irreducible water saturation, i.e. $S_{b\infty}=\phi(1-S_{wir})$:

$$\log P_c = -F_g / \ln(\frac{1-S_w}{1-S_{wir}}) + \log P_d \qquad (5\text{-}13)$$

The shaly sandstone samples from Purcell (1949) are illustrated here to show the improvement of Thomeer's (1960) model. The three samples come from Frio Formation in the Gulf of Mexico area, showing irreducible water saturation of 30% to 50%. $P_d$ is read from capillary-pressure curves, *Fg* is estimated from equation 5-12. The original Thomeer's model displays poor agreement between calculation and experiment (Figure 5.2 a). The discrepancy increases with mercury saturation. A better match is obtained while the modified Thomeer's model (equation 5-13) is applied (Figure 5.2b).

Thomeer (1960, 1983) model has been widely used (Hawkins et al., 1993, Ma, 1994, Haynes, 1995, Wu and Berg, 2003). The Thomeer model usually gives better fit to experimental data than other empirical models. The drawback of Thomeer's model is that not all capillary pressure curves are hyperbolic and suitable to assignment of $F_g$ values (Pittman, 1992). In addition, equation 5-10 is an empirical equation based on 279 samples. Most of the samples are from oil field reservoirs so this equation might not be valid for low-permeability (< 10 md) samples.

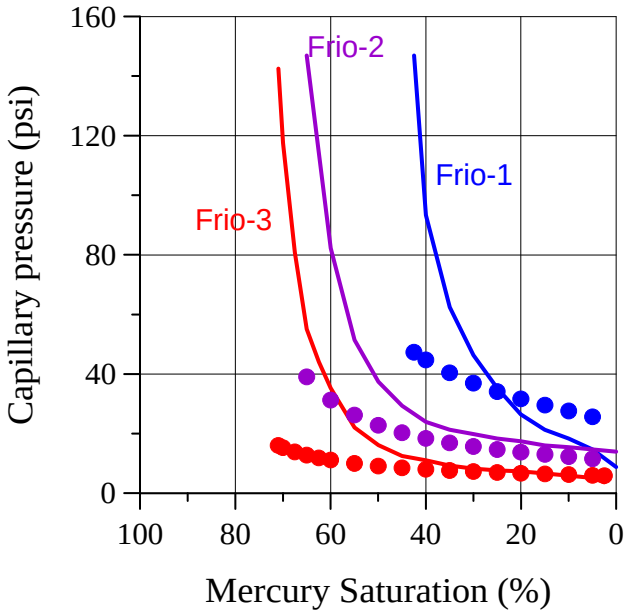


(a)

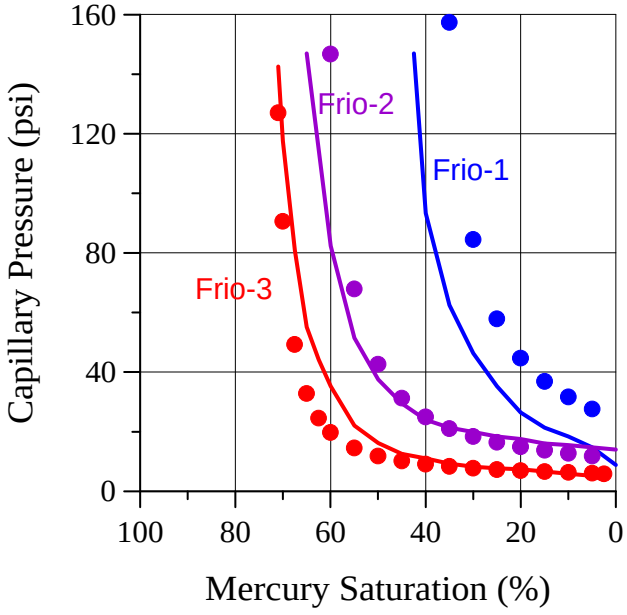


(b)

**Figure 5.2 Comparison between calculated (dots) and measured capillary pressures (solid curves). (a) Thomeer's model (1960); (b) Modified Thomeer's model (equation 5-13) (data from Purcell, 1949).**

## 5.4 Pore-Throat Size Distribution

Pore-throat size distribution is an important property of porous media. It affects both permeability and capillary pressure. Several variables have been proposed to quantify this property (Archie, 1950, Jennings, 1987, Thomeer, 1960, Brooks and Corey, 1966). Among these valiables, Brooks and Corey's λ (1966) and Thomeer's Fg (1960, 1983) are the most popular.

### 5.4.1 Brooks and Corey's λ (1966)

The λ is measured directly from the best-fit line drawn through the data points on a log-log plot of $S_e$ vs. $P_c/P_d$. The negative slope of the fitted line is λ. According to Brooks and Corey (1966), porous media having narrow pore-throat size distributions (well-sorted) tend to have large values of λ, while porous media having wide pore-throat size distributions (poorly-sorted) tend to have small values of λ. If this assumption is correct, then λ should be correlated with other variables, such as permeability and irreducible water saturation, since these variables are sensitive to pore-throat distribution. A plot of Brooks and Corey's original data shows no relationship between λ and these two variables (Figure 5.3).

Seven samples from the dolomites in Frobisher-Alida Interval in Southwest North Darkota are analyzed here (Table 5.1). Porosity and permeability are obtained from routine laboratory measurements. MICP data are available for the samples. Figure 5.4a shows the selected three samples with distinctive pore-throat distribution. Figure 5.4b shows Brooks and Corey's method (1966) to determine λ. In spite of distinctive pore-

throat distributions, the three samples have similar λ values. It appears that λ is insufficient to distinguish the varying pore-throat distributions.

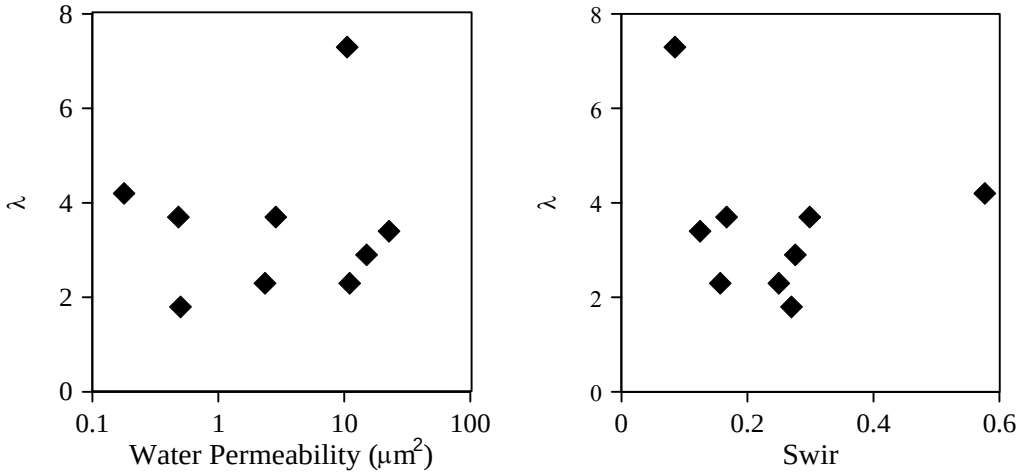


**Figure 5.3 Correlations of λ with permeability and $S_{wir}$ (data from Brooks and Corey, 1966)**

**Table 5.1 Measured rock properties and parameters obtained from mercury injection capillary pressure curves**

| *k* (md) | *ϕ* | $P_d$ (psi) | $S_{wir}$ | λ | λ1 | λ2 | Fg |
|---|---|---|---|---|---|---|---|
| 14.5 | 0.164 | 40 | 0.02 | 1.59 | 3.12 | 1.28 | 0.06 |
| 2.2 | 0.154 | 69 | 0.05 | 1.34 | 1.86 | 1.07 | 0.09 |
| 0.7 | 0.149 | 79 | 0.15 | 1.08 | 0.91 | 1.24 | 0.17 |
| 0.2 | 0.151 | 145 | 0.3 | 0.95 | 0.95 | .095 | 0.24 |
| 222 | 0.32 | 18 | 0.01 | 1.29 | 2.81 | 1.14 | 0.09 |
| 11 | 0.21 | 44 | 0.02 | 1.31 | 2.44 | 1.10 | 0.09 |
| 1 | 0.144 | 76 | 0.1 | 1.27 | 1.29 | 1.06 | 0.12 |

Data from Petty (1988). k and ϕ are measured from core plugs. Other variables are read or calculated from MICP curves.

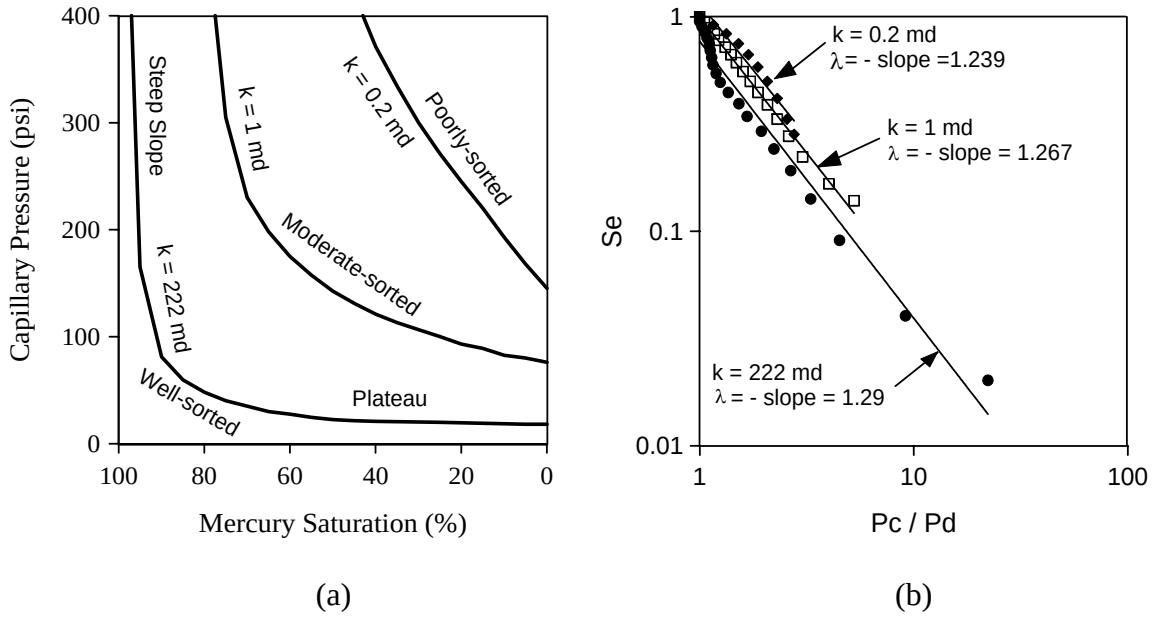


**Figure 5.4 (a) MICP curves showing distinctive pore-throat distribution; (b) Brooks and Corey's method of determining λ (data from Petty, 1988).**

Archie (1950) pointed out that reservoir rock with high permeability exhibits a plateau and a steep slope, and these two distinctive sections tend to merge as the range of pore-size distribution increases. Swanson (1981, 1985) used the apex between the plateau and steep slope as the cutoff between macropores (plateau) and micropores (steep slope). Here, I propose to fit the plateau and steep slope separately (Figure 5.5). The negative slope of these two sections are labeled as λ1 and λ2, respectively. λ1 is a measure of macropore sorting, whereas λ2 is a measure of micropore sorting. They show strong and weak correlations with porosity and permeability, respectively (Figure 5.6, Figure 5.7).

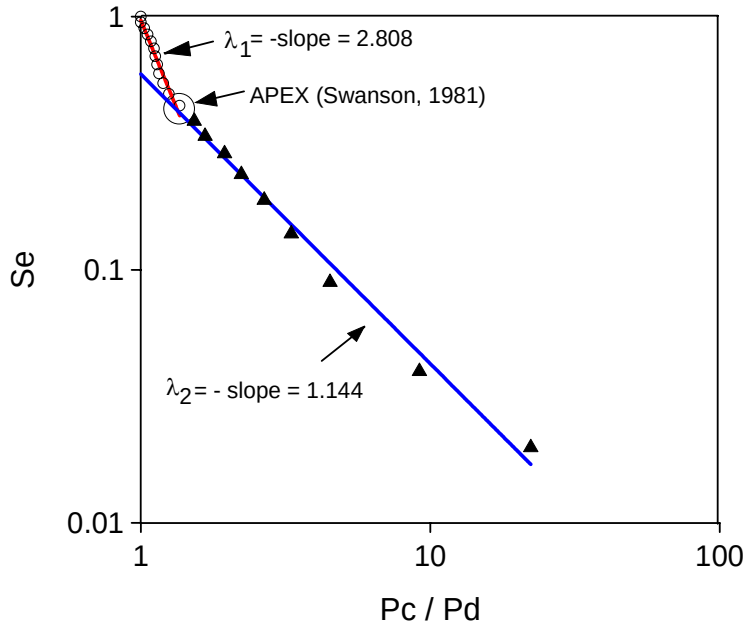


**Figure 5.5 Cross plot Se and Pc/Pd. Two fit lines are obtained. The negative slopes are designated as λ1 and λ2, respectively.**

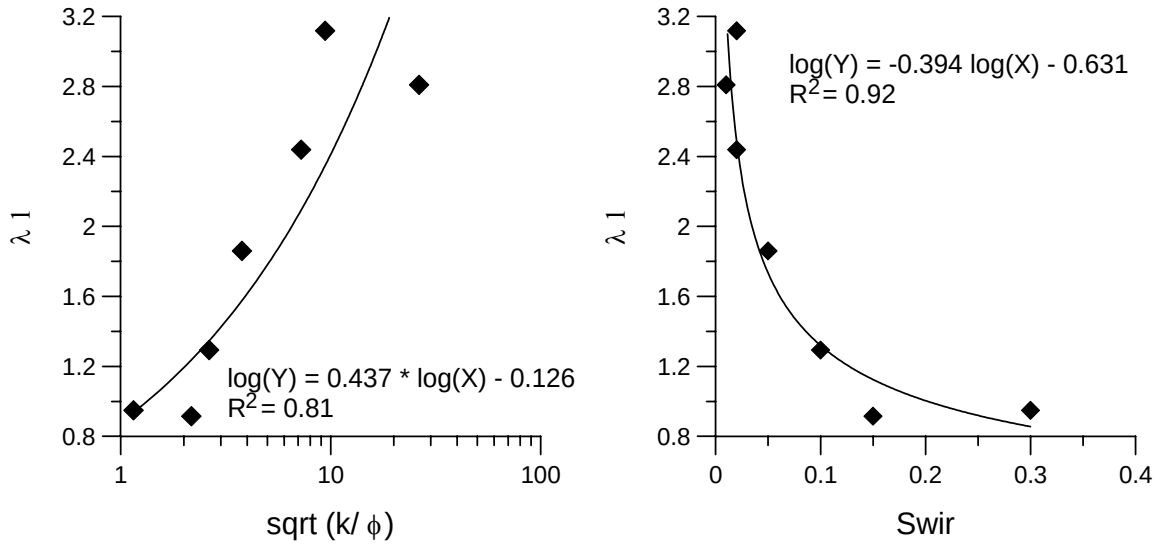


**Figure 5.6 Correlation between λ1with $\sqrt{k/\phi}$ and $S_{wir}$ (data from Petty, 1988).**

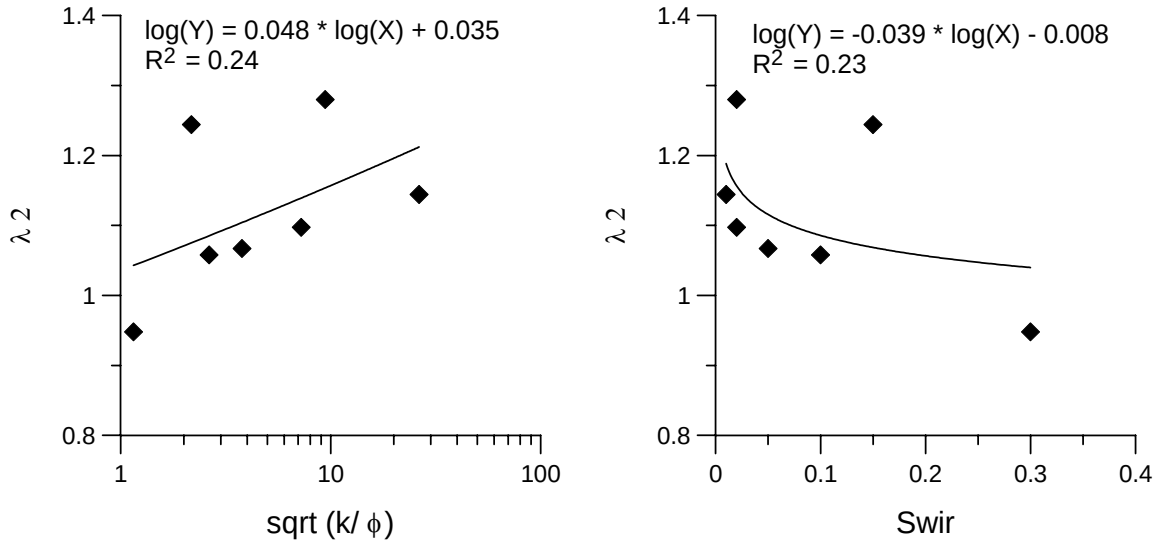


**Figure 5.7 Correlation between λ2 with $\sqrt{k/\phi}$ and $S_{wir}$ (data from Petty, 1988).**

### 5.4.2 Thomeer's Fg (1960, 1983)

Thomeer's (1960, 1983) pore geometrical factor (*Fg*) is another widely used parameter to delineate pore-throat distribution. According to Thomeer (1960), well-sorted pore-throats tend to have smaller *Fg* values, while poorly-sorted pore-throats tend to have larger *Fg* values. Here, a simple method is proposed to calculate *Fg*. Rearranging equation 5-13, we have:

$$\log(P_c/P_d) = -F_g/\ln(1-S_e) \qquad (5\text{-}14)$$

The *Fg* is the negative slope of $\log(P_c/P_d)$ vs. $-1/\ln(1-S_e)$ plot. Usually, Se < 0.1 should not be used in the plot (Figure 5.8). The *Fg* displays a good correlation with $\sqrt{k/\phi}$ and $S_{wir}$ (Figure 5.9).

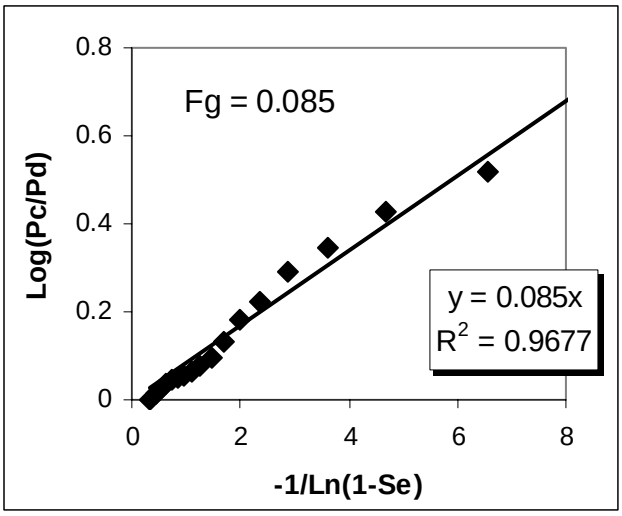


**Figure 5.8 A cross plot of Log (Pc/Pd) vs. –1/ln(1-Se) showing a linear relationship. The slope is the pore geometric factor, Fg.**

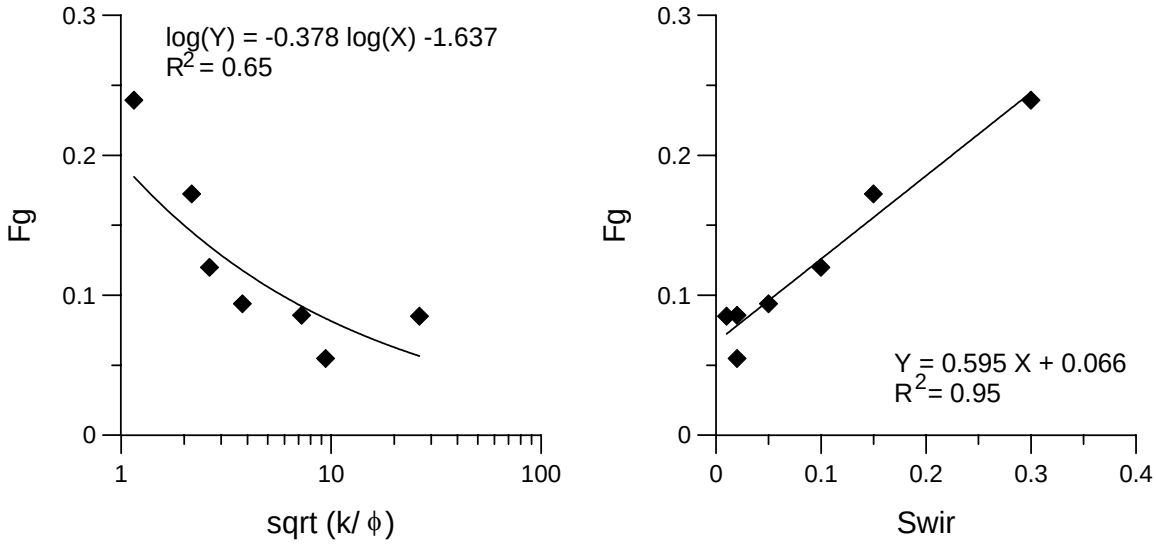


**Figure 5.9 Correlation between Fg with $\sqrt{k/\phi}$ and $S_{wir}$ (data from Petty, 1988).**

### 5.4.3 Correlation between permeability and pore-throat distribution

Thomeer (1983) proposed a permeability equation based on the correlation between permeability and the three parameters: pore geometrical factor, total porosity, and displacement pressure (equation 5-11).

Substituting $\phi(1\text{-}S_{wir})$ to $S_{b\infty}$ in equation 5-11 yields:

$$k = 3.8068 F g^{-1.3334} \left[100\phi(1 - S_{wir}) / P_d\right]^2 \qquad (5\text{-}15)$$

Nakornthap and Evans (1986) derived an expression for permeability based on the previous investigation of Purcell (1949) and Brooks and Corey (1966). The authors utilized pore geometry terms and incorporated the saturation terms developed by Brooks and Corey to account for tortuosity:

$$k = 10.66\left[\phi(1 - S_{wir})\right]^3 (\sigma \cos\theta)^2 \frac{\omega}{n} \int_0^1 \frac{d_{Se}}{P_c} \qquad (5\text{-}16)$$

where ω and n are empirical pore geometry terms that account for pore-throat distribution and the numbers of pore-throat per pore body, respectively.

The results of a previous investigation by Blasingame and Ali (1995) indicated that the ω and n can be substituted for in the following manner:

$$\frac{\omega}{n} = a\frac{(1 - S_{wir})}{\phi} \qquad (5\text{-}17)$$

where a is an empirical adjustment constant that is typically set equal to 1.

Incorporating equation 5-17 and 5-7 into equation 5-16, Blasingame and Ali developed the following expression for permeability:

$$k = 10.66(1 - S_{wir})^4 (\sigma \cos\theta)^2 \left(\frac{\phi}{P_d}\right)^2 \left(\frac{\lambda}{\lambda + 2}\right) \qquad (5\text{-}18)$$

Figure 5.10 shows the comparison between calculated and measured permeability of the seven dolomite samples from Petty (1988). Both Thomeer's (1983) equation (equation 5-15) and Blasingame and Ali's (1995) equation (equation 5-18) give a good agreement between calculation and measurements.

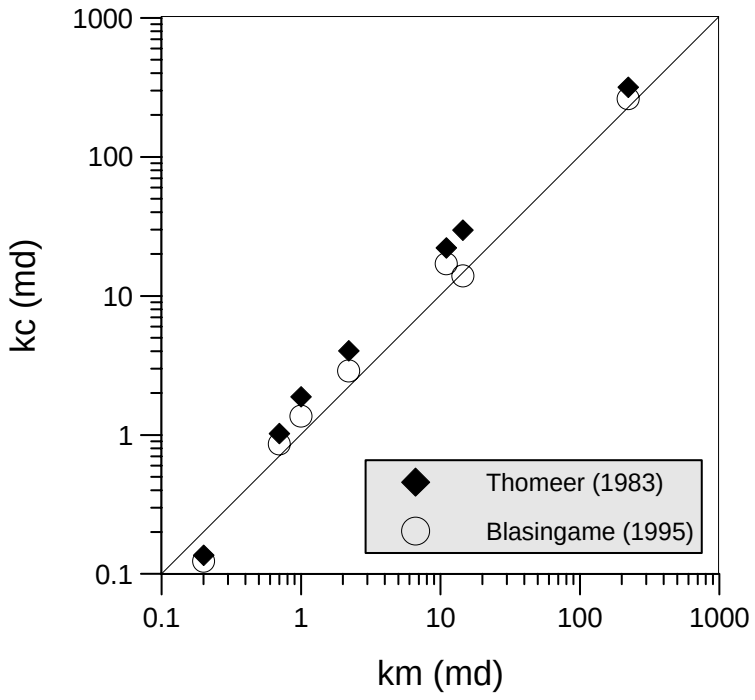


**Figure 5.10 Comparison between calculated (kc) and measured permeability. Permeabilities are calculated with equation 5-15 and 5-18, respectively. The diagonal line denotes the 1:1 correlation (data from Petty, 1988).**

Equation 5-15 and 5-18 incorporate three most important aspects of a porous network: the largest pore-throat (represented by $P_d$), the total connected pore volume, and pore-throat distribution. Equation 5-15 is purely empirical correlation, while equation 5-

18 has some physic basis. The merit of equation 5-18 is that the interfacial tension and contact angle are included, which makes it applicable to different fluid systems. The λ, as discussed above, is not a well-defined parameter. A more accurate approach should be to fit the plateau and steep slope separately. But the influence of λ on permeability is much less than the other two parameters. In addition, it usually varies in a small range, and the role of λ is somewhat muted by the grouped term of $\lambda/(\lambda+2)$.

To extend Thomeer's equation to air-brine systems, a data set of 25 air-brine centrifugal capillary-pressure measurements (Appendix D) from the Yowlumne field was used, and the following equation is proposed:

$$k = 404.6Fg^{-1.33}\left[\phi(1-S_{wir})/P_d\right]^{1.614} \qquad (5\text{-}19)$$

Figure 5.11 shows the results of the calculated permeabilities from equation 5-19. A good fit is obtained. The exponent of Fg in equation 5-19 is almost the same as that in equation 5-15. The exponent, 1.614, is close to the average cementation factor (Archie, 1942) of the 25 samples, which is equal to 1.65. Thus, I postulate that a general equation might holds for different lithology and fluid systems:

$$k = CFg^{-1.33}\left[\phi(1-S_{wir})/P_d\right]^{m} \qquad (5\text{-}20)$$

where C is a coefficient that need to be adjusted with experimental data. "m" is the Archie's (1942) cementation factor.

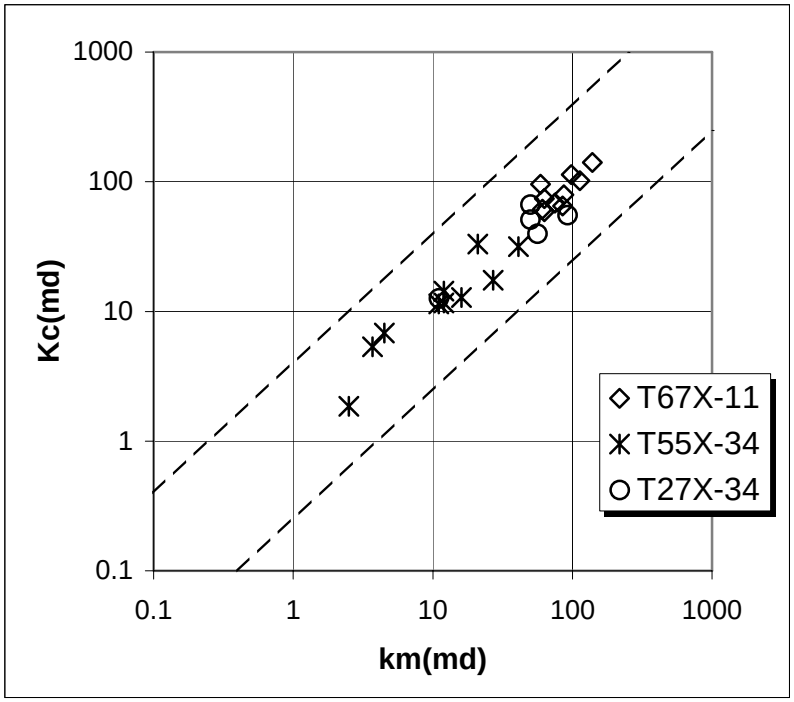


**Figure 5.11 Comparison between calculated (kc) and measured permeability (km). The dashed lines represent the range of 0.25 < kc/km < 4. Samples are from Yowlumne field (Appendix E).**

## 5.5 Summary

Widely used drainage capillary-pressure models are reviewed. Two groups of models can be defined: models based on capillary-pressure tubes and models based on curve-fitting. All these models are empirical, and based on some simplified assumptions. Although capillary-pressure tube based models usually work well for some type of reservoir rocks and fluid saturations (such as 35% and 50% non-wetting phase saturation), they provide no information of pore-throat distribution, and are insufficient to generate a continuous capillary pressure curve. The models based on curve-fitting involve a parameter of pore-

throat distribution, which affects the curvature of capillary pressure curves. They can provide a continuous curve from 100% water saturation ($S_e$=1) to irreducible water saturation ($S_e$ =0). The limitation of these types of models is that it can be difficult to estimate the parameter of pore-throat distribution from other properties, such as permeability and porosity.

Of the published models, Thomeer's (1960) may be the most widely used. A modified Thomeer's (1960) model (equation 5-13) is proposed.

Two widely used parameters of pore-throat distribution are discussed, i.e., Brooks and Corey's (1964) λ, and Thomeer's (1960, 1983) *Fg*. It is insufficient to use a single parameter to depict the pore-throat distribution of the entire curve. The pore-throat distribution of macropores ($\lambda_1$) shows good correlation with permeability and $S_{wir}$, while the pore-throat distribution of micropores ($\lambda_2$) shows poor correlation with permeability and $S_{wir}$. A new approach is proposed to determine *Fg*, and a general permeability equation (equation 5-20) is also proposed.

# CHAPTER VI

# A REVISED CAPILLARY PRESSURE MODEL

## 6.1 A Revised Capillary Pressure Model

Bentsen and Anli (1976) proposed a mathematical model to fit capillary pressures. Their model is based on the following mathematical criteria: (1) the slope of the capillary pressure curve tends to minus infinity as the effective water saturation, Se, decreases to zero (water saturation approaches irreducible saturation; (2) the capillary pressure curve tends to a fixed value as the water saturation approaches to 1; and (3) the area under the capillary pressure curve must be finite. These criteria can be met with the following equation:

$$\frac{dP_c}{dS_e} = -\frac{C}{S_e} \qquad (6\text{-}1)$$

which, on integration, yields

$$P_c = P_d - C \ln S_e \qquad (6\text{-}2)$$

The parameter “C” in equations 6-1 and 6-2 is a constant that incorporates the effects of interfacial tension, wettability and pore size distribution. “C” is the area under the capillary pressure curve and, as such, it is related to the amount of reversible work needed to create the fluid-solid surfaces located in the porous medium (Bentsen. 2003. personal communication). Although equation 6-2 is empirical, it is based on some physical principles in that it satisfies various mathematical constraints.

Harris and Goldsmith (2001) proposed that:

$$C = \sigma \cos\theta \sqrt{\phi / k} \qquad (6\text{-}3)$$

For a particular rock, the parameters σ and θ usually are assumed constants. Thus, a capillary pressure curve can be generated if $\phi$, $k$, $P_d$, and $S_{wir}$ are known.

Applications of equation 6-2 show that it works well as $S_e$ approaches 0 and 1, but less well in the interval between these points. From a statistical point of view, $P_c$ and $\ln(S_e)$ typically have nonlinear relationships. Equation 6-2 can be improved by introducing an exponent to the independent variable, $\ln(S_e)$:

$$P_c = P_d + \sigma \cos\theta \sqrt{\phi / k} (\ln 1 / S_e)^{\beta} \qquad (6\text{-}4)$$

The parameter "β" is called a "shape factor". It controls the curvature of a $P_c$ vs. $S_w$ curve, and usually varies between 1-3.

## 6.2 Testing the Revised Model

### 6.2.1 Interfacial tension and contact angle

Laboratory measurements of interfacial tension (σ) and contact angle ($\theta$) are difficult and expensive, so approximations are commonly used (Table 6.1). For the purpose of modeling drainage process, it is reasonable to assume $\theta = 0°$, since most rocks are water wet in their original depositional environment (Berg, 1975). Interfacial tension can be better estimated if the density of reservoir oil and water are known because surface tension is a function of density difference (Firoozabadi and Ramey, 1988).

**Table 6.1 Commonly used contact angle and interfacial tension values**

| *System* | *Contact Angle ($\theta$) (°)* | *Interfacial Tension ($\sigma$) (dynes/cm)* |
|---|---|---|
| Methane/Brine | 0 | 72 |
| Air/Mercury | 140 | 485 |
| Crude Oil/Brine (< 30 ° API) | 0 | 30 |
| Crude Oil/Brine (30 ° - *40 ° API)* | 0 | 21 |
| Crude Oil/Brine (>40 ° *API)* | 0 | 15 |

(From Vavra et al., 1992)

### 6.2.2 Displacement pressure

Estimating displacement pressure, $P_d$, is critical in capillary pressure modeling. Wu and Berg (2003) proposed the following empirical relationship between $P_d$ (air-mercury) and porosity and permeability:

$$\ln P_d = 5.458 - 1.255 \ln \sqrt{k/\phi} + 0.081 (\ln \sqrt{k/\phi})^2 \qquad (6\text{-}5)$$

Equation 6-5 is based on 96 samples from seven published data sets (Figure 6.1). They cover a wide range of lithology, porosity, and permeability. Porosity ranges from 7.3% to 40.7%, permeability ranges from 0.02 md to 2580 md, and displacement pressure ranges from 2 psi to 900 psi. The coefficient of correlation ($R^2$) is 0.92. Most of the predicted $P_d$ values fall into the range of 1:2 < $P_d$ (calculated)/$P_d$ (measured) < 2:1. This range is considered acceptable because permeability is a function of capillary pressure square (Purcell, 1949).

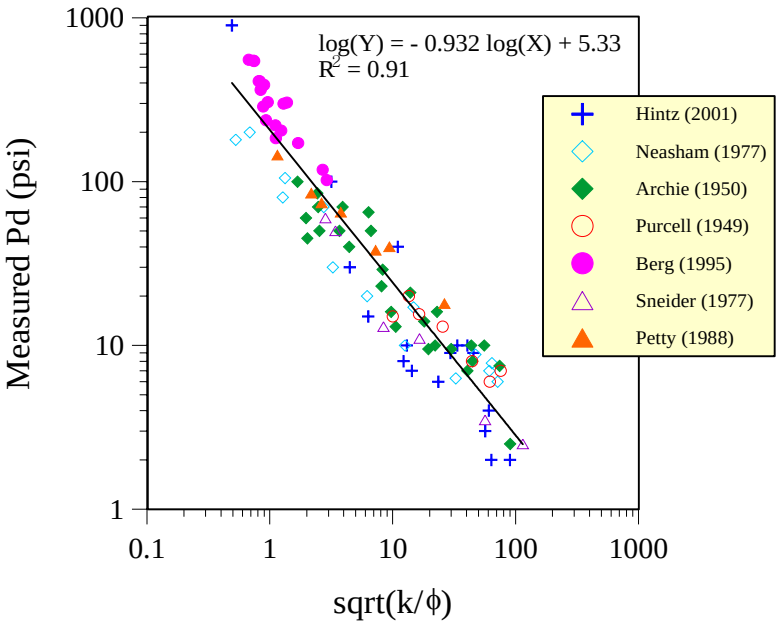


(a)

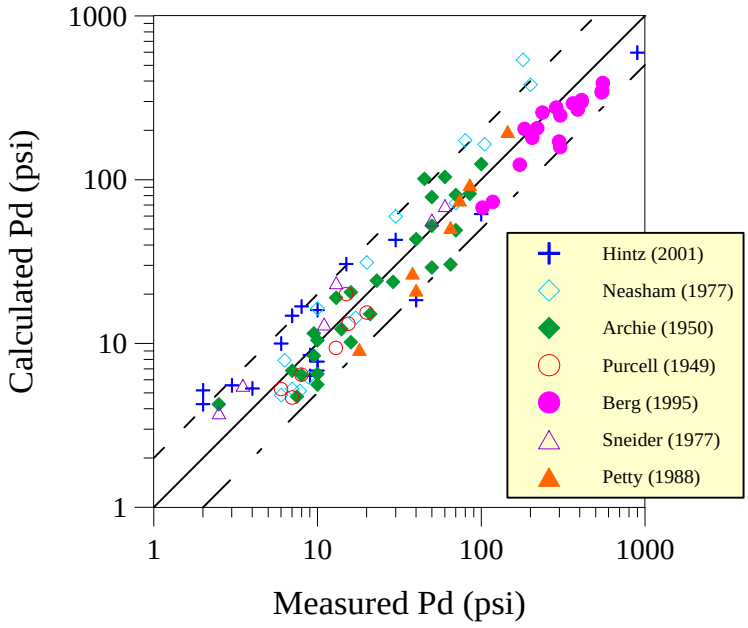


(b)

**Figure 6.1 (a) Correlation between Pd (air-mercury) and $\sqrt{k/\phi}$; (b) Comparison between calculated and measured Pd. Dashed lines denote 2:1 and 1:2 correlation lines.**

### 6.2.3 Shape factor, β

The shape factor, β, is an empirical variable. It is tested with over 200 samples, and found varying in a narrow range of 1 to 3. It depends on lithology, pore geometry and connection. Table 6.2 provides a rule of thumb to estimate β. A default value of 2 works well for a wide range of lithology and permeability.

**Table 6. 2 Empirical values of β as a function of lithology, pore type, and permeability**

| Lithology | Pore Type | Permeability | β |
|---|---|---|---|
| Clean Sandstone<br>Carbonate | Intergranular or<br>Intercrystalline Pores | 100s ~ 1000s md | 3 |
| Sandstone<br>Shaly sandstone | Micropores,<br>Dissolution Pores | 1 ~ 100s md | 2 |
| Shale<br>Tight sandstone | Micropores | < 1 md | 1 |

### 6.2.4 Results

The revised model is tested with published data sets and our own data sets (over 200 samples). These samples cover a wide range of lithology including sandstone, shaly sandstone, shale, and carbonates with dominant intergranular or intercrystalline pores. Calculated results are visually compared with experiments because it is hard to conduct quantitative comparison for an entire curve. Three published data sets and one unpublished data set are selected here to show the results of the model.

The three published data sets come from Archie (1950), Purcell (1949), and Berg & Avery (1995). The data sets cover a wide range of lithology (Table 6.3). Capillary pressures were measured using mercury-injection method.

**Table 6.3 Parameters used in synthesizing capillary pressure curves**

| Data source | Sample number | Formation | Lithology | $\phi$ | $k$ (md) | $P_d$ (psi) | $S_{wir}$ | $\beta$ |
|---|---|---|---|---|---|---|---|---|
| Archie (1950) | 33797B | Pennsylvanian | Friable Sandstone | 0.282 | 870 | 10 | 0.08 | 3 |
| | 18972 | Upper Wilcox | Friable Sandstone | 0.22 | 116 | 18 | 0.2 | 3 |
| | 10811 | Nacatoch | Shaly Sandstone | 0.358 | 117 | 16 | 0.2 | 2 |
| | 23964 | Lower Wilcox | Hard Sandstone | 0.122 | 8 | 27 | 0.1 | 2 |
| | 11094 | San Andres | Limestone | 0.193 | 37.2 | 25 | 0.1 | 2 |
| | 28418 | Devonian | Limestone | 0.371 | 16.4 | 60 | 0.25 | 2 |
| Purcell (1949) | 1 | Frio | Shaly Sandstone | 0.23 | 23 | 18 | 0.5 | 2 |
| | 2 | Frio | Shaly Sandstone | 0.26 | 170 | 15 | 0.32 | 2 |
| | 3 | Frio | Shaly sandstone | 0.25 | 950 | 5 | 0.28 | 2 |
| Berg & Avery (1995)* | 13849 | Wilcox | Shale | 0.162 | 0.09 | 450 | 0.4 | 1 |
| | 13863 | Wilcox | Shale | 0.167 | 0.11 | 400 | 0.3 | 1 |
| | 14102 | Wilcox | Shale | 0.12 | 0.15 | 200 | 0.4 | 1 |
| | 14111 | Wilcox | Shale | 0.1 | 0.19 | 225 | 0.5 | 1 |

Note: $P_d$ and $S_{wir}$ are read from original figures. β values are assigned based on lithology and permeability.
* original data come from Berg, 2003, personal communication. The $P_d$ values are a little different from those published.

The three Frio shaly sandstones from Purcell (1949) are the same samples shown in Figure 5.3. A better fit between calculation and experiments is obtained with the revised model (Figure 6.2).

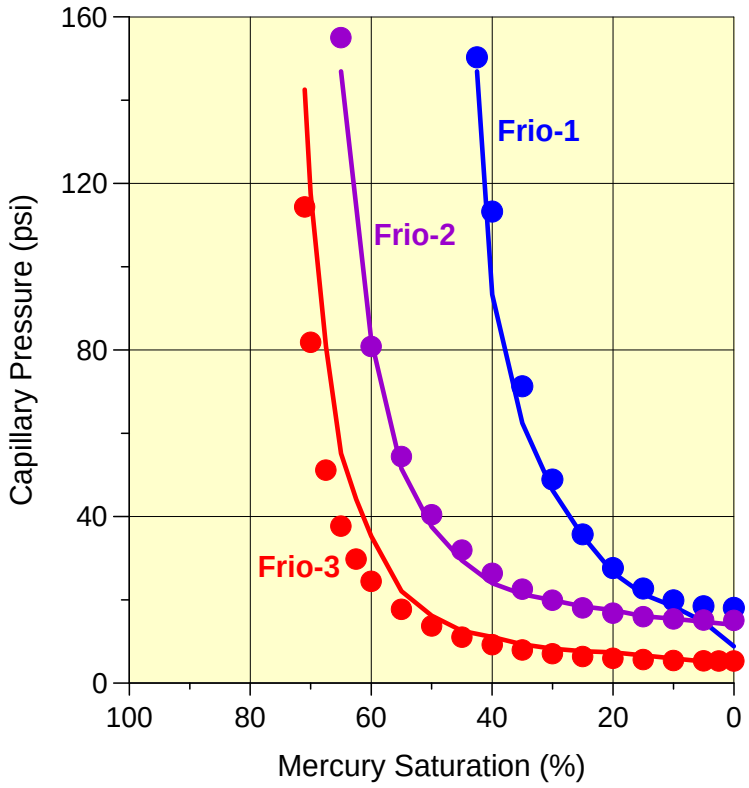


**Figure 6.2 Comparison between calculated and measured capillary pressures of shaly sandstones. Solid curves denote experiments, and dots denote calculation (data from Purcell, 1949)**

Archie's data set comes from six formations in North America: (1) Pennsylvanian sand with high permeability and well-sorted grains; (2) Upper Wilcox sandstone with moderate porosity and permeability; (3) Nacatoch shaly sandstones characterized by

comparatively high porosity for permeability; (4) Lower Wilcox sandstone with comparatively low porosity for permeability; (5) San Andres limestone with considerable secondary pores due to dissolution; (6) Devonian cherty limestone, highly granular to earthy texture, comparatively high porosity for its lower permeabilities. Results of the calculation are shown in Figure 6.3.

Berg and Avery's (1995) data set comes from the sheared fault zone in the Shell Stegall 1A core, Rosita field, Texas. Four samples are selected to illustrate the calculation. These samples show very low permeability (< 1 md), and high displacement pressure (> 200 psi). The porosity ranges from 10% to 16.7%. A large amount of microporosity exists because of high clay content and relative high porosity for low permeability. The irreducible water saturation ranges from 30% to 50%. These values are arbitrary because of the pressure limit of the instrument; but the estimations are reasonable for such low permeability samples with abundant micropores. Results of the calculation are shown in Figure 6.4.

One unpublished data set comes from Calhoun (2002, personal communication, Appendix D). Nine samples from oil fields in Erath and Eastland County, middle Texas, are selected here because they represent typical good, moderate, and poor (non) reservoirs. The samples were cored from the depth of 2500 ft to 3000ft. Lithology is sandstone to shaly sandstone, and shale. Porosity ranges from 16.2% to 6.3%, and permeability ranges from 1150 md to 0.24 md. Capillary pressures were measured by air-brine centrifugal method. Results of the calculation are shown in Figure 6.5.

All these examples (Figure 6.3, 6.4, and 6.5) show good agreements between calculated and measured capillary pressures.

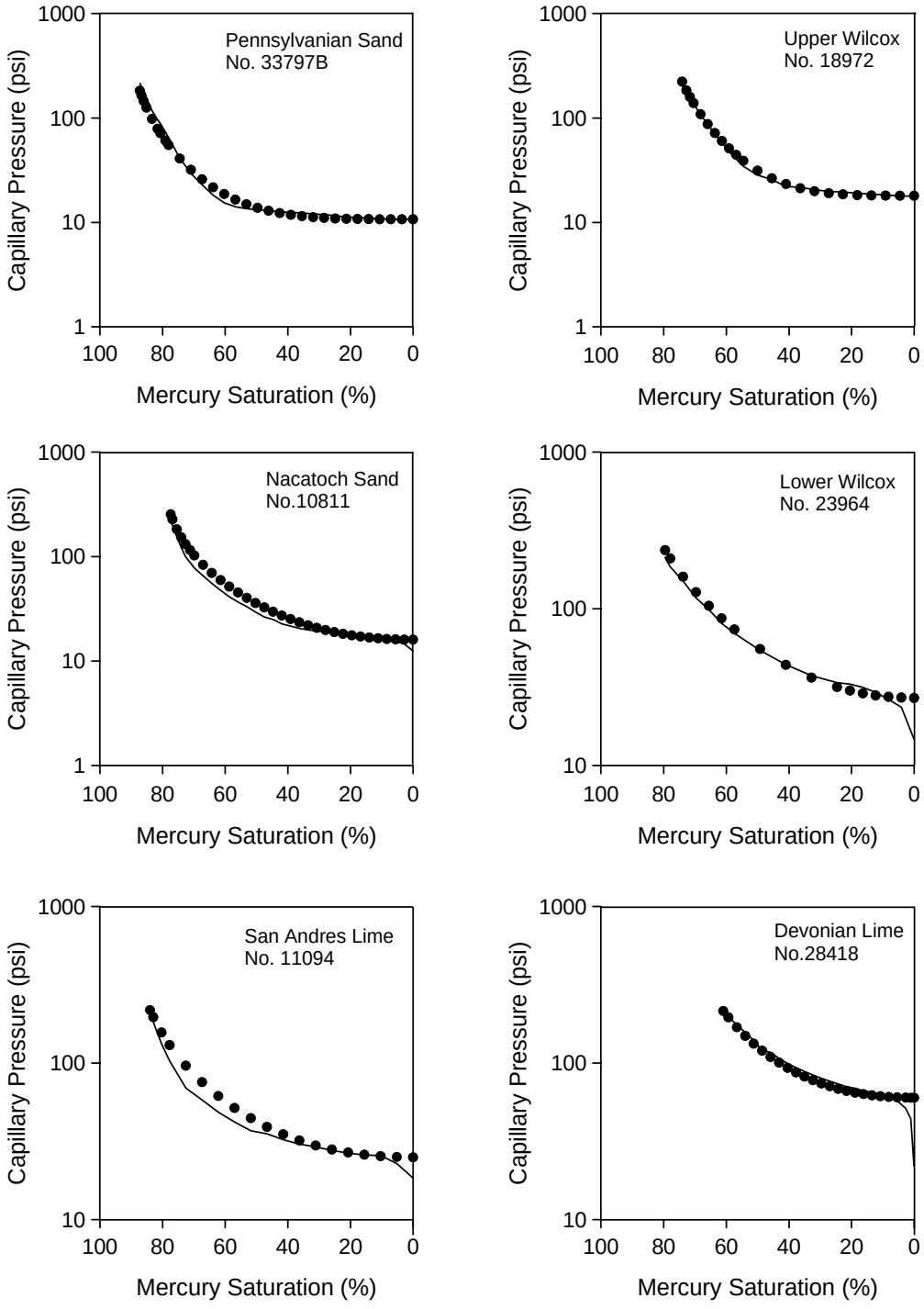


**Figure 6.3 Comparison between calculated and measured capillary pressures. Solid curves denote measurements, and dots denote calculation (data from Archie, 1950).**

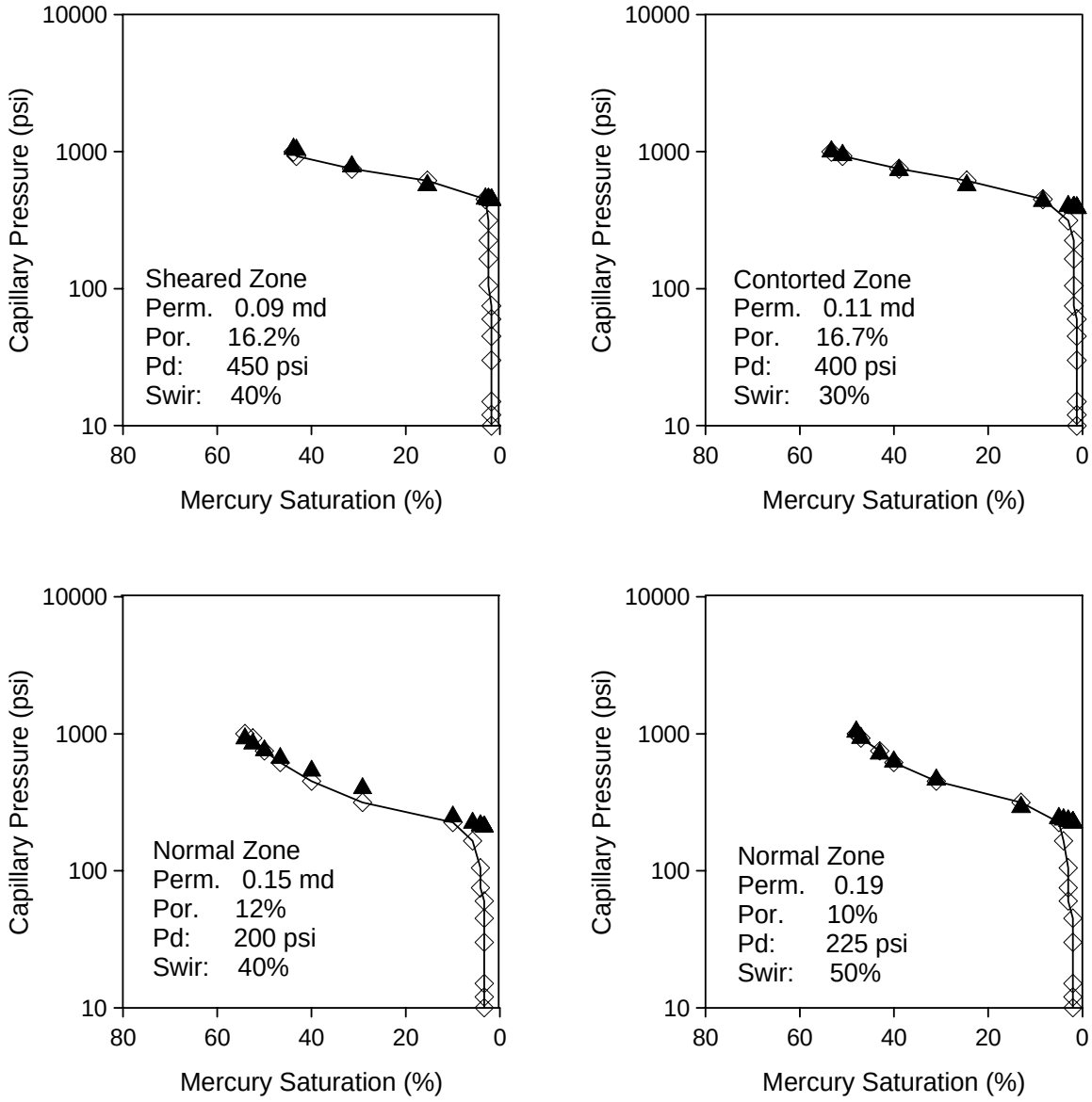


**Figure 6.4 Comparison between calculated and measured air-mercury capillary pressures. Solid lines (diamonds) denote measurements, and triangles denote calculations, Shell Stegall 1A well (data from Berg and Avery, 1995).**

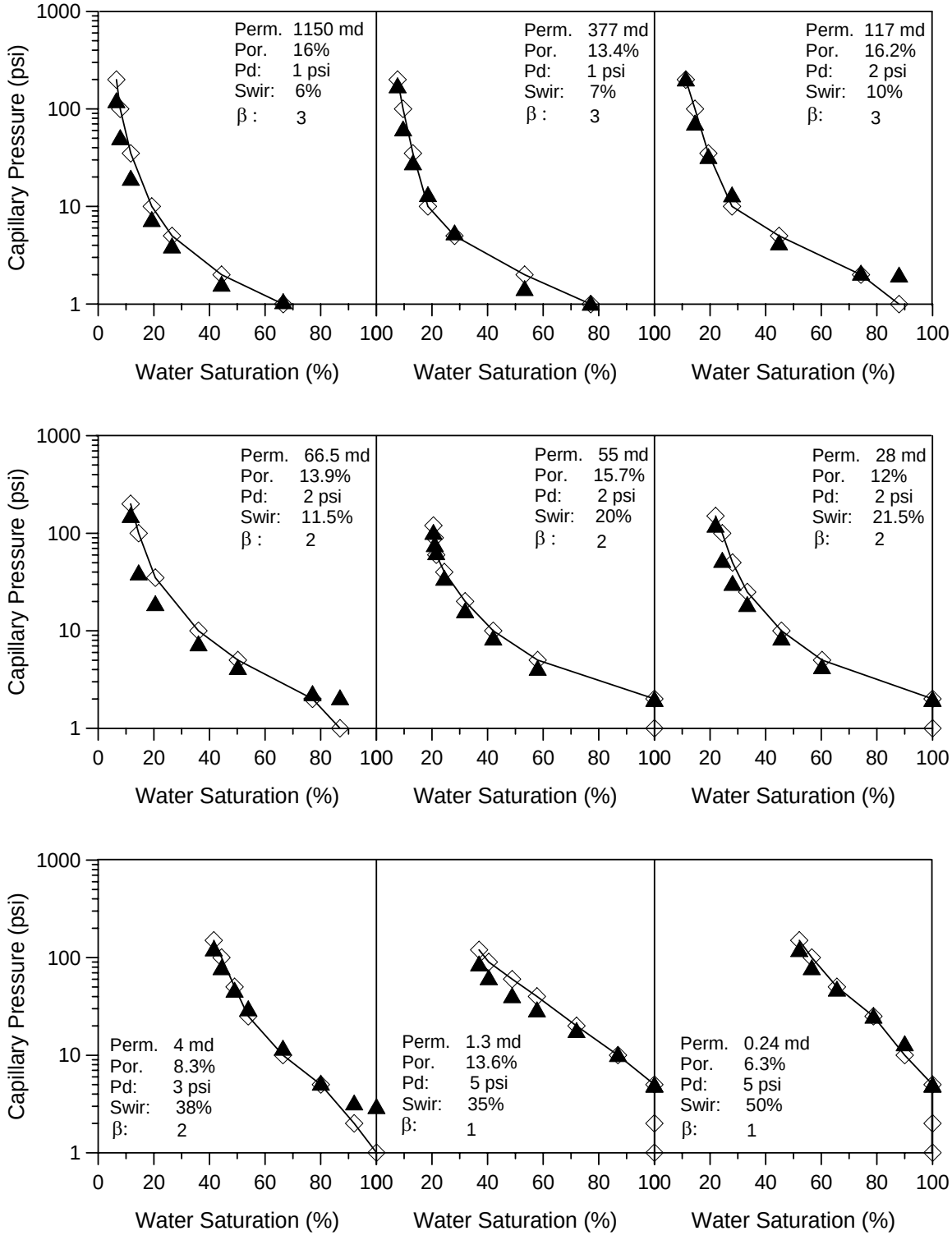


**Figure 6.5. Comparison between measured (diamond-curve) and calculated (triangle) centrifugal air-water capillary pressures (data from Dr. John C. Calhoun, personal communication, 2002).**

### 6.3 Summary

A revised capillary-pressure model is proposed based on Bentsen and Anli's (1976), and Harris and Goldsmith (2001) work. The model is largely empirical, but meets some reasonable assumptions. The new contribution is the introduction of a "shape factor", $\beta$, which accounts for the influence of lithology and pore-type on capillary pressures. Empirical rules are proposed to guide choosing the values of $\beta$. This model is tested with a large data set (over 200 samples) covering a wide range of lithology, porosity, and permeability. Good results are observed. Exceptions do exist for low-permeability (<1 md) samples, which may be caused my complex pore network and experimental errors.

# CHAPTER VII

# UPSCALING CAPILLARY PRESSURES

## 7.1 Introduction

It can be difficult to relate capillary pressure data measured on core plugs to properties of the entire reservoir. For homogeneous reservoirs, a common approach is to correlate capillary pressures with porosity, permeability, and water saturation to define relationships between these parameters. Once such relationships are established, an "average" capillary-pressure vs. water saturation curve for the reservoir can be estimated. This process is called "up-scaling" or correlation (Amyx et al. 1960). For heterogeneous reservoirs, the approach usually involves dividing the reservoir into different flow units, each unit with slightly varying properties (Ebanks et al., 1993). Once the "average" capillary pressure curve for each flow unit is generated, the saturation distribution can be inferred provided the free water level of the reservoir is known.

## 7.2 Statistical Correlation

A simple approach of up-scaling is to plot water saturation against the logarithm of permeability for a constant value of capillary pressure (Amyx et al. 1960). A straight line can be fitted to the data of each constant capillary pressure (Figure 7.1). The average capillary pressure curve can then be calculated from the average permeability of the reservoir. The straight line can be expressed as (Guthrie and Greenburger, 1955):

$$S_w = a \log k + c \qquad (7\text{-}1)$$

where a and c are constants.

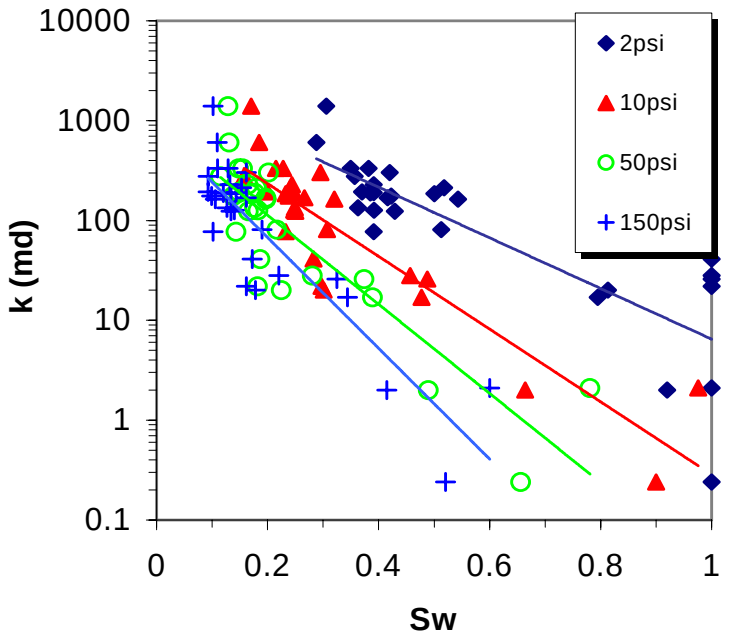


**Figure 7.1 Correlation between permeability and water saturation. Straight lines denote exponential fit lines (equation 7-1) for selected capillary pressures (data from Dr. John C. Calhoun, 2002, personal communication, Appendix D).**

Porosity can be introduced in equation 7-1 because the water saturation at a constant capillary pressure is not only a function of permeability but also a function of porosity as suggested by:

$$S_w = a \log k + b\phi + c \qquad (7\text{-}2)$$

where a, b, and c are constants determined from sample data.

Johnson (1987) proposed a similar correlation as Guthrie and Greenburger (1955):

$$\log S_w = a \log k + c \qquad (7\text{-}3)$$

where a and c are constants for a given capillary pressure. The c can be correlated with capillary pressures. Equation 7-3 can be graphically expressed as Figure 7.2. It shows better fits than equation 7-1, but the improvement is not very significant (Table 7.1).

Heseldin (1974) correlated capillary pressure with the bulk volume of hydrocarbon (BVH) and porosity. The method involves plotting porosity vs. BVH at a constant value of capillary pressure. The relationship between porosity and BVH can be expressed as:

$$V_{bh} = a + b \log \phi \qquad (7\text{-}4)$$

where $V_{bh}$ is the BVH, a and b are the intercept and slope of the fit line, respectively. The water saturation is implied in BVH through:

$$V_{bh} = \phi(1 - S_w) \qquad (7\text{-}5)$$

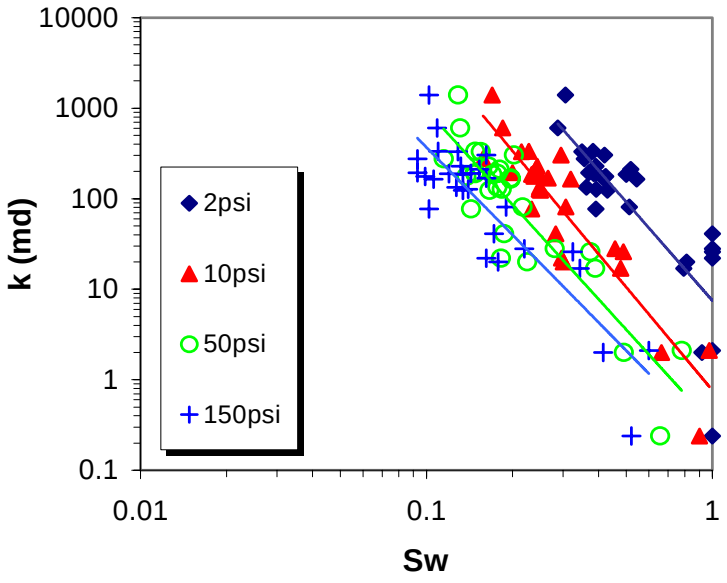


**Figure 7.2 Correlation between permeability and water saturation (logarithm). Straight lines denote power-law fit lines (equation 7-3) (same data set as Figure 7.1).**

**Table 7.1 Correlation equations between permeability and water saturation at different capillary pressures**

| Methods | Pc (psi) | Equations | $R^2$ |
|---|---|---|---|
| Guthrie & Greenburger (1955) | 2 | $\ln k = 7.708 - 5.839Sw$ | 0.70 |
| | 5 | $\ln k = 7.473 - 7.968Sw$ | 0.87 |
| | 10 | $\ln k = 7.132 - 8.385Sw$ | 0.82 |
| | 25 | $\ln k = 6.811 - 8.975Sw$ | 0.78 |
| | 50 | $\ln k = 6.782 - 10.275Sw$ | 0.77 |
| | 100 | $\ln k = 6.803 - 11.948Sw$ | 0.78 |
| | 150 | $\ln k = 6.767 - 12.772Sw$ | 0.79 |
| Johnson (1987) | 2 | $\ln k = 2.013 - 3.615 \ln Sw$ | 0.70 |
| | 5 | $\ln k = 0.270 - 3.905 \ln Sw$ | 0.86 |
| | 10 | $\ln k = -0.270 - 3.783 \ln Sw$ | 0.84 |
| | 25 | $\ln k = -0.776 - 3.591 \ln Sw$ | 0.83 |
| | 50 | $\ln k = -1.132 - 3.471 \ln Sw$ | 0.81 |
| | 100 | $\ln k = -1.369 - 3.310 \ln Sw$ | 0.78 |
| | 150 | $\ln k = -1.488 - 3.214 \ln Sw$ | 0.78 |

(data from John Calhoun, 2002, personal communication)

Although equation 7-4 usually shows better correlations than equations7-1 and 7-2, it appears to be invalid because the variable $\phi$ on the right side is included in the dependent variable, $V_{bh}$.

There are similar correlations in the literatures (Alger et al., 1989, Cuddy et al., 1993, Skelt and Harrison, 1995). All these methods involve correlations among the following variables: capillary pressure (or converted to height above FWL), water saturation (or bulk volume of water/hydrocarbon), porosity and/or permeability. These correlations, however, are empirical, and have to be adjusted from field to field. To be statistically valid, a large number of measurements have to be made, which is usually unavailable.

### 7.3 Leverett's (1941) J-Function

The most popular up-scaling method is Leverett's (1941) J-function:

$$J(S_w) = \frac{P_c}{\sigma \cos\theta}\sqrt{k/\phi} \qquad (7\text{-}6)$$

A power-low relationship between the J values and water saturation:

$$J(S_w) = \frac{P_c}{\sigma \cos\theta}\sqrt{k/\phi} = a(S_w)^{-b} \qquad (7\text{-}7)$$

The "a" and "b" are coefficients. The J-function was originally proposed as a means of converting all capillary pressure data into a universal curve, but it has been found that the J-function is valid only for single rock types (Brown, 1951). One problem of J-function is that it doesn't take into account pore-size distribution. Better correlations can be obtained if the $S_w$ in equation 7-7 is replaced by effective water saturation, $S_e$:

$$J(S_e) = \frac{P_c}{\sigma \cos\theta}\sqrt{k/\phi} = a(S_e)^{-b} \qquad (7\text{-}8)$$

Figure 6 shows the plots of J-function against water saturation (equations 7-7) and against effective water saturation (equation 7-8), respectively. Capillary pressures were measured on 10 core plugs from the T67X-11 well, Yowlumne Field (Appendix D). The samples are fine-grained sandstones interpreted to be a turbidite channel deposit. The reservoir is homogeneous. Permeability ranges from 59 md to 139 md, with an average value of 84.3 md. Porosity ranges from 16.9% to 19.5%, with an average value of 18.4%. The relationship between J-function and water saturation ($S_w$) has a coefficient of correlation ($R^2$) of 0.87, while the relationship between J-function and effective water saturation ($S_e$) has a $R^2$ value of 0.97.

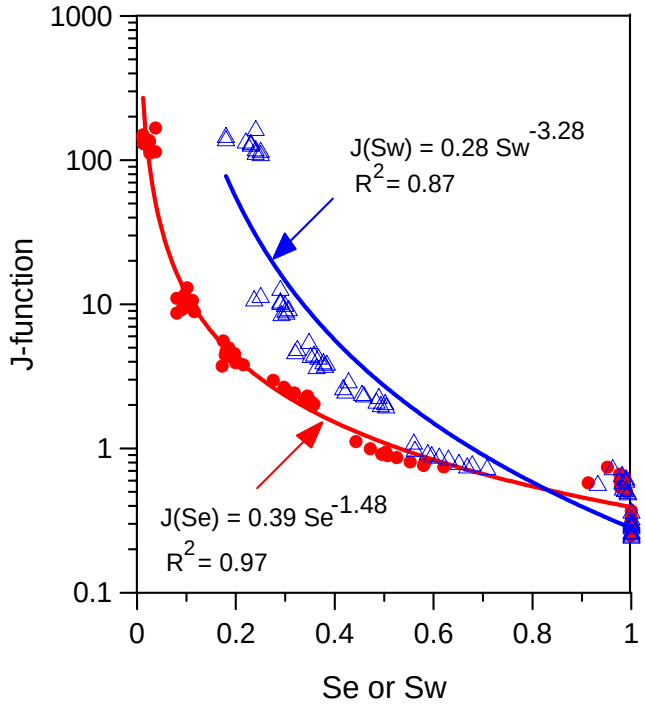


**Figure 7.3 Leverett's (1941) J-function as a function of water saturation (triangles), Sw, and as a function of effective water saturation (dots), Se, respectively. Solid curves are the best fits. Samples are from Stevens Sandstone, T67X-11 well, Yowlumne Field, Kern County, California**

Once the J-function is obtained, capillary pressures can be calculated by rearranging equation 7-8:

$$P_c = a\sigma\cos\theta\sqrt{\phi/k}(S_e)^b \qquad (7\text{-}9)$$

Comparison equation 7-9 with Brooks and Corey's equation (equation 5-7), it is easy to find that $b = -1/\lambda$, and $a$ is related with $P_d$. Merging the constants yields (Corbett et al., 1992, and Ringrose et al., 1993):

$$P_c = C\sqrt{\phi/k}(S_e)^{-1/\lambda} \qquad (7\text{-}10)$$

where C is a constant ($C=a\sigma\cos\theta$). Corbett et al. (1992) and Ringrose et al. (1993) used equation 7-10 to generate capillary-pressure curves by assuming a constant value (1.5) for $\lambda$. From practical point of view, $\lambda$ is not easy to predict (see Chapter V). Amaefule et al. (1988) pointed out " For most rocks, $\lambda$ normally falls between 0.4 and 4.0. As $\lambda$ approaches infinity, the uniformity of pore size increases. Wide range of pore size is evidenced when $\lambda$ is between 0.5 and 2.0……". They found an average value of 1.15 for the Travis Peak Formation characterized by low permeability and wide range of pore size. Brooks and Corey (1966) used a default value of 2 in relative permeability calculation. Therefore, in order to apply equation 7-10, experimental data must be available to estimate $\lambda$.

This limitation of the above methods can be overcome with the model proposed in this study (equation 6-4) because all the parameters can be estimated from independent sources like well log, or be assumed. To illustrate this, we again use data from well T67X-11. Since the reservoir is homogeneous, the average petrophysical properties from core analysis are approximated as the average properties of the whole reservoir. The displacement pressure can be calculated with porosity and permeability. The irreducible water saturation, $S_{wir}$, can be assigned either an empirical value, or estimated from well log data. Since the reservoir is clean sandstone, a $\beta$ value of 3 is used. Figure 7.4 shows the comparison among the measurements and calculated average capillary-pressure curves from equations 7-10 and 6-4. The calculated average capillary-pressure curves from equations 7-10 and 6-4 agree well with each other, and both represent the average trend of the ten measurements. The merit of equation 6-4 is that no capillary-pressure measurements are required.

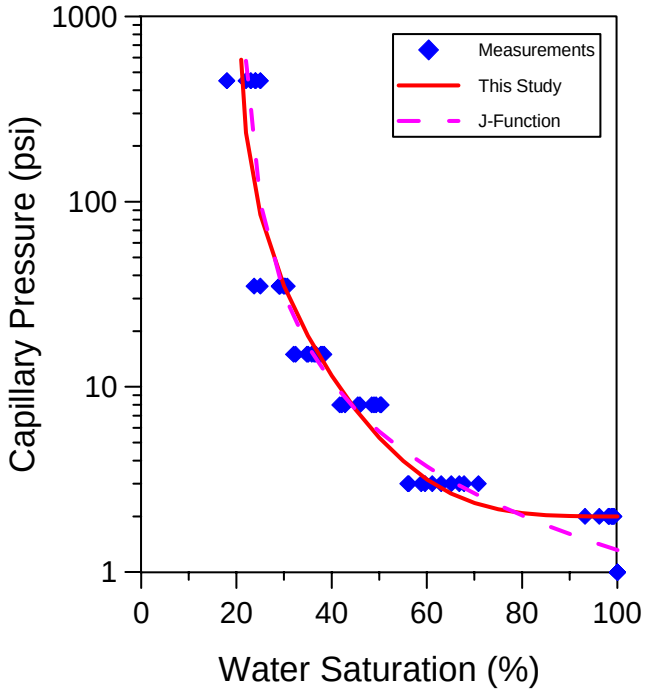


**Figure 7.4 Measured capillary pressures (diamonds), and calculated average capillary-pressure curve from equation 6-4 (solid curve) and equation 7-10 (dash curve), respectively. Samples are from the Stevens Sandstone, T67X-11 well, Yowlumne Field, Kern County, California (Appendix D)**

## 7.4 Reservoir Zonation

For homogeneous reservoirs, the average capillary pressure curve of the reservoir can be generated by correlating capillary pressure with water saturation, permeability, and/or porosity (as discussed in the above sections). But for heterogeneous reservoirs, it is difficult to use a single capillary pressure curve to delineate the whole reservoir. A common approach is to divide the reservoir into several flow units (or rock types) according to porosity, permeability, pore-throat size, and pore type (Martin et al, 1997, Hartmann and Beaumont, 1999). A flow unit is defined as “a mappable portion of the total reservoir within which geological and petrophysical properties that affect the flow of

fluids are consistent and predictably different from the properties of other reservoir rock volumes" (Ebanks et al, 1993). Flow units can be identified from an interrelated series of petrophysical crossplots and from the calculation of Winland's $r_{35}$ (Martin, et al, 1997).

Figure 7.5 shows how flow units are identified with Winland's $r_{35}$. The samples come from Yowlumne Field, Kern County, California. The Yowlumne sandstone is interpreted to be deposits from turbidity currents (Royo, 1986, Berg and Royo, 1990). The sands were deposited within a channel as indicated by the dominance of incomplete turbidites of A, AB, and AE Bouma sequence types (Bouma, 1962). Five flow units are distinguished by ranges of $r_{35}$. Flow units 1 and 2 make up the major reservoirs in the field, they have permeabilities ranging from 10s md to 100s md, porosities ranging from 13% to 20%, and $r_{35}$ ranging between 2 to 8 μm (Table 7.2). They are central channel deposits characterized by massive to laminated sands, i.e., A and B sequences. Flow units 3 and 4 are poor reservoirs with permeabilities between 1.3 md to 5.2 md, porosities between 10% and 17%, and r35 between 1 and 2μm. These two units are usually composed of turbidites C and D. The presence of clay does not significantly reduces the porosity, but dramatically reduce the permeability because of the introduction of microporosity. Flow unit 5 has r35 less than 0.5 μm, which represents non-reservoir shale deposits, i.e., turbidites E.

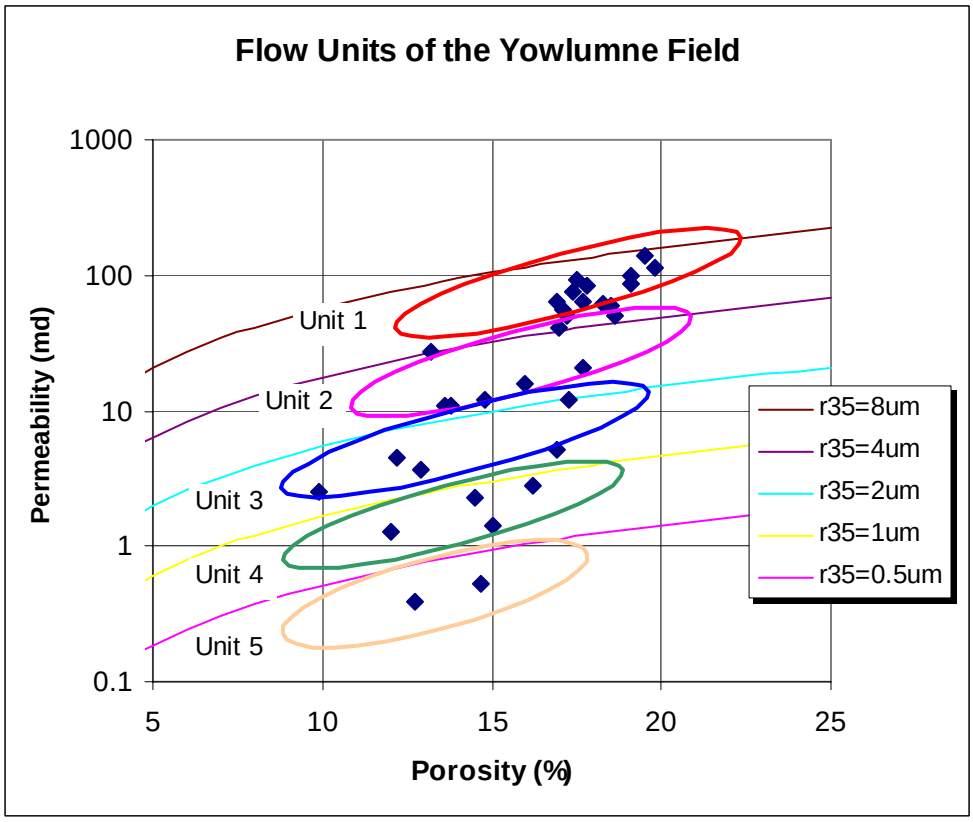


**Figure 7.5 Cross plot of permeability and porosity. Diagonal contour lines are Winland's r35 values (1980). Ellipsoids enclose samples of equal pore-throat radii within each flow unit. Samples are from the Stevens Sandstone, Yowlumne Field, Kern County, California (Appendix E)**

**Table 7.2 Average petrophysical properties of the flow units in Yowlumne Field.**

| Flow Units | Number of Samples | Permeability (md) | Porosity | $r_{35}$ (μm) | $S_{wir}$ | β | $P_d$ (psi)* |
|---|---|---|---|---|---|---|---|
| 1 | 15 | 75.47 | 0.18 | 4 – 8 | 0.2 | 3 | 1.65 |
| 2 | 6 | 16.33 | 0.15 | 2 – 4 | 0.21 | 2 | 2.87 |
| 3 | 4 | 3.98 | 0.13 | 1 – 2 | 0.3 | 2 | 5.16 |
| 4 | 4 | 1.95 | 0.14 | 1 – 0.5 | 0.49 | 2 | 7.68 |
| 5 | 2 | 0.46 | 0.14 | < 0.5 | 0.6 | 1 | 16.99 |

* $P_d$ was calculated from permeability and porosity with equation 5-17, and converted to air-water system.

Air-brine centrifugal, capillary pressures were measured on 31 samples, most of the measurements represent flow units 1 and 2 since they are the dominate reservoirs. Average capillary pressure curves for each flow unit are synthesized by substituting the average petrophysical properties (Table 7.2) into equation 6-4. The β values are empirically determined based on lithology and permeability. The calculated average capillary pressure curves and measured data of each flow unit are plotted in Figure 7.6 (the average capillary pressure curve of flow unit 5 is not calculated because of limited data). As can be seen, the calculated capillary pressure curves fit the measurements well.

If capillary pressure curves of each flow units are known, the water saturation profile in a single well can be inferred, as long as the free water level is known. Figure 7.7 is a schematic diagram showing the saturation profile of a heterogeneous reservoir. Two facies (A and B) are identified with different capillary pressure curves. The free water level (fw) is the same for all facies, but the different displacement pressure results in different oil-water contact elevations, and sharp changes in vertical water saturation profile.

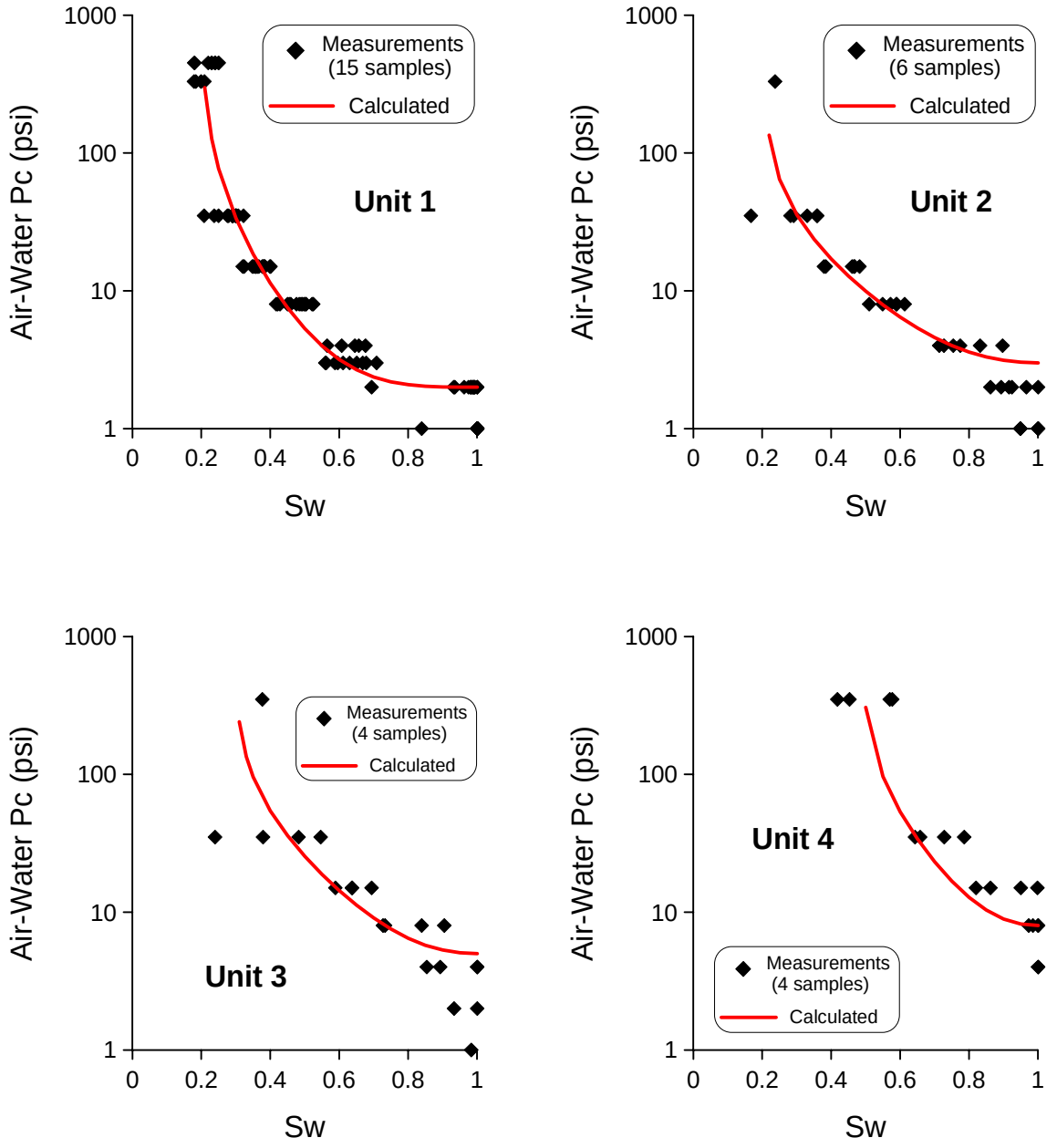


**Figure 7.6 Measured and calculated capillary pressures of the four flow units in Yowlumne Field. The solid curves are calculated (equation 6-4) average capillary pressure with the average petrophysical properties shown in Table 7.2.**

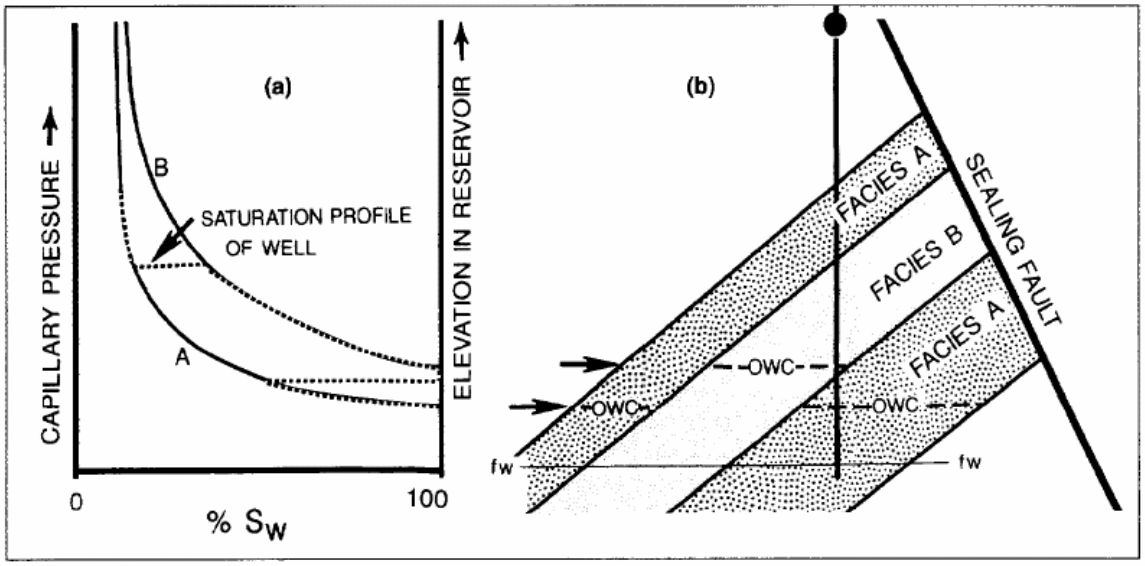


**Figure 7.7 Effect of reservoir heterogeneity on fluid contacts and distribution. (a) Capillary pressure curves for facies A and B within the reservoir. The dashed line cooresponds to the saturation profile of the well in part (b). (b) Oil-water contacts (OWC) corresponding to capillary pressure curves. The vertical line is the well position corresponding to the saturation profile shown in (a). (From Brown, 1993)**

### 7.5 Summary

Several methods of up-scaling capillary pressure from core-plug to reservoir scale have been discussed. Most approaches are based on empirical correlations among capillary pressure, porosity, permeability, and water saturation. These methods usually work well for homogeneous reservoirs. There is no significant difference in predictions made by these methods. To be statistically valid, a large number of measurements are required, which is not possible in many cases because core measurements are sparse. The revised model proposed in this study (equation 6-4) can be used to describe reservoir-scale capillary behaviors if the average porosity, permeability, and irreducible water saturation

of the reservoir can be reliably measured or estimated. The merit of the modified model is no capillary-pressure measurements are required.

The “up-scaling” procedure for heterogeneous reservoirs involves the following two steps: (1) divide a particular reservoir into several flow units (or rock types) according to porosity, permeability, and pore-throat radius. Each flow unit is assumed to be internally homogenous; (2) calculate (or estimate) the average porosity, permeability, irreducible water saturation, and displacement capillary pressure for each flow unit. The average capillary pressure curve for each flow unit (or rock type) can then be generated with equation 6-4.

# CHAPTER VIII

# APPLICATION OF CAPILLARY PRESSURE MODELS

## 8.1 Introduction

In the petroleum industry, capillary pressure data have been used to evaluate reservoir rock properties, sealing capacity (the maximum column of hydrocarbon a seal can hold before it leaks), pay versus nonpay and transition zone thickness (Jennings, 1987, Vavra, et al., 1992). Capillary pressure is the main resisting force to secondary hydrocarbon migration. A thorough understanding of capillary pressure is helpful in tracing hydrocarbon migration routes and predicting vertical and lateral sealing capacity. Such knowledge is critical in exploring for and exploiting subtle stratigraphic traps (Arps, 1964, Berg, 1975, Berg and Avery, 1995, Schowalter, 1979, 1982). In development programs, capillary pressure data are used to analyze pore structures of reservoir rocks, which significantly influence sweep efficiency and distribution of residual oil. Combination of capillary pressure and relative permeability is helpful to understand fluid distribution and oil-water contact (Arps, 1964). Capillary pressure can also be used to calculate relative permeability (Burdine, 1953, Brooks and Corey, 1966).

The focus of this chapter is to illustrate the application of capillary pressure models, i.e., to generate capillary pressure vs. saturation curves from other petrophysical properties (e.g., porosity and permeability), and then to use the synthetic curves to evaluate sealing capacity of seals and fluid distribution in reservoirs.

## 8.2 Sealing Capacity Evaluation

If displacement pressures of seal and reservoir are known, the maximum hydrocarbon column the seal can hold before it begins leaking can be calculated by (Smith, 1966, Schowalter, 1979, Jennings, 1987, Vavra et al., 1992):

$$h_{\max} = \frac{P_{dS} - P_{dR}}{0.433(\rho_w - \rho_{hc})} \qquad (8\text{-}1)$$

where $h_{max}$ is the height of hydrocarbon column (in ft); $P_{dS}$ and $P_{dR}$ are the brine-hydrocarbon displacement pressure (in psi) of the seal and reservoir, respectively; $\rho_w$ and $\rho_{hc}$ are the specific density (in $g/cm^3$) of brine and hydrocarbons at ambient conditions, respectively.

### 8.2.1 Wilcox sandstone, Milbur Field, Texas

The Lower Wilcox sandstone reservoir at Milbur field, Burleson County, Texas, is a simple lenticular reservoir at shallow depth (Chuber, 1972). The reservoir sandstones were formed as littoral marine bars deposited in a generally regressive sequence (Berg, 1975). The reservoir is presumed to grade laterally to a thinner lagoonal facies, which forms the seal of the reservoir. Although normal faults are present at the field, oil accumulation is predominately controlled by facies changes. The rock and fluid properties of the reservoir and seal are known from the Clark Cotton 1 well (Table 8.1). These values are assumed to be representative of the field. The well log and core saturation measurements are shown in Figure 8.1.

**Table 8.1 Basic data and oil-column calculations for selected fields**

| Field | Milbur, Texas | | East McCook, Texas | Martens Prairie, Texas |
|---|---|---|---|---|
| | Reservoir | Seal | Fault Seal | Reservoir |
| Permeability (md) | 900 | 25 | 0.09 | 910 |
| Porosity | 0.32 | 0.25 | 0.166 | 0.21 |
| $P_d$ (oil/gas-water, calculated) | 0.5 | 1.48 | 31.2 | 0.43 |
| $P_c$ at 35% oil saturation (oil/gas-water, calculated) | 0.57 | 2.77 | 75.5 | |
| $S_{wir}$ (assumed) | 0.1 | 0.3 | 40 | 0.1 |
| Oil/Gas density, $\rho_o$, (g/cm$^3$) | 0.91 | | 0.2 | 0.74 |
| Water density, $\rho_w$, (g/cm$^3$) | 1.0 | | 0.95 | 1.0 |
| Interfacial tension (dynes/cm) | 30 | | 40 | 31 |
| Contact angle (0°) | 0 | | 0 | 0 |
| β (assumed) | 3 | 2 | 1 | 2 |
| Oil/Gas Column (ft) | 60 to 75 | | 180 | |
| Calculated oil/gas column (ft) | 57 to 72 | | 125 to 233 | |

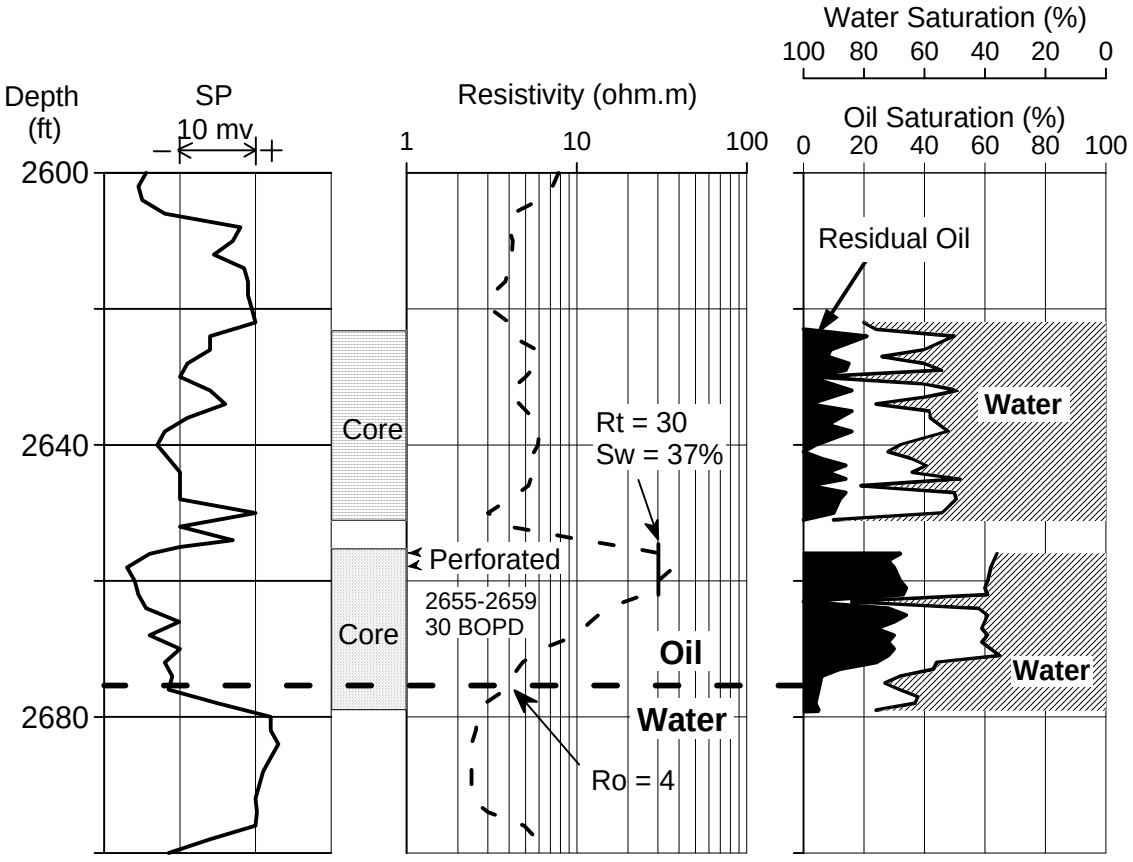


**Figure 8.1 Well log and core-measured saturation, Lower Wilcox Formation, well Clark Cotton 1, Milbur Field, Burleson County, Texas.**

Displacement pressures for the reservoir and seal are calculated by equation 6-5, and converted to subsurface condition. Substituting these values into equation 8-1 gives an oil column of 25 ft, while the actual oil column in the field ranges between 60 to 75 ft (Chuber, 1972). We believe this disagreement results from the choice of capillary pressure. The $P_{dS}$ and $P_{dR}$ used in the calculation are the capillary pressure corresponding to 100% water saturation, and thus, the calculated oil column is the oil column before the oil leaks into the seal. As can be seen from the core analysis (Figure 8.1), the seal is a leaking seal showing 10% residual oil saturation. The average water saturation in the core is about 65%. We believe the subsurface water saturation in the seal is close this value because the seal is shaly sandstone with low permeability, that means it may not be affected significantly by water-flushing during coring. We assume the oil is trapped from further leaking by capillary pressure at 35% oil saturation ($P_{c35}$), this assumption is consistent with Windland (published by Kolodzie, 1980) and Pittman's (1992) observation. Substituting $P_{c35}$ values of seal and reservoir into equation 15 gives an oil column of 57 ft, which is close to the actual oil column of the field. From the calculated capillary-pressure curve of the seal (Figure 8.2), 65% water saturation in the seal suggests an oil column of 72 ft, which also agrees well with the actual oil column.

The reservoir in Clark Cotton 1 well has a thickness of 25 ft. The reservoir was perforated at 2655 – 2659 ft, and has a production of 30 barrel of oil per day (BOPD). The majority of the reservoir is believed within transition zone, which is supported by core and well log (Figure 8.1). Oil-water contact is located at 2675 ft. One evidence is the core beneath that depth displays no oil stain. Water saturation at the top of reservoir is calculated by Archie (1942) equation (assume n = m = 2), and is equal to 37%. From the

calculated capillary-pressure curve, this saturation suggests a transition zone of 20 ft, which is identical to the actual thickness.

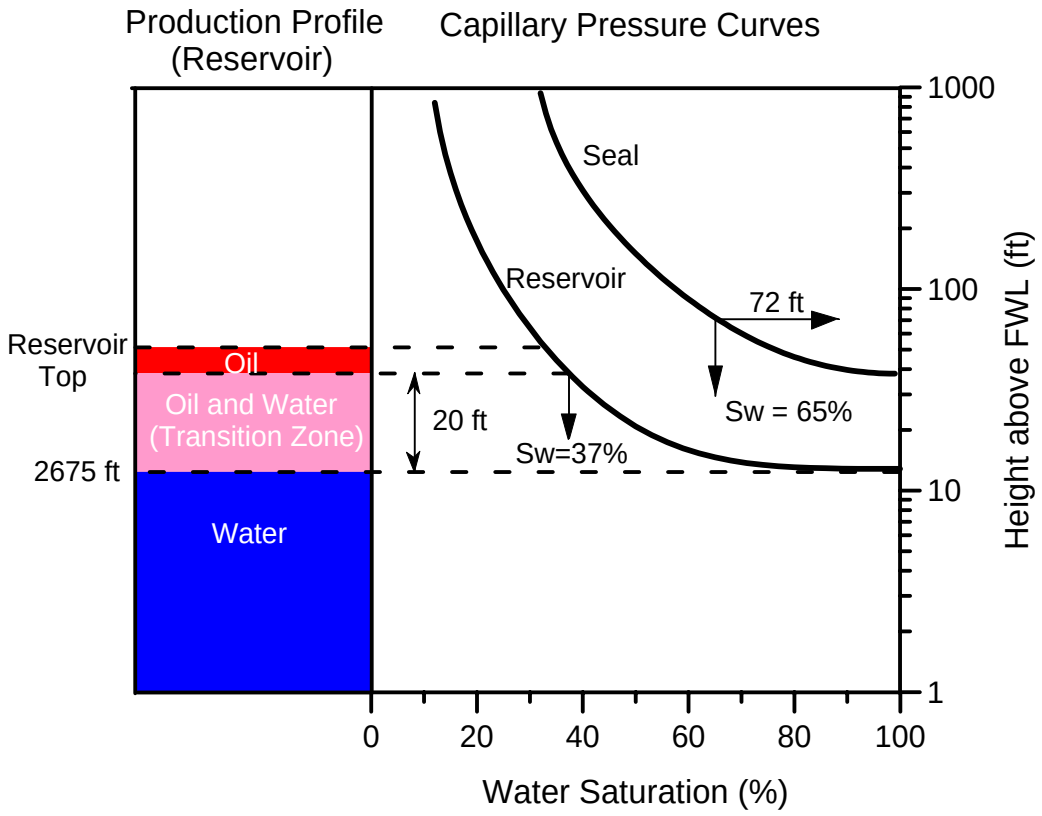


**Figure 8.2 Synthetic capillary-pressure curves of the seal and reservoir, and production profile of the reservoir, Lower Wilcox Formation, well Clark Cotton 1, Milbur Field, Burleson County, Texas.**

If Clark Cotton 1 was happen to be a discovery well, the above calculation would provide valuable information to define the boundary and fluid distribution of the reservoir (Figure 8.3). Clark Cotton 1 penetrated 25 ft of porous and highly permeable bar sands. The top 5 ft produces pure oil, while the remaining 20 ft produces oil and water (transition zone). If we know the lagoonal facies is capable of sealing 60 – 75 ft of oil,

then we can estimate how far updip we will produce only oil and how far downdip we will produce only water. A second test well might be proposed, and is expected to penetrate the reservoir. If we have such a clear geological model, the above information may also lead to discovery of a new stratigraphic trap (Figure 8.3).

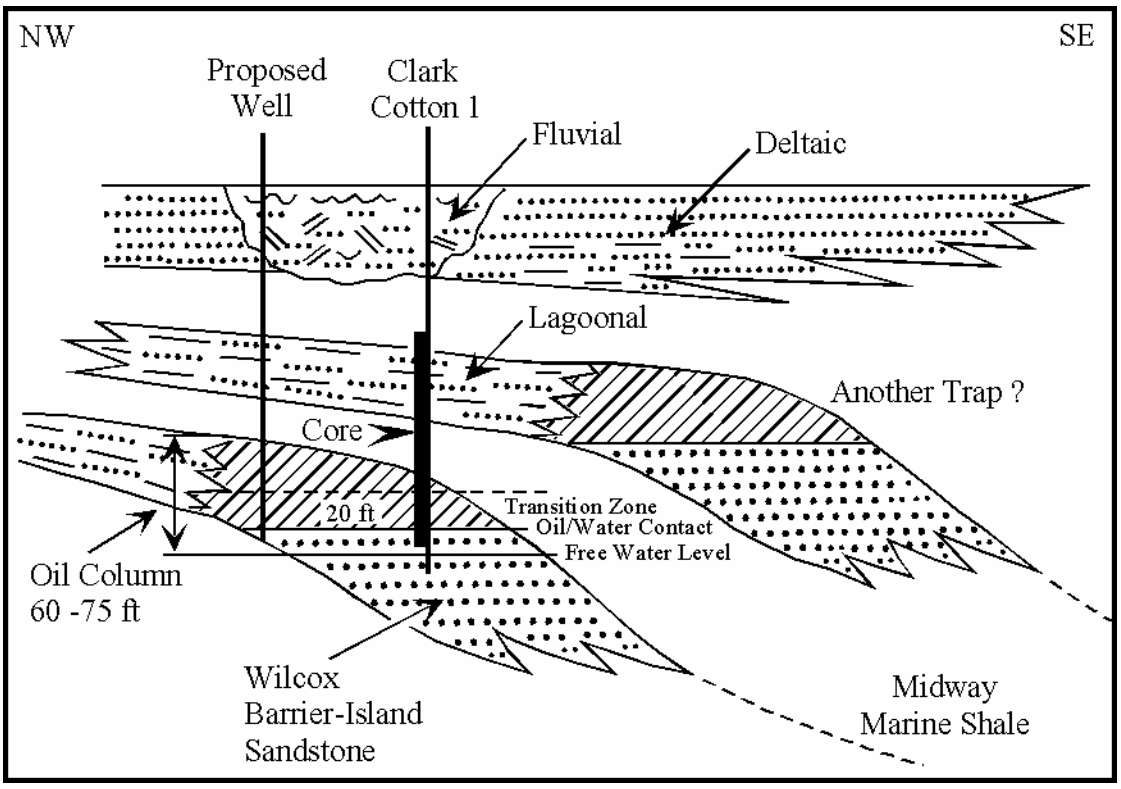


**Figure 8.3 A schematic diagram showing depositional environment and stratigraphic trap in the Milbur Field, Burleson County, Texas (modified from Berg, personal communication, 2003).**

### 8.2.2 Vicksburg sandstone, East McCook Field, Texas

This is an example of fault trap. Faults are commonly effective seals because of zones of sheared sediment, or clay smear, injected along the fault surface. The sheared zones

originated by ductile flow of shale and may occur on either side of the fault (Berg and Avery, 1995). In listric growth faults, the sheared zones are most likely to occur on the upthrown block as the fault propagates upward through highly pressured shale.

Sheared zones can be detected by dip log patterns (Figure 8.4). For example, regularly increasing dips over a short interval may record drag on the downthrown block and indicate an adjacent fault surface (Figure 8.4A). Erratic dips below a fault represent a sheared zone of shale injected along the fault by ductile flow. A reservoir sandstone below on the upthrown block abuts the sheared zone, assuring an effective seal.

In Figure 8.4B, the section of erratic dips represents a sheared zone adjacent to the downthrown block. Below the sheared zone is the fault surface which is indicated by the more regular drag pattern of decreasing dips downward. In this case, a sandstone on the upthrown block that abuts the fault surface might not be sealed because the fault surface is a plane of extension and can leak during periods of movement along the fault.

The sheared zone is an effective seal because ductile flow has homogenized the fine-grained sediment, and capillary displacement pressures are relatively high and uniform. If undercompacted shale is present along the fault, the sheared zone can form either on the upthrown or downthrown blocks. However, planar faults through compacted rocks may not have sheared zones. Listric faults may not have reverse dip, or rollover, on the downthrown blocks and sheared zones only along the upthrown side.

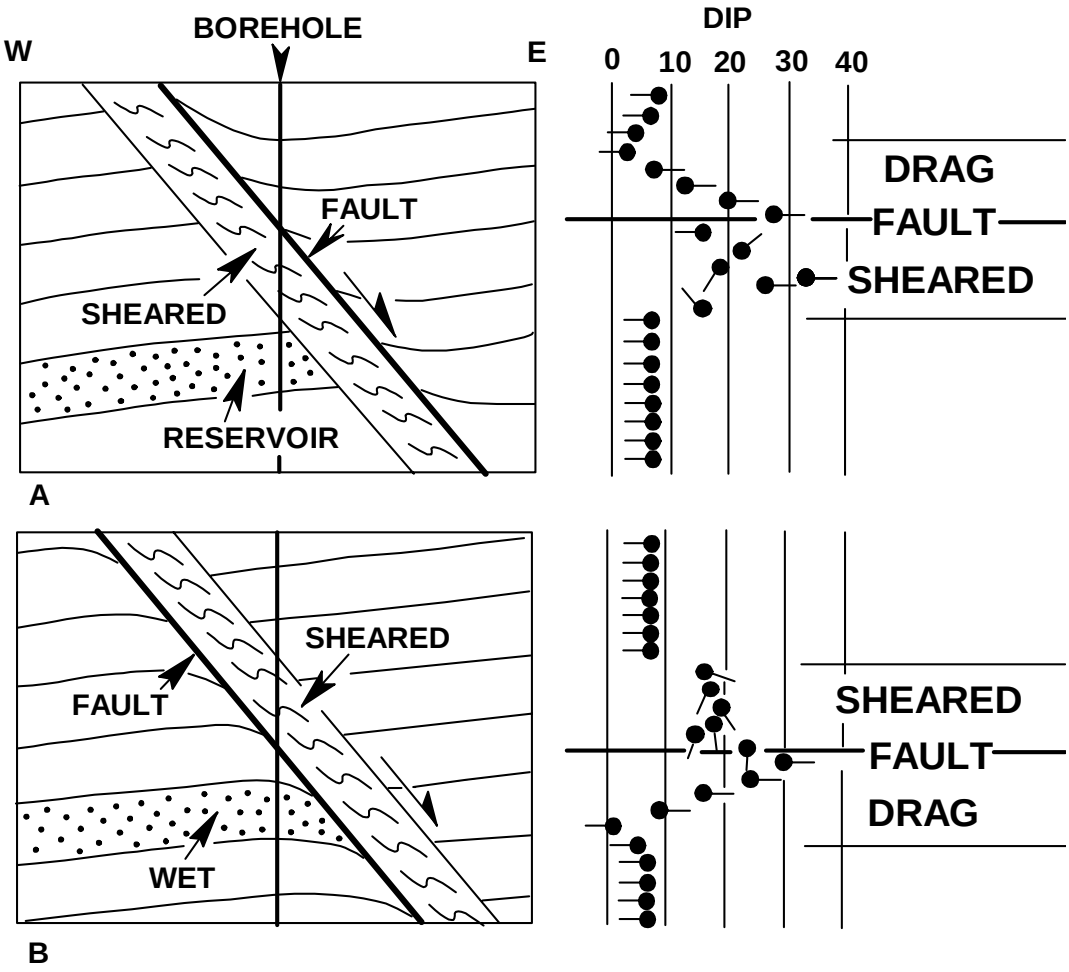


**Figure 8.4 Diagrammatic cross sections and dip logs through a normal-faulted section of sandstones (stippled) and shales (blank). (A) Sheared zone on the upthrown block seals reservoir. (B) Fault surface is a poor seal on the upthrown block (modified from Berg, personal communication, 2003).**

In the East McCook field, multiple sandstones in the Vicksburg Formation produce gas, and many reservoir seals are clearly related to normal faulting. Regional dip in the area is about five degrees to the east, but at the producing level, some beds show dip reversal to the west. The Shell Davis 3 well (Figure 8.5) shows a typical reservoir section with resistivity in the sandstone through perforations from 12,674 to 12,854 ft.

The producing interval of 180 ft is the gas column sealed by the sheared zone. The initial potential was 12 million $ft^3$/day, and cumulative production was 8 billion $ft^3$ in 13 years.

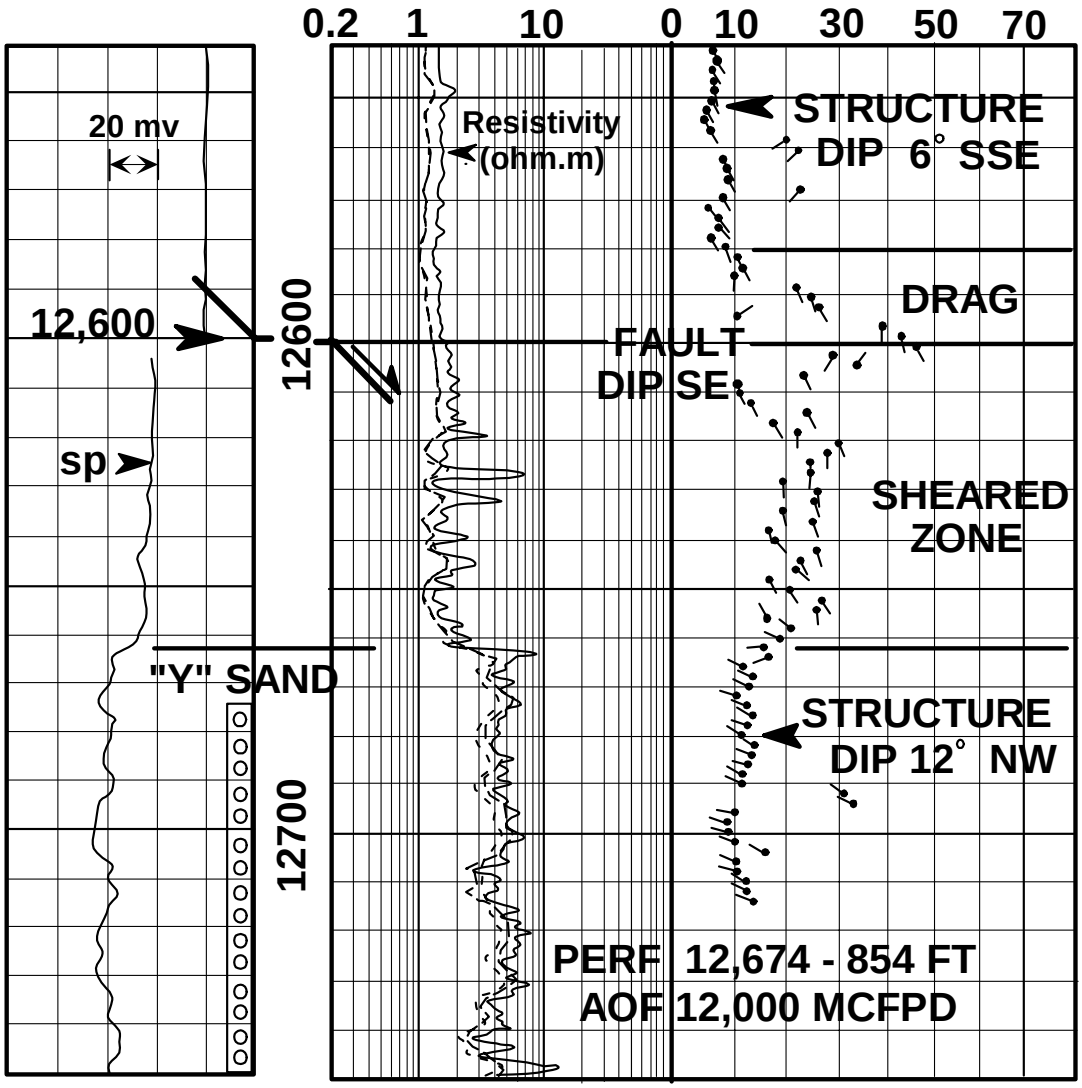


**Figure 8.5 Well logs through a section of Vicksburg sandstone and shale in the Davis 3 well, East McCook field. Logs are the spontaneous potential (SP, left), induction resistivity (middle), and interpreted true dips (right) (modified from Berg and Avery, 1995)**

From the dip pattern (Figure 8.5), it is most likely that a normal fault surface is present at 12,600 ft, a normal drag zone at 12,585 to 12,600 ft, and a sheared zone at 12,600 to 12,622 ft. Since no cores are available in this well, the properties from a similar sheared zone in Shell Segall are used. The sheared zone from Shell Segall has an average 16.6% porosity and 0.09 md permeability (Berg and Avery, 1995). Other properties are listed in Table 8.1. Synthetic capillary-pressure curve (converted to height) is generated with equation 6-4 (Figure 8.6). The synthetic capillary-pressure curve suggests that a column of 125 ft of gas can be sealed at 10% gas saturation, and a column of 233 ft can be sealed at 35% gas saturation. Thus, the total gas column that can be sealed by the sheared zone is expected to range between 125 ft to 233 ft (44 to 71 m) which agrees well with the observed gas column of 180 ft (55 m) as based on the perforated interval.

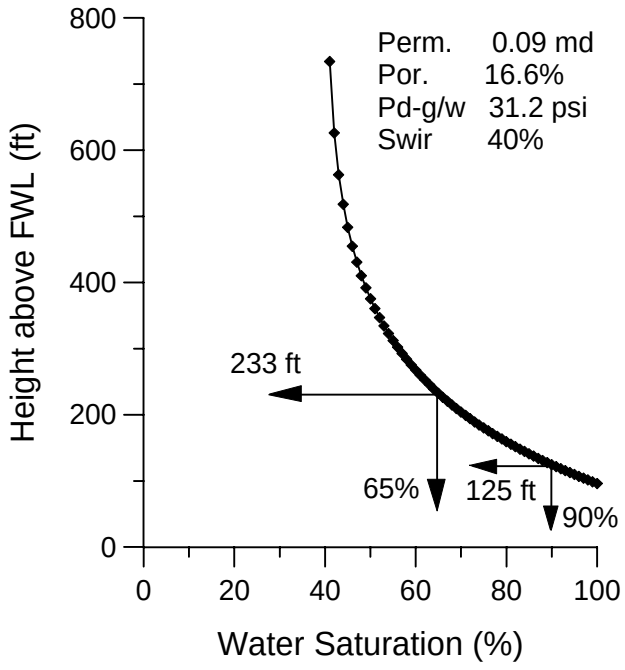


**Figure 8.6 Synthetic capillary-pressure curve of the sheared zone, Davis 3 well, East McCook field. It suggests a gas column of 125 ft to 233 ft can be held by the fault.**

### 8.3 Height Above the Free Water Level

The height of hydrocarbon column above the free water level (FWL) can be calculated by (Smith, 1966, Vavra, et al., 1992):

$$h = \frac{P_c}{0.433(\rho_w - \rho_{hc})} \qquad (8\text{-}2)$$

This information can be used to compare expected fluid saturations at given levels in the reservoir (Vavra, et al., 1992). Three examples are illustrated here: a shaly sandstone reservoir, an unconsolidated sandstone reservoir, and a dolomite reservoir.

#### 8.3.1 Wilcox unconsolidated sandstone, Texas

Eocene Wilcox sandstones in the Cashco Hicks 1 well, Martens Prairie Field, Grimes County, TX, are unconsolidated sandstones interpreted as fluvial channel deposits. No cores are available. The oil/water contact is located at 4975ft. Well log indicates the reservoir is shaly sandstone with an average GR of 60 API (Figure 8.7). Calculated average shale volume is 12%. Porosity is calculated from well log, and has an average value of 21%. Water saturation is calculated with effective medium model (Berg, 1996). Irreducible water saturation is assumed 10%, which is based on water saturation at the top of reservoir. Permeability is calculated by three empirical equations: Morris and Biggs (1967), Timur (1968), and Schlumberger (1988):

$$k = \left( 250 \frac{\phi^3}{S_{wir}} \right)^2 \qquad (8\text{-}3)$$

$$k = 0.136 \frac{(100\phi)^{4.4}}{(100 S_{wir})^2} \qquad (8\text{-}4)$$

$$k = \left[ \frac{100\phi^2 (1 - S_{wir})}{S_{wir}} \right]^2 \qquad (8\text{-}5)$$

Geometrical mean of the three equations, 910 md is assumed the average permeability of the reservoir, which is believed reasonable for the lithology, age, and shallow depth. Other properties are listed in Table 8.1. Capillary-pressure curve for the reservoir is calculated by equation 6-4, and converted to height above FWL (equation 8-2). The water saturation profile from the calculated capillary pressure agrees well with that from log interpretation (Figure 8.7).

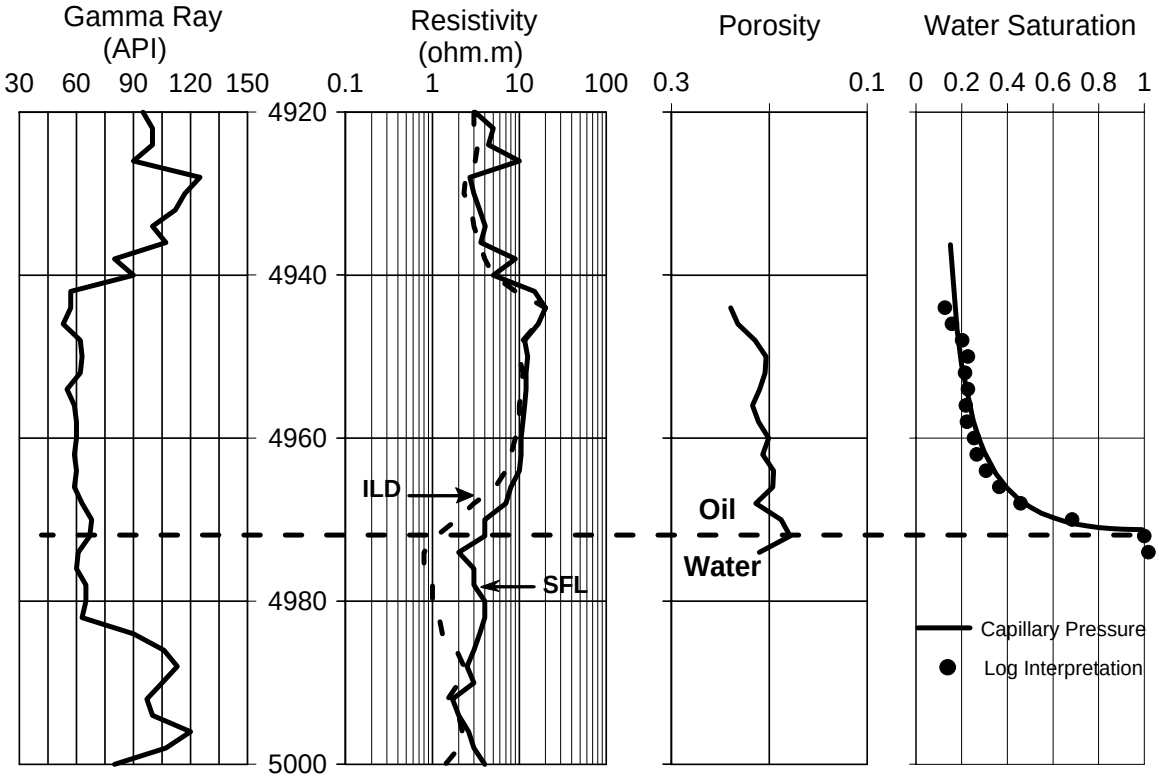


**Figure 8.7 Well log, log interpretation, and capillary pressure of the Eocene Wilcox sandstone in well Cashco Hicks 1, Martens Prairie Field, Grimes County, TX**

### 8.3.2 Pennsylvanian Dolomite, West Texas

A carbonate example comes from a well in the Pennsylvanian dolomite (Aufricht and Koepf, 1957). The porosity and permeability values were measured at 1 ft intervals on a 50 ft cored section (Figure 8.8). Water saturation and water cut were not measured. They were derived by correlating $P_c$, $S_w$, and water cut (Aufricht and Koepf, 1957). Here, I assume these values are "true". The reservoir is heterogeneous displaying a "gig-saw" pattern of porosity, permeability, and water saturation, which is attributed to alternating lithofacies. The FWL is known at 5450 ft.

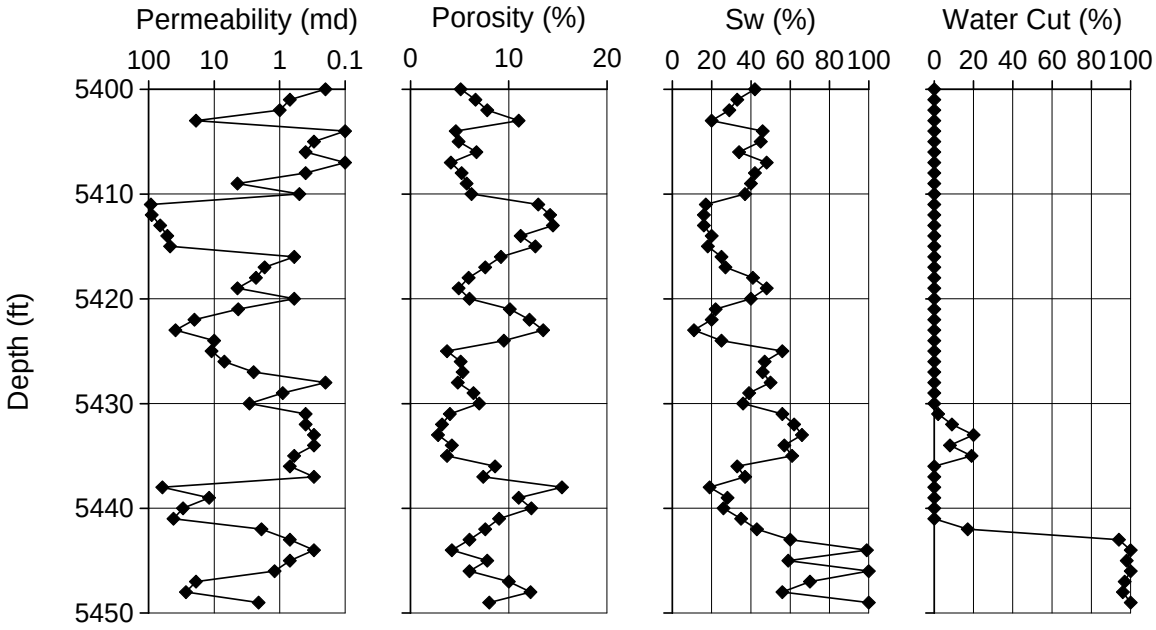


**Figure 8.8 Measured permeability, porosity, and capillary-pressure derived water saturation and water cut, Pennsylvanian Dolomite (data from Aufricht and Koepf, 1957)**

If we approximately divide the reservoir into two lithofacies: “A” and “B”, representing good and poor reservoir, respectively, then capillary-pressure curves for these two lithofacies can be generated based on the average properties of each lithofacies (Figure 8.9).

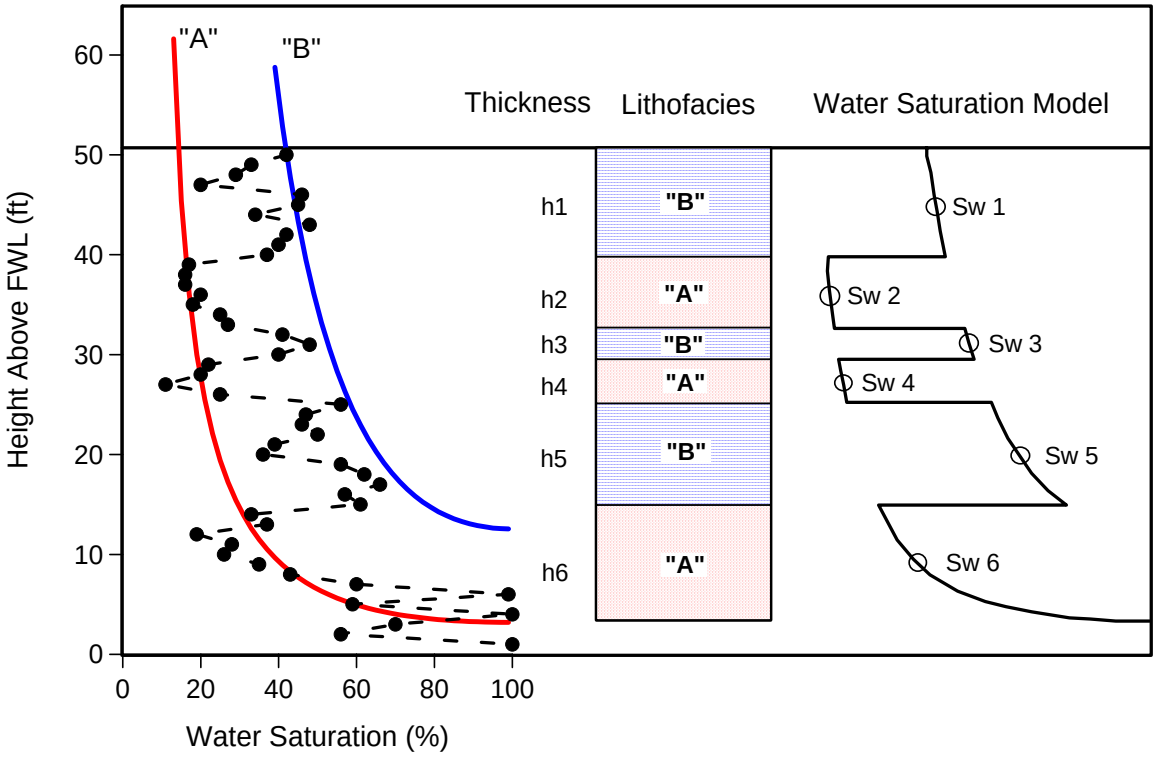


**Figure 8.9 A conceptual saturation model showing effects of reservoir heterogeneity on fluid distribution. The dots are actual water saturations in the reservoir, which is divided into two lithofacies “A” and “B”, and six units. Water saturation model is generated by integrating capillary-pressure curves of the two lithofacies. The mid-depth saturation is approximated as average water saturation of each unit. This model is based on the interpretation of data from Aufricht and Koepf (1957)**

To evaluate the saturation of a heterogeneous reservoir, we can first divide the reservoir into several flow units based on lithofacies (Figure 8.9). A water-saturation model for the entire reservoir can be generated by integrating the capillary-pressure curves of each lithofacies. If we take the mid-depth saturation of each flow unit as the average saturation of that unit, then the overall average saturation of the reservoir weighted by thickness can be calculated by (Amyx et al., 1960):

$$\overline{S_w} = \frac{\sum_{i=1}^{n} S_{wi} h_i}{\sum_{i=1}^{n} h_i} \qquad (8\text{-}6)$$

where $S_{wi}$ is the mid-depth water saturation of flow unit *i*, $h_i$ is the thickness of unit *i*, and *n* is the total number of units. If the area information is available, the average saturation can also be weighted by area. With such information, the initial oil in-place can be evaluated.

### 8.4 Calculating Relative Permeability

Purcell (1949) developed a theoretical equation to calculate absolute permeability from capillary pressure data. This equation can be readily extended to the calculation of relative permeability (Amyx, et al., 1960):

$$k_{rw} = \frac{\int_0^{Sw} dS_w / (P_c)^2}{\int_0^1 dS_w / (P_c)^2} \qquad (8\text{-}7)$$

$$k_{rnw} = \frac{\int_{Sw}^1 dS_w / (P_c)^2}{\int_0^1 dS_w / (P_c)^2} \qquad (8\text{-}8)$$

where $k_{rw}$ and $k_{rnw}$ are the relative permeabilities of wetting-phase and non-wetting phase, respectively.

Burdine (1953) developed equations similar to Purcell's equations by introducing a tortuosity factor as a function of wetting phase saturation. The relative permeability of the wetting phase can be calculated as follows:

$$k_{rw} = (\lambda_{rw})^2 \frac{\int_0^{Sw} dS_w/(P_c)^2}{\int_0^1 dS_w/(P_c)^2} \qquad (8\text{-}9)$$

where $\lambda_{rw}$ is the tortuosity ratio of the wetting phase, and can be calculated as follows:

$$\lambda_{rw} = \frac{S_w - S_{wir}}{1 - S_{wir}} \qquad (8\text{-}10)$$

The relative permeability of nonwetting phase can be calculated by introducing a nonwetting phase tortuosity ratio:

$$k_{rnw} = (\lambda_{rnw})^2 \frac{\int_{Sw}^1 dS_w/(P_c)^2}{\int_0^1 dS_w/(P_c)^2} \qquad (8\text{-}11)$$

where $\lambda_{rnw}$ is the tortuosity ratio of the nonwetting phase, and can be calculated as:

$$\lambda_{rnw} = \frac{1 - S_w - S_{or}}{1 - S_{wir} - S_{or}} \qquad (8\text{-}12)$$

where $S_{or}$ is the residual oil saturation (or residual nonwetting phase saturation)

Honarpour et al. (1986) pointed out that the expression for the wetting-phase relative permeability (equation 8-9) fits the experimental data much better than the expression for the nonwetting phase (equation 8-11). A better fit can be obtained by adjusting the exponent of the nonwetting-phase tortuosity ratio, $\lambda_{rnw}$ in equation 8-11. An exponent of 3 works well in some cases:

$$k_{rnw} = (\lambda_{rnw})^3 \frac{\int_{Sw}^{1} dS_w/(P_c)^2}{\int_{0}^{1} dS_w/(P_c)^2} \qquad (8\text{-}13)$$

Li and Horne (2002) compared different relative permeability models and concluded that although Purcell's model best fit experimental data of wetting-phase relative permeability but it poorly fit nonwetting phase. The Purcell's model (equation 8-7) is used here to calculate wetting-phase relative permeability, and the Burdine's model (equations 8-9 and 8-11) is used to calculate nonwetting-phase relative permeability. Five samples from TX27-34, Yowlumne Field, California, were measured air-water capillary pressures by using centrifuge method. The average capillary pressure curve is calculated with the equation 1. It agrees well with the average trend of the five individual samples (Figure 8.10).

Oil-water capillary pressures can be generated directly from the average properties of the reservoir, or converted from the air-water capillary pressures presented in Figure 8.10. Residual oil saturation, $S_{or}$, is estimated from the water-flood test, which gives an average value of 32%. The calculated relative permeabilities and the measured ones are presented in Figure 8.11. Good agreements between the calculation and measurements have been achieved. Relative permeabilities are affected by many factors, such as saturation history and temperature (Amyx et al., 1960). The calculations are thus somewhat simplified because these factors are not considered. Where direct measurements are unavailable, however, such calculations are valuable because they provide insight into the characteristics of two-phase flow.

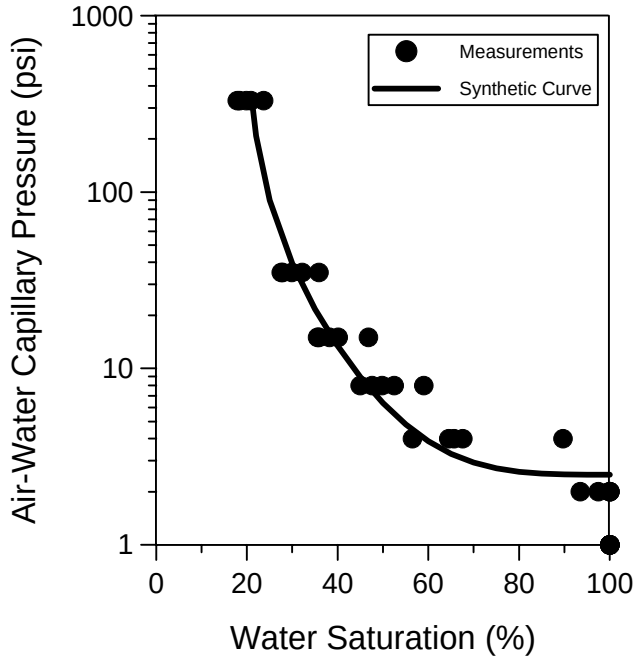


**Figure 8.10 Measured capillary pressures and synthetic average capillary-pressure curve, Stevens Sandstone, T27X-34, Yowlumne Field, Kern County, California.**

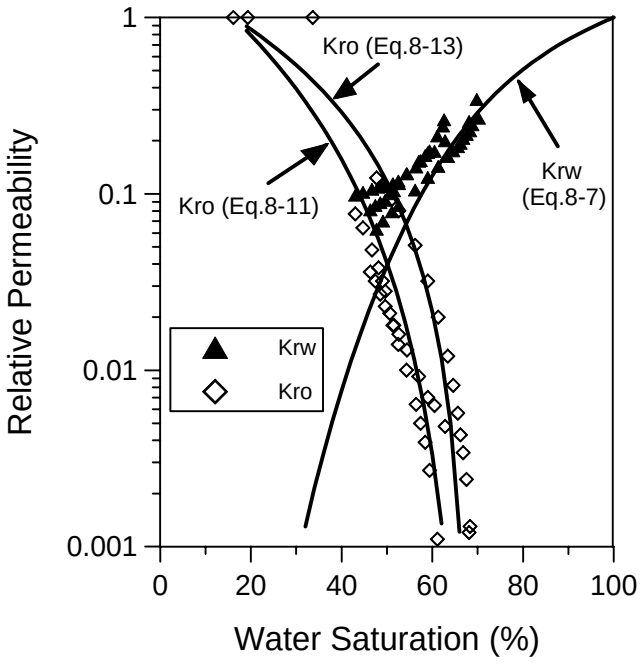


**Figure 8.11 Measured relative permeabilities and calculated relative permeability curves, Stevens Sandstone, T27X-34, Yowlumne Field, Kern County, California.**

# CHAPTER IX

# DISCUSSION

The two objectives of this study are to predict permeability and capillary pressure from other sources like well log. Although good results have been achieved with the methods proposed, uncertainty exists at every step of the prediction of permeability and capillary pressure.

## 9.1 Porosity

Comparison of log interpretation to core analysis need to consider measurement scale. Core analysis is performed on samples varying in size from a few cubic centimeters to a few cubic decimeters, and well logs are measurements over a few cubic meters. This difference in measurement scale causes scatter between these two types of data. Figure 9.1 shows the correlation between core plug porosity and log porosity. The samples come from three wells with a wide range of porosity (10.7 – 31.8%) and permeability (0.6 – 3216 md). The scatter of points tends to cancel off each other, which results in good agreements between averaged values of log porosity and core porosity.

## 9.2 Permeability

Permeability measured on core plugs provide accurate values. Although permeability can not be directly measured from well logs, it can be correlated with well log estimated porosities. Permeability models of well log data are evaluated by comparison with core

plug values. The scale effects also exist in comparison of well log porosity in permeability prediction. Scatters are frequently observed (Figure 9.2). Most of the sample fall into the acceptable range of 0.25 < kc/km < 4. The scatter increases with decreasing permeability. A good fit of average permeabilities is obtained by using the average log porosity, and average grain size (Table 9.1).

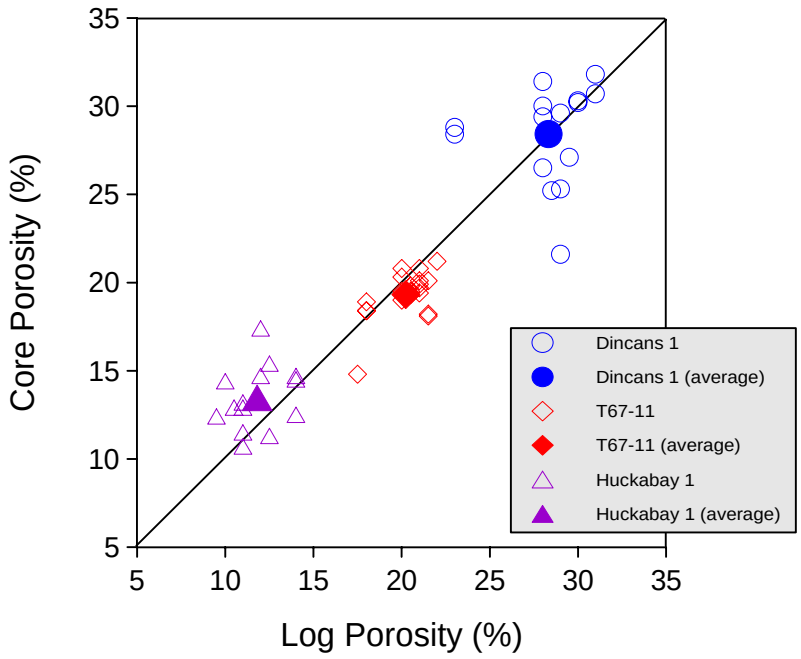


**Figure 9.1 Comparison between core porosity and well log (density) porosity of three different wells. Although the data points scatter around the 1:1 correlation line (diagonal line), the average values fit reasonably well.**

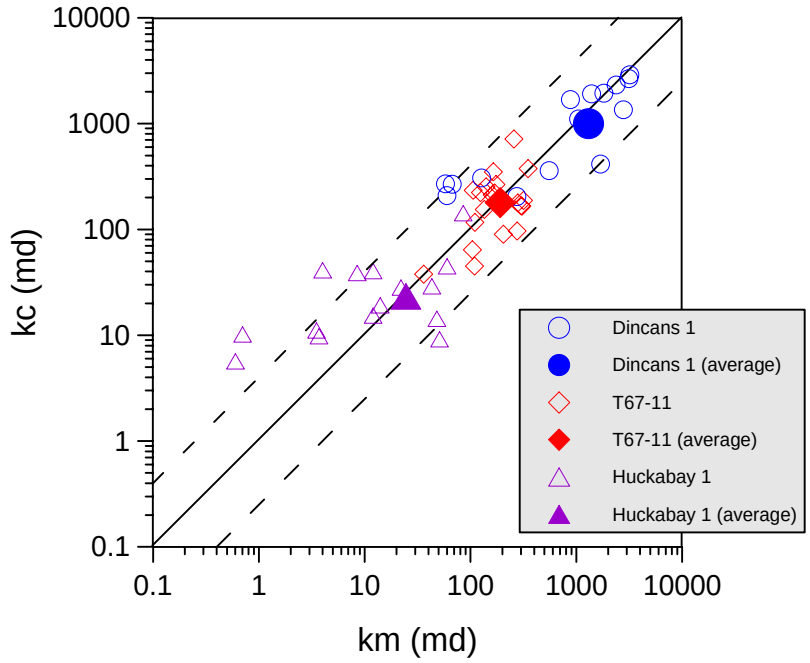


**Figure 9.2 Comparison between measured core permeability (km) and calculated permeability (kc) of the same data sets in Figure 9.1. Permeabilities are calculated with equation 3-19. Dashed lines represent the range of 0.25 < kc/km < 4. The solid diagonal line indicates 1:1 correlation. Core porosities are used in the calculation.**

**Table 9.1 Average properties from core plug and well logs**

| Field | Well | Depth (ft) | Core Porosity (%) | Log Porosity (%) | $P_{90}$ (μm) | km (md) | kc (md) |
|---|---|---|---|---|---|---|---|
| Yegua | Dincans 1 | 8219.3 – 8479 | 28.4 | 28.3 | 0.086 | 1302.9 | 995.3 |
| Yowlumne | T67-11 | 11155.0 –11246.5 | 19.3 | 20.23 | 0.086 | 190.8 | 178.8 |
| J Sandstone | Huckabay 1 | 6179 – 6226 | 13.5 | 11.8 | 0.123 | 24.53 | 23.3 |

$P_{90}$: ninetieth percentile of grain size distribution; km: measured permeability from core plug; kc: calculated permeability with Berg's (1975) equation, $k = 5.3\times10^{-3}\phi^{5.1}(P_{90})^2$.

More often, we need to predict the average porosity and permeability of a reservoir or a section of the reservoir, instead of individual points, which can vary up to four orders of magnitude in closely spaced samples (Bradely et al., 1972). Good

prediction of average permeabilities can be obtained if additional information such as grain size is available, because the permeability-porosity relationship itself is usually not so strong to support a reliable prediction of permeability.

### 9.3 Irreducible Water Saturation

In equation 6-4, a hidden parameter is irreducible water saturation, $S_{wir}$. Irreducible water occurs because small volumes of water lose hydraulic connection with the surrounding water and become trapped in the rock (Morrow, 1971). The water remains as thin films on the grains and round point contacts by adhesion tension in the form of pendular rings (Figure 9.3)

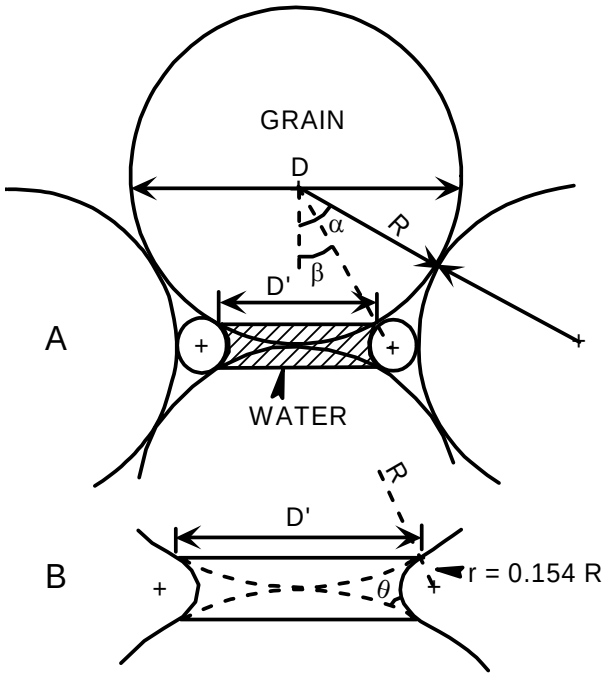


**Figure 9.3 Configuration of pendular rings forming at spherical grain contacts. (A) dimensions of the water and spheres, (B) enlargement showing pore-throat radius and contact angle θ (modified from Berg, 1986).**

Theoretically, hexagonal and cubic packing of equal spheres have $S_{wir}$ of 5.5% and 4.2%, respectively, held entirely as discrete pendular rings of liquid at points of contact between particles (Harris and Morrow, 1964). Other well-mixed packing (including artificial sands of log-normal size distribution) give saturations in the range of 6 – 10% (Table 9.2). The irreducible water saturations for sedimentary rocks are commonly in the range of 15 – 40% (Morrow, 1971). These theoretical and experimental values provide reasonable estimation of $S_{wir}$ for clean sandstones and unconsolidated sands if other information is unavailable.

**Table 9.2 Irreducible water saturation of different sphere packing**

| Sources | Sphere Packing | $\phi$ | $S_{wir}$ | Note |
|---|---|---|---|---|
| Harris and Morrow (1964) | Cubic | 0.476 | 0.042 | Theoretical |
| Harris and Morrow (1964) | Hexagonal | 0.259 | 0.055 | Theoretical |
| Brooks and Corey (1966) | Random | 0.383 | 0.085 | Experimental |
| Morrow (1971) | Random | N/A | 0.06 ~ 0.1 | Experimental |

Mercury injection is commonly used in capillary pressure measurements. However, mercury injection test does not always lead to a definite $S_{wir}$ (Figure 9.4a). High applied externally pressure (i.e., greater than 1000 psi) may fracture the sample and allow greater than expected mercury volume to be injected and no $S_{wir}$ recorded. Another explanation is that air is not a perfect wetting phase, it can slip away from the smallest pore space without being adhered to grain surface. In this case, it does not make too much sense to estimate $S_{wir}$, although it can be approximately defined by the inflection point at high-pressure section. As shown in figure 10a, both 0% and 10% of $S_{wir}$ give good match to experimental data. In fact, what we are interested is real capillary pressure behavior

under subsurface conditions. If we can simulate that behavior directly, there is no need to concern $S_{wir}$ in mercury-injection test.

It is relatively easy to define $S_{wir}$ in centrifugal method. Air is commonly used as non-wetting phase, and water is used as wetting phase. It is closer to subsurface condition than air-mercury system and usually displays $S_{wir}$. Sometimes, $S_{wir}$ might be absent because of pressure limit of the instrument or small pores of the sample. In Figure 9.4b, a $S_{wir}$ of 35% is estimated, it is arbitrary, but reasonable based on the sample's lithology (shaly) and low permeability. This estimation also gives a perfect fit to the measurement.

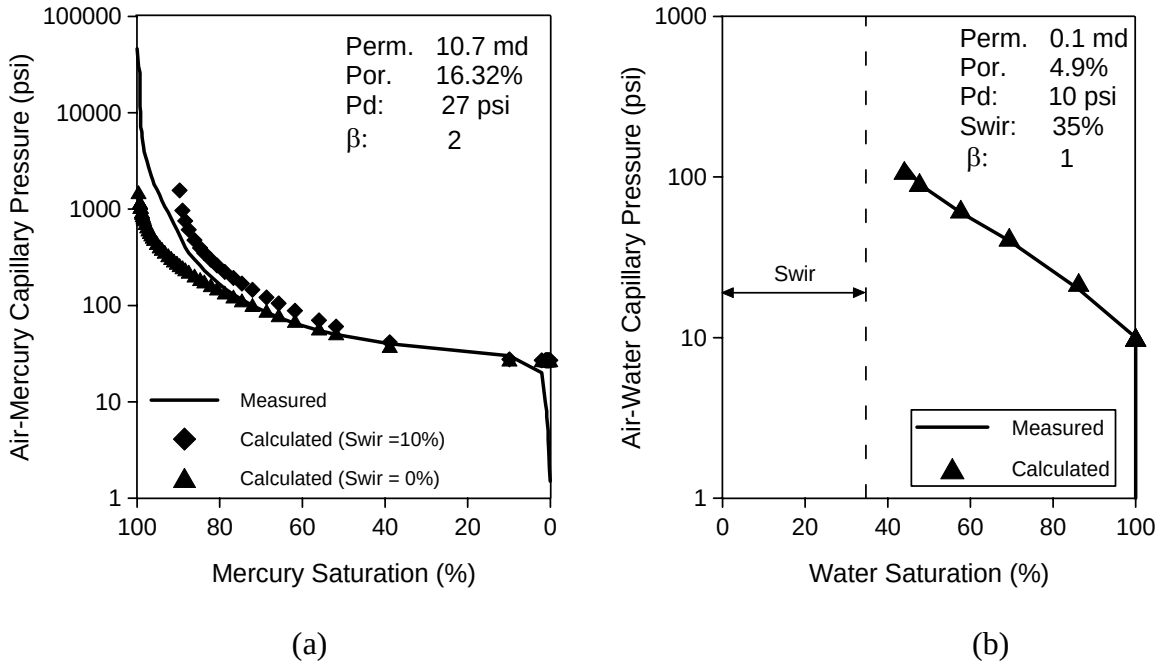


**Figure 9.4 Capillary pressure curves showing (a) zero $S_{wir}$, for high-pressure mercury injection test (data from Doublet, 1999); and (b) no definite $S_{wir}$ for air-water centrifugal test (data from John Calhoun, personal communication).**

In practice, a useful tool to estimate $S_{wir}$ is NMR log. Hodgkins and Howard (1999) claimed that $S_{wir}$ estimation from NMR-based pore-size distributions correspond well with independent measures from special core flood tests. Another approach is though empirical correlations. There are numerous empirical equations in literature that correlate $S_{wir}$ with porosity and permeability (Morris and Biggs, 1967, Timur, 1968, and Schlumberger, 1988). Such kind of empirical correlations can be easily established if lots of data are available.

### 9.4 Displacement Pressure

Displacement pressure ($P_d$) was obtained by extending capillary pressure curve to 100% percent wetting phase saturation. When the plateau is obvious (Figure 9.4), it is easy to estimate $P_d$. If the plateau is absent (Figure 9.5), it would be difficult to apply this method. In Figure 9.5, three values (20 psi, 10 psi and 3 psi) can be obtained by extending the three different segments of the curve to 100% water saturation. Based on the low permeability, 10 psi or 20 psi is a more reasonable estimation of displacement pressure. In such case, $P_d$ can be estimated from equation 6-5 because that equation is based on 96 samples with definite plateau. The calculated Pd (converted to air/water system) is 20 psi. For low permeability (<1md )samples, the model proposed in this study (equation 6-4) does not always work well. But low permeable rocks are usually seals, for which our major concern is how much oil can be trapped, instead of the saturation distribution within the seals. Oil column is controlled by $P_d$, or $P_{c35}$, which can be satisfactorily estimated from equation 6-5 or Winland's equation (equation 5-4).

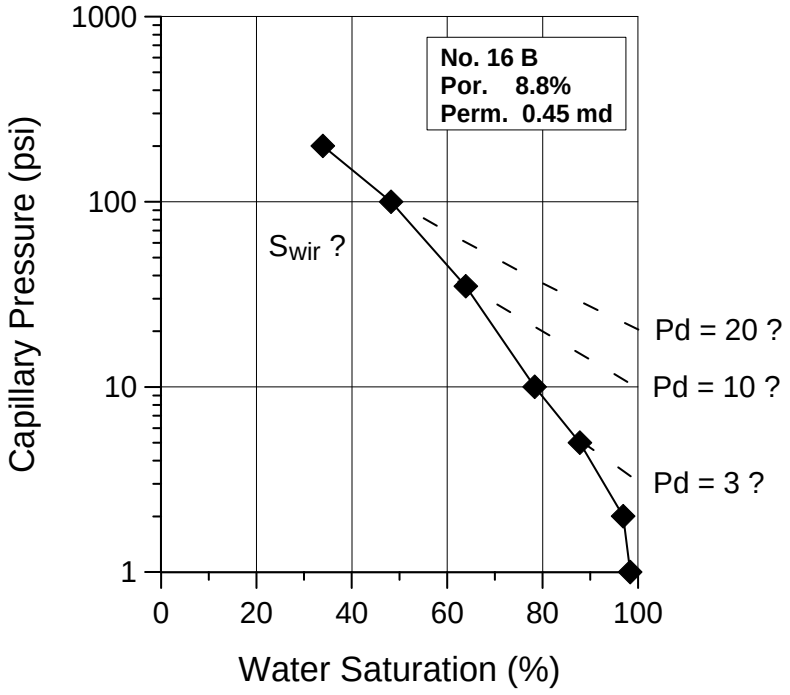


**Figure 9.5 A air-water plate capillary pressure curve showing no definitive $S_{wir}$ and $P_d$ (data from Dr. John Calhoun, 2002, personal communication).**

## 9.5 Interfacial Tension and Contact Angle

Approximations are commonly used for interfacial tension ($\sigma$) and contact angle ($\theta$) (Chapter VI). Because most sandstones are initially water wet (Berg, 1975), it is reasonable to assume 0° contact angle in the calculation of drainage capillary-pressure curve. More accurate estimates of interfacial tension can be made from recent correlations (Firoozabadi and Ramey, 1988). For pure compounds, the interfacial tension is a function of hydrocarbon/water density difference and temperature (Figure 9.6).

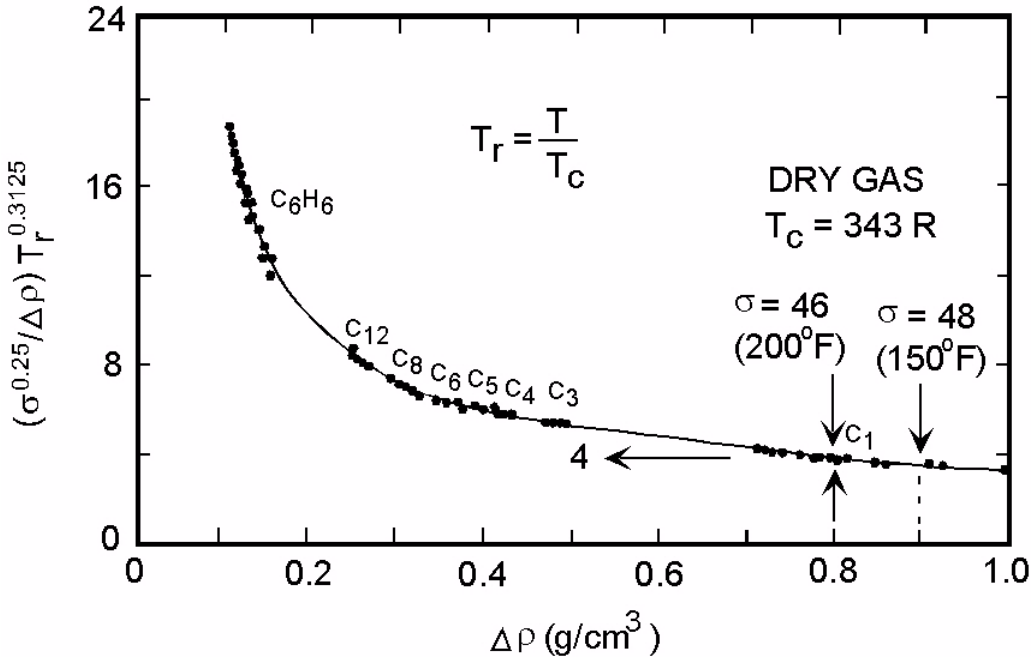


**Figure 9.6 Surface tensions between water and pure compounds correlated with reduced temperature (Tr) showing the range of values for dry gas (methane) in the subsurface (modified from Firoozabadi and Ramey, 1988).**

The following example shows the procedure to estimate interfacial tension of dry gas and water (from Berg, 2003, personal communication).

| | |
|---|---|
| Depth: | 10,000 ft |
| Gas density: | 0.2 g/cm3 |
| Water density: | 1.0 g/cm3 |
| Density difference ($\Delta\rho$): | 0.8 g/cm3 |
| Reservoir temperature: | 200 °F + 460 ° = 660 °R |

(based on a normal geothermal gradient)

A density difference of 0.8 g/cm3 (Figure 9.6) gives:

$$(\sigma^{0.25} / \Delta\rho) T_r^{\,0.3125} = 4.0$$

and the reduced temperature, $T_r$, is:

$$T_r = T/ T_c$$

Where T is the reservoir temperature and Tc is the critical temperature for pure methane (343 °R), so

$$T_r = 660°R/343°R = 1.92$$

Rearranging the terms of the correlation equation and inserting values gives:

$$\sigma = (4.0 \times 0.8 / 1.92^{0.3125})^4 = 46 mN/m$$

This value agrees with other measurements.

Oil-water interfacial tensions were based only on oil-water density difference (Figure 9.7). The correlations give interfacial tensions of 23 to 39 mN/m, which compare well with other measured values.

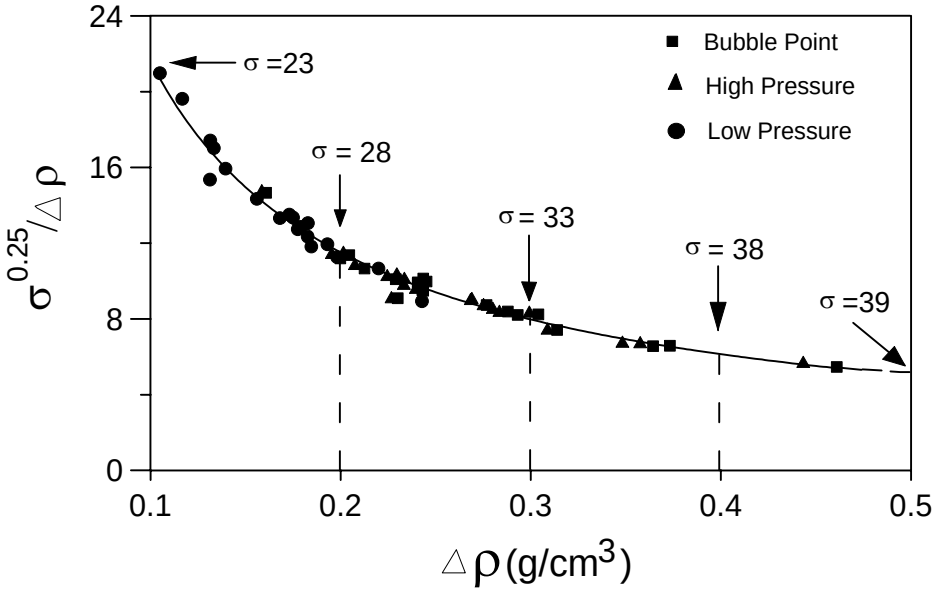


**Figure 9.7 Surface tensions between water and reservoir oils showing values for a wide range of oil-water density difference (modified from Firoozabadi and Ramey , 1988).**

# CHAPTER X

# CONCLUSIONS

Knowledge of reservoir porosity, permeability, and capillary pressure is essential to exploration and production of oil and gas. Porosity can be interpreted from well logs, but permeability and capillary pressure must be measured in cores or estimated from well logs.

A detailed literature review has been conducted. The variables that affect permeability and capillary pressures have been investigated. Permeability is directly controlled by pore-throat size and distribution, especially the largest connected pore-throat size. Although porosity, grain size, and specific surface area vary with permeability, they are considered as secondary variables. Capillary pressure is a function of pore-throat size and can be estimated if permeability and/or porosity are known.

Permeability is correlated with porosity to predict permeability and capillary pressures. Diagenetic processes (compaction, cementation, dissolution, and occurrence of clay minerals) reduce the effective porosity available to fluid flow. To better predict permeability, effective porosity is estimated. The general equation for effective porosity is expressed as:

$$\phi_e = \phi_t - \phi_{cl} - \phi_d \qquad (10\text{-}1)$$

where $\phi_d$ is the dissolution porosity, and $\phi_{cl}$ is the clay-bound microporosity.

The clay-bound microporosity is estimated as:

$$\phi_{cl} = \sum_j V_{clj}\phi_{mj} \qquad (10\text{-}2)$$

$V_{clj}$ is the volume of clay mineral j, $\phi_{mj}$ is the average microporosity of 100% clay mineral j. Direct measurements of the microporosity of each clay mineral is difficult and time consuming. Empirical values are proposed for each category of diagenetic clay, i.e., 20% for discrete clays, 70% for pore-lining clays, and 90% for pore-bridging clays.

A large number of sandstone samples of different composition, grain size, and sorting were examined. Porosity ranges from 5% to 35%, and permeability ranges from less than 0.1 md to over 1000 md. The samples examined were collected from publications, including a large number of samples reported in studies at Texas A&M.

The following regression equation is applied to estimate permeability from effective porosity:

$$\ln k = 21.42 + 11.425 \ln \phi_e + 1.327(\ln \phi_e)^2 \qquad (10\text{-}3)$$

Theoretical models, such as Kozeny-Carman equation and its derivatives can be improved by using effective porosity, if additional information, such as specific surface area or grain size, is available.

The following equation can be used to estimate air-mercury displacement pressure:

$$\ln P_d = 5.458 - 1.255 \ln \sqrt{k/\phi} + 0.081(\ln \sqrt{k/\phi})^2 \qquad (10\text{-}4)$$

Equation 10-4 is based on 7 published data sets including 96 sandstone, shaly sandstone, and carbonate samples, with a wide range porosity (7.3 to 40.7%) and permeability (0.02 to 2580 md). The coefficient of correlation ($R^2$) is 0.92.

A modified Thomeer's equation (1960) is used to generate a continuous mercury injection capillary pressure vs. saturation curve:

$$\log P_c = -F_g / \ln(\frac{1-S_w}{1-S_{wir}}) + \log P_d \qquad (10\text{-}5)$$

where the pore geometrical factor, Fg, can be estimated by rearranging Thomeer's equation (1983) as:

$$F_g = e^{[1.3368+2\ln(100S_{b\infty}/P_d)-\ln k]/1.3334} \qquad (10\text{-}6)$$

Because some samples are unsuitable to assign a *Fg* value (shaly sandstone and low permeable samples). A new equation is proposed based on the work of Bentsen and Anli (1976) and Harris and Goldsmith (2001):

$$P_c = P_d + \sigma\cos\theta\sqrt{\phi/k}(\ln 1/S_e)^{\beta} \qquad (10\text{-}7)$$

Parameter "β" is the "shape factor". It controls the curvature of a $P_c$ vs. $S_w$ curve, and usually varies between 1-3. Empirical rules are proposed to assume a suitable β value. The merits of this model lie in: (1) all the parameters have physical meanings, and can be measured from routine core analysis, estimated from well log, and assumed; (2) capillary-pressure curves start at $P_d$ as water saturation equal to 1 (i.e., Se = 1); (3) the β varies in a small range, and a default value of 2 works well for a wide range of lithology; (4) interfacial tension and wettability are included.

Equation 10-7 has been tested with a large data set (over 200 samples) covering a wide range of lithology (limestone, dolomite, sandstone, shaly sandstone, and shale), and different laboratory methods (mercury injection, centrifugal, and porous plate). It provides a good empirical fit to experimental capillary pressures. The major challenge in application is to estimate the parameters from other sources, such as well log. The model

is applied to evaluate sealing capacity of seals, to calculate transition zone thickness and water saturation above free water level in reservoirs. Goods results are achieved through integration of well log data, production data, core, and geological concepts. The model will find more applications for defining reservoirs and seals.

# NOMENCLATURE

$\phi$ = porosity, fraction

$\phi_{sd}$ = clean sand or sandstone porosity, fraction

$\phi_{sh}$ = pure shale porosity, fraction

$\phi_m$ = microporosity, fraction

$\phi_d$ = dissolution porosity, fraction

$\varphi_v$ = clay volume, fraction

$k$ = permeability, millidarcy

$k_{sd}$ = clean sandstone permeability, millidarcy

$k_m$ = measured permeability, millidarcy

$k_c$ = calculated permeability, millidarcy

$\tau$ = tortuosity, dimensionless

$S_g$ = specific internal surface, $\mu m^{-1}$

$d_w$ = mean grain diameter (by weight in mm)

$\sigma_{phi}$ = standard deviation of grain diameter in phi units, where phi = $-\log_2 d$ (mm)

$d_N$ = mean grain diameter by number in mm, where $d_N = d_w \exp(-1.44\sigma_{phi}^2)$

d = median grain size in mm,

msd = cementation exponent for clean sandstone, $1.5 \leq msd \leq 2$

mcs = cementation exponent for clayey sand, dimensionless

$S_w$ = water/wetting phase saturation, fraction

$S_{wir}$ = irreducible water saturation, fraction

$S_e$ : effective water saturation, fraction

$S_{nw}$ = non-wetting phase saturation, fraction

$S_b$ = bulk volume occupied by non-wetting phase, percent

$S_{b\infty}$ = bulk volume occupied by non-wetting phase at infinite pressure, percent

$V_{sh}$ = shale volume, fraction

$f$ = lithology factor, dimensionless

$F_g$ = pore geometrical factor, dimensionless

$\lambda$ = pore size distribution factor, dimensionless

$P_c$ = capillary pressure, psi

$P_d$ = displacement pressure, psi

$T_1, T_2$ = nuclear magnetic resonance decay time, milliseconds

$r$ = pore-throat size, μm

$r_{10}$ = pore-throat size corresponding to 10% non-wetting phase saturation

$r_{35}$ = pore-throat size corresponding to 35% non-wetting phase saturation

$l_c$ = effective pore size (diameter), μm

$\gamma$ = interfacial tension, dynes/cm

$\theta$ = contact angle

$\sigma$ = electrical conductivity of the rock

$\sigma_0$ = electrical conductivity of the saturant

$\beta$ = shape factor, varies between 1 - 3

# REFERENCES CITED

Aguilera, R., 2002, Incorporating capillary pressure, pore throat aperture radii, height above free-water table, and Winland r35 values on Pickett plots: AAPG Bulletin, v.86, p. 605-624

Amaefule, J. O., D. G. Kersey, D. M. Marschall, J. D. Powell, L. E. Valencia, and D. K. Keelan, 1988, Reservoir description: a practical synergistic engineering and geological approach based on analysis of core data, SPE paper 18167: Society of Petroleum Engineers, presented at 63th Annual Technical Conference and Exhibition, 30p.

Amyx, 1960, J. W., D. M. Bass, and R. L. Whiting, 1960, Petroleum reservoir engineering: McGraw-Hill, New York, 610 p

Anguy, Y., R. Ehrlich, C. M. Prince, V. L. Riggert, and D. Bernard, 1994, The sample support problem for permeability assessment in sandstone reservoirs, *in* J.M., Yarus and R.L. Chambers, eds. Stochastic modeling and geostatistics, AAPG Computer Application in Geology, No.3, Chapter 5, p.37-54

API document, 1998, Recommended practices for core analysis, 2nd ed., American Petroleum Institute, document No. API-RP 40, 200 p.

Archie, G. E., 1942, The theoretical resistivity log as an aid in determining some reservoir characteristics: American Institute of Mining and Metallurgical Engineers, Transactions, v.146, p.54-61

Archie, G. E., 1950, Introduction to petrophysics of reservoir rocks: AAPG Bulletin, v.34, p.943-961

Arps, J. J., 1964, Engineering concept useful in oil finding: AAPG Bulletin, v.48, p. 157-165

Asquith, G.B., 1990, Log evaluation of shaly sandstones: a practical guide, AAPG continuing education course note series #31, 59 p.

Aufricht W. R. and E. H., Koepf, 1957, The interpretation of capillary pressure data from carbonate reservoirs: American Institute of Mining and Metallurgical Engineers Transactions, v. 210, p. 402-405

Basan, P. B., B. B. Lowden, P. R. Whattler, and J. J. Attard, 1997, Pore-size data in petrophysics: a perspective on the measurement of pore geometry, *in*: M. A. Lovell, and P. K. Harvey, ed., Development in petrophysics: Geological Society Special

Publication no.122, p.47-67

Bass, D. M. Jr., 1992, Properties of reservoir rocks, *in*: H. B. Bradley, ed. Petroleum engineering handbook: Society of Petroleum Engineering, Chapter 26. 33p.

Beard, D. C., and P. K. Weyl, 1973, Influence of texture on porosity and permeabilityof unconsolidated sand: AAPG Bulletin, v. 57, p. 349-360

Bentsen, R. G., 1984, A functional relationship for macroscopic capillary pressure: SPE paper 13831, 25p.

Bentsen, R. G. and J. Anli, 1976, A new displacement capillary pressure model: The Journal of Canadian Petroleum Technology, v. 15, p. 75-79

Berg, C. R., 1996, Effective–medium resistivity models for calculating water saturation in shaly sands: The Log Analyst, v.37, p.16-28

Berg, R. R., 1970, Method for determining permeability from reservoir rock properties, Transaction: Gulf Coastal Association of Geological Societies, v.XX, P.303-317.

Berg, R. R., 1975, Capillary pressure in stratigraphic traps: AAPG Bulletin, v.59, p.939-956

Berg, R. R., 1986, Reservoir sandstones: Prentice-Hall, Inc., Englewood Cliffs, New Jersey, 481p.

Berg, R. R. and G. R. Royo, 1990, Channel-fill turbidite reservoir, Yowlumne Field, California: in J. H. Barwis, J. G. McPherson, and J. R. J. Studlick eds., Sandstone Petroleum Reservoirs, Springer-Verlag, New York , p. 467-487

Berg, R. R. and A. H. Avery, 1995, Sealing properties of Tertiary Growth faults, Texas Gulf Coast: AAPG Bulletin, v.79, p.375-393

Bradley, J. S., R. W. Duschatko, and H. H. Hinch, 1972, Pocket permeameter: Hand-held device for rapid measurement of permeability: AAPG Bulletin, v. 56, p. 568-571

Brooks, R. H. and A. T. Corey, 1966, Properties of porous media affecting fluid flow: Journal of Irrigation and Drainage Division, Proceedings of the American Society of Civil Engineers, v.92, No. IR 2, p.61-88

Brown, A. A., 1993, Fluids contact, *in* D. Morton-Thompson and A. M. Woods, eds., Development geology reference manual: AAPG Methods in Exploration Series. No. 10, Tulsa, Oklahoma, AAPG, p. 221-225

Brown, H. W., 1951, Capillary pressure investigations: American Institute of Mining and Metallurgical Engineers, Transactions, 192, 67-74

Burdine, N. T., L. S. Gournay, and P. P. Reichertz, 1950, Pore size distribution of petroleum reservoir rocks: American Institute of Mining and Metallurgical Engineers, Transactions, v.189, p.195-204

Byrant, S., C. Cade, and D. W. Mellor, 1993, Permeability prediction from geologic models: AAPG Bulletin, v.77, p.1338-1350.

Carman, P.C., 1937, Fluid flow through granular beds: American Institute of Chemistrical Engineers Transactions, v.15, p.150-166

Carman, P. C., 1956, Flow of gases through porous media, Butterworth's Scientific Publications, London, 128 p.

Chatzis, I. and F. A. L. Dullien, 1985, The modeling of mercury porosimetry and the relative permeability of mercury in sandstones using percolation theory: International Chemical Engineers, v. 25, p. 47-66

Chuber, S., 1972, Milbur (Wilcox) field, Milam and Burleson counties, Texas, *in* R. E. King, eds., Stratigraphic oil and gas fields: AAPG Memory, no. 16, p. 399-405

Coates, G. R., R. C. A. Peveraro, A. Hardwick, and D. Roberts, 1991, The magnetic resonance imaging log characterized by comparison with petrophysical properties and laboratory core data, Paper 22723, Proceedings of the Society of Petroleum Engineers 66th Annual Technical Conference and Exhibition, 4p.

Corbett, P.W.M., P. S. Ringrose, J. L. Jensen, and K. S. Sorbie,1992, Laminated clastic reservoirs: the interplay of capillary pressure and sedimentary architecture: SPE-24699: Society of Petroleum Engineers, presented at 67th annual technical conference, 12p

Cornell D. and D. L. Katz , 1953, Flow of gases through consolidated porous media: Industry Engineering Chemistry, v. 45, p. 2145-2152

Cuddy, S., G. Allinson, and R. Steele, 1993, A simple, convincing model for calculating water saturations in Southern North Sea gas fields: Paper H, SPWLA 34th Annual Logging Symposium, June 13th – 16th .

Darcy, H., 1856, Determination des lois d'ecoulement del'eau a travers le sable, *in* Hubbert, M. K., 1969, The theory of ground water motion and related papers: Hafner Publishing Company, New York, p. 303-311.

Doublet L. E., 2001, An integrated geologic and engineering reservoir characterization of the North Robertson (Clear Fork) Unit, Gaines County, TX: Ph.D. Dissertation, Texas A&M University, College Station, TX, Volume Ⅱ, 660p

Dullien, F. A. L., 1992, Porous media: fluid transport and pore structure, 2nd edition:

Academic Press, San Diego, 574 p.

Ebanks, W. J., Jr., M. H. Scheihing, and C. D. Atkinson, 1993, Flow units for reservoir characterization, *in* D. M. Thompson and A. M. Woods, eds., Development geology reference manual: AAPG Methods in Exploration Series, no. 10, Tulsa, Oklahoma, AAPG, p.282-285

Ehrenberg, S. N., 1990, Relationship between diagenesis and reservoir quality in sandstone of the Garn formation, Haltenbanken, mid-Norwegian continental shelf, AAPG Bulletin, v.74, p.1538-1558

Ehrlich, R., S. J. Crabtree, K. O. Horkowitz, and J. P. Horkowitz, 1990, Petrography and reservoir physics I: objective classification of reservoir porosity: AAPG Bulletin, v.70, p.1547-1562.

Fatt, I., 1956, The network model of porous media, parts I: American Institute of Mining and Metallurgical Engineers Transactions, v. 207, p. 144-159

Firoozabadi, A., and H. J. Ramey, Jr., 1988, Surface tension of water-hydrocarbon systems at reservoir conditions: Canadian Petroleum Technology Journal, v. 27, p. 41-48

Folk, R. F., 1974, Petrology of sedimentary rocks: Hemphill Publishing, Austin, Texas, 182 p.

Gangi, A. F., 1985, Permeability of unconsolidated sands and porous rocks: Journal of Geophysical Research, v.90, p.3099-3104

Graton L. C. and H. J. Fraser, 1935, Systematic packing of spheres with particular relation to porosity and permeability: Journal of Geology, v. 43, p. 785-909

Guthrie, R. K. and M. H. Greenburger, 1955, The use of multiple correlation analyses for interpreting petroleum engineering data: presented at the Spring Meeting of the S.W. District Divison of Production, New Orleans, LA

Hagiwara, T., 1984, Archie's *m* for permeability, SPE paper 13100, Proceedings of the Society of Petroleum Engineers 59th Annual Technical Conference and Exhibition, 9p

Harris, C. C. and N. R. Morrow, 1964, Pendular moisture in packings of equal spheres: Nature, v. 203, p. 706-708

Harris, R. G. and P. J. Goldsmith, 2001, Water saturation analysis and interpretation of a tilted free-water level in the Joanne/Judy chalk field, U.K. North Sea, paper EEE, *in* 42nd Annual Logging Symposium Transactions: Society of Professional Well Log Analysts

Hartmann, D. J. and E. A. Beaumont, 1999, Predicting reservoir system quality and performance: in E.A. Beaumont and N.H. Foster ed., Treatise of Petroleum Geology/Handbook of Petroleum Geology: Exploring for Oil and Gas Traps, Ch9, p.1-154

Hawkins, J. M., D. L. Luffel, and T. C. Harris, 1993, Capillary pressure model predicts distance to gas/water,oil/water contact, Oil & Gas Journal, Jan.18, p.39-43

Haynes, B., 1995, An evaluation of a method to predict unknown water levels in reservoirs and quantifying the uncertainty: Society of Petroleum Engineers, Production Operations Symposium, Oklahoma City, OK, SPE paper 29466, p.225-232

Hearst, J. R., P. H. Nelson, and F. L. Paillet, 2000, Well logging for physical properties, 2nd edition, John Wiley & Sons Ltd., West Sussex, England, 483p

Heseldin, G. M., 1974, A method of averaging capillary pressure curves: Society of Professional Well Log Analysts 15th Annual Logging Symposium Transactions: paper I

Hintz, J. C., 2001, Trapping capacity of fault zones, downdip Yegua Formation, Texas Gulf Coast Basin: M.S. thesis, Texas A&M University, College Station, TX, 188p

Hodgkins, M. A., and J. J Howard, 1999, Application of NMR logging to reservoir characterization of low-resistivity sands in the Gulf of Mexico: AAPG Bulletin, v.83, p.114-127

Honarpour, M. M., L. Koederitz, and A. H. Harvey, 1986, Relative Permeability of Petroleum Reservoirs, *CRC* press, Boca Raton, Florida, 143p

Houseknecht, D. W., 1993, Thins section analysis, *in* D. M. Thompson and A. M. Woods, eds., Development geology reference manual: AAPG Methods in Exploration Series, no. 10, Tulsa, Oklahoma, AAPG, p.233-236

Hubbert, M. K., 1940, The theory of groundwater motion: Journal of Geology, v. 48, p.785-944

Hurst, A. and P. H. Nadeau, 1995, Clay microporosity in reservoir sandstones: an application of quantitative electron microporosity in petrophysical evaluation: AAPG Bulletin, v.79, p.563-573

Jennings, J. B., 1987, Capillary pressure techniques: application to exploration and development geology: AAPG Bulletin, v.71, p. 1196-1209

Johnson A., 1987, Permeability averaged capillary data: a supplement to log analysis in field studies: Society of Professional Well Log Analysts 28th Annual Logging

Symposium Transactions: paper EE,

Kamath J., 1988, Evaluation of accuracy of estimating air permeability from mercury injection data, SPE paper 18181, 14 p.

Katz, A. J. and A. H. Thompson, 1986, Quantitative prediction of permeability in porous rocks, Physical Review B, v.34, p.8179-8181

Keelan, D. K. 1972, A critical review of core analysis techniques: Journal of Canadian Petroleum Technology, v. 2., p. 42-55

Kenyon, W. E., P. I. Day, C. Straley, and J. E. Willemsen, 1988, A three-part study of NMR longitudinal relaxation properties of water-saturated sandstones: SPE Formation Evaluation, v.3, p.622-636

Klinkenberg, L. J., 1941, The permeability of porous media to liquids and gases: API drilling and production practices, p. 200-213

Kolodzie Jr. S., 1980, Analysis of pore throat size and use of the Waxman-Smits equation to determine OOIP in Spindle field, Colorado:Society of Petroleum Engineers 55th Annual Technical Conference, SPE paper 9382, 10p.

Korvin, G., 1992, Fractal models in the earth sciences: Elsevier, Amsterdam, New York, 396 p.

Kozeny, J., 1927, Ober kapillare Leitung des Wassers in Boden: Sitzungsbericht der Wiener Akademie, Abteilung Πa, v.136, p.271

Krumbein, W. C., and G. D. Monk, 1942, Permeability as a function of the size parameters of unconsolidated sand: American Institute of Mining and Metallurgical Engineers, Transactions, v.151, 153-162

Kwon, B. B., and G. R. Pickett, 1975, A new pore structure model and pore structure interrelationships: Society of Professional Well Log Analysts 16th Annual Logging Symposium, 14p.

Leverett, M. C., 1941, Capillary behavior in porous solids: American Institute of Mining and Metallurgical Engineers, Transactions, v.142, 152-169

Li, K. and R. N. Horne, 2002, Experimental verification of models to calculate relative permeability using capillary pressure data: SPE paper 76757, presented at the SPE Western Regional/AAPG Pacific Section Joint Meeting, Anchorage, Alaska

Ma, S., N. R. Morrow, and X. Zhang, 1994, Determination of Archie's cementation exponent from capillary pressure measurements: The International Symposium on Well-Logging Technology, Xian, China, 12p

Mavko G. and A. Nur, 1997, The effect of a percolation threshold in the Kozeny-Carman relation: Geophysics, v. 62, p. 1480-1482.

Martin, A. J., S. T. Solomon, and D. J. Hartmann, 1997, Characterization of petrophysical flow units in carbonate reservoirs: AAPG Bulletin, v. 81, p. 734-759.

McDougall, S. R., J. Cruickshank, and K. S. Sorbie, 2002, Anchoring methologies for pore-scale network models: application to relative permeability and capillary pressure prediction: Petrophysics, v.43, p.363-375

Milliken, K. L., 2001, Diagenetic heterogeneity in sandstone at the outcrop scale, Breathitt Formation (Pennsylvanian), eastern Kentucky: AAPG Bulletin, v.85, p.795-815

Morris, R. L., and W. P. Biggs, 1967, Using log-derived values of water saturation and porosity: Society of Professional Well Log Analysts Annual Logging Symposium, 26 p.

Morrow, N. R., 1971, Small scale packing heterogeneities in porous sedimentary rocks: AAPG Bulletin, v. 55, p.514-522

Nadeau, P. H., and A. Hurst, 1991, Application of back-scattered electron microscopy to the quantification of clay mineral microporosity in sandstones: Journal of Sedimentary Petrology, v.61, p.921-925

Nakornthap, K. and R. D. Evans, 1986, Temperature-dependent relative permeability and its effect on oil displacement by thermal methods: SPE Reservoir Engineering, May, p. 230-242

Neasham, J. W., 1977, The morphology of dispersed clay in sandstone reservoirs and its effect on sandstone shaliness, pore space, and fluid flow properties: SPE paper 6858.

Nelson, P. H., 1994, Permeability-porosity relationships in sedimentary rocks, Log Analyst, May-June, 38-62

Nelson, P. H., 2000, Evolution of permeability-porosity trends in sandstones: Society of Professional Well Log Analysts 41st Annual Logging Symposium, June 4-7

Ohen, H. A. and D. G. Kersey, 1993, Permeability, *in* D. M. Thompson and A. M. Woods, eds., Development geology reference manual: AAPG Methods in Exploration Series, no. 10, Tulsa, Oklahoma, AAPG, p.210-213

Pape, H., C. Clauser, and J. Iffland, 1999, Permeability prediction based on fractal pore-space geometry: Geophysics, v.64, p.1447-1460

Patchett, J. G., 1975, An investigation of shaly sand conductivity, paper U, *in* 16th

Annual Logging Symposium Transactions: Society of Professional Well Log Analysts

Petty, D. M., Depositional facies, texture characteristics, and reservoir properties of dolomites in Frobisher-Alida interval in southwest North Darkota: AAPG Bulletin, v.72, p.1229-1253.

Pike, J. D., 1981, Feldspar diagenesis in the Yowlumne sandstone, Kern County, California: M.S. thesis, Texas A&M University, College Station, TX, 132p.

Pittman, E. D., 1979, Porosity, diagenesis and productive capability of sandstone reservoir, *in* Scholle, P.A. and P.R. Schluger, eds. Aspects of Diagenesis, SEPM Special Publication, No.26, p.159-173

Pittman, E. D., 1992, Relationship of porosity and permeability to various parameters derived from mercury injection-capillary pressure curves for sandstone: AAPG Bulletin, v.76, p.191-198

Poiseuille, J.L.M., 1840, Le Movement des liquids dans des tubes de petite diameters: Comp. Rendus Acad. Sci., v.11, p.961-967

Purcell, W. R., 1949, Capillary pressures-their measurement using mercury and the calculation of permeability therefrom: American Institute of Mining and Metallurgical Engineers, Transactions, v.186, p.39-48

Revil, A., and L. M. Cathles Ш, 1999, Permeability of shaly sands: Water Resources Research, v.35, p.651-662

Ringrose, P.S., K. S. Sorbie, O. W. M. Corbett, and J. L. Jensen, 1993, Immiscible flow behaviour in laminated and cross-bedded sandstones: Journal of Petroleum Science and Engineering, v.9, p.103-124

Royo, G. R., 1986, Environment of desposition of the Yowlumne sandstone: internal morphology and rock properties, Kern County, California: M.S. thesis, Texas A&M University, College Station, TX, 167p

Schlumberger, 1988, Probing for permeability: an introduction to measurements: The Technical Review, v. 36, p. 6-20

Schlumberger, 2003, http://www.glossary.oilfield.slb.com/Display.cfm?Term=effective%20porosity

Schowalter, T. T. 1979, Mechanics of secondary hydrocarbon migration and entrapment: AAPG Bulletin, v. 63, p.723-760

Schowalter, T. T. and P. D. Hess, 1982, Interpretation of subsurface hydrocarbon shows:

AAPG Bulletin, v. 66, p. 1302-1327

Sen, P. N., C. Straley, W. E. Kenyon, and M. S. Whittingham, 1990, Surface-to-volume ratio, charge density, nuclear magnetic relaxation, and permeability in clay-bearing sandstones: Geophysics, v.55, p.61-69

Sigal, R., 2002, Coates and SDR permeability: two variations on the same theme: Petrophysics, v.43, no.1, p.38-46

Skelt, C., and B. Harrison, 1995, An integrated approach to saturation height analysis: *in* 36th Annual Logging Symposium Transactions: Society of Professional Well Log Analysts, Paper NNN.

Smith, 1966, Theoretical considerations of sealing and non-sealing faults: AAPG Bulletin, v. 50, p. 363-374

Sneed, D. R., 1988, Reservoir rock-property calculations from thin section measurements: M. S. Thesis, Texas A&M University, College Station, TX, 105p.

Sneider, R. M., F. H. Richardson, D. D. Paynter, R. E. Eddy, I. A. Wyant, 1977, Predicting reservoir rock geometry and continuity in pennsylvanian reservoirs, Elk City Field, Oklahoma: Journal of Petroleum Technology, July, 1977, p.851-866.

Spain, D. R., 1992, Petrophysical evaluation of a slope fan/basin-floor fan complex: Cherry Canyon Formation, Ward County, Texas: AAPG Bulletin, v. 76, p. 805-827

Swanson, B. F., 1981, A simple correlation between permeabilities and mercury capillary Pressures: Journal of Petroleum Technology, p.2498-2504

Swanson, B. F., 1985, Microporosity in reservoir rocks: its measurement and influence on electrical resistivity: The Log Analyst, v.26, p.42-52

Thomas, L. K., D. L. Katz, and M. R. Tek, 1968, Threshold pressure phenomena in porous media: Society of Petroleum Engineers Journal, v.8, p.174-183

Thomeer, J. H. M., 1960, Introduction of a pore geometrical factor defined by the capillary pressure curve, Journal of Petroleum Technology, p.73-77

Thomeer, J. H. M., 1983, Air permeability as a function of three pore network parameters: Journal of Petroleum Technology, p.809-814

Thompson, A.H., A. J. Katz, and C. E. Krohn, 1987, The microgeometry and transport properties of sedimentary rock: Advances in Physics, v. 36, p.625-694

Tieh, T. T., R. R.Berg, R. K. Popp, J. E. Brasher, and J. D. Pike, 1986, Deposition and diagenesis of Upper Miocene Arkoses, Yowlumne and Rio Viejo fields, Kern

County, California: AAPG Bulletin, v. 70, p. 953-969

Timur, A., 1968, An investigation of permeability, porosity, and residual water saturation relationships for sandstone reservoirs: The Log Analyst, v. 9, p. 8-17.

Taylor, T. R. and C. H. Soule, 1993, Reservoir characterization and diagenesis of the Oligocene 64-zone sandstone, North Belridge field, Kern County, California: AAPG Bulletin, v. 77, p. 1549-1566

Vavra C. L., J. G. Kaldi, and R. M. Sneider, 1992, Geological applications of capillary pressure: a review: AAPG Bulletin, v.76, p.840-850

Walder, N. C. and J. P. Cassan, 1979, Oil recovery efficiency and the rock-pore properties of some sandstone reservoirs: Canadian Petroleum Geology Bulletin, v. 27, p. 117-138

Walderhaug, O., 2000, Modeling quartz cementation and porosity in middle Jurassic Brent Group sandstones of the KvitebjØrn field, Northern North Sea: AAPG Bulletin, v.84, p.1325-1339

Washburn, E. W., 1921, Note on a method of determining the distribution of pore sizes in a porous material: Proceedings of the National Academy of Science, v. 7, p. 115–116.

Wells, J. D. and J. O. Amaefule, 1985, Capillary pressure and permeability relationships in tight gas sands, SPE paper 13879, presented at the SPE/DOE Low Permeability Reservoirs held in Denver, Colorado, May 19-22.

Worthington, P. F., 1998, Conjunctive interpretation of core and log data through association of the effective and total porosity models, *in*: Harvey, P.K. and M.A., Lovell (eds.), Core-log interpretation, Geological Society, London, Special Publications, v.136, p.213-223

Wu, T. and R. R. Berg, 2003a, A method for synthesizing and averaging capillary pressure curves: extended abstract, AAPG Annual Meeting, Salt Late City.

Wu, T. and R. R. Berg, 2003b, Relationship of reservoir properties for shaly sandstones based on effective porosity: Petrophysics, v.44, p. 328-341

Xu, S. and R. White, 1998, Permeability prediction in anisotropic shaly formations, *in*: Harvey, P. K. and Lovell, M. A. ed., *Core-log integration*, Geological Society, London, Special Publication, no.136, p.225-236

# APPENDIX A

# LITERATURE SURVEY OF PERMEABILITY AND CAPILLARY PRESSURE MODELS

**Table A-1 Selected permeability models**

| Authors | Equations | Note |
|---|---|---|
| Berg (1970) | Original:<br>$k = 5.1\times10^{-3}(100\phi)^{5.1} d_w^{\,2} \exp(-1.385 PD_{phi})$<br>Modified by Gangi (1985):<br>$k = 4.49\times10^{-3}(100\phi)^{5.1} d_N^{\,2} \exp(1.78\sigma_{phi}^{\,3})$ | Theoretical |
| Coates (1981) | $k = [\frac{100\phi^2(1-S_{wir})}{S_{wir}}]^2$<br>$k = C\phi^4(\frac{FFI}{BVI})^2$ | Empirical |
| Gangi (1985) | $k = 665000 d_N^{\,2} \exp(1.78\sigma_{phi}^{\,3})$<br>$= 665000 d_w^{\,2} \exp(-2.88\sigma_{phi}^{\,2} + 1.78\sigma_{phi}^{\,3})$<br>$k = 648000 d_N^{\,2} \exp(1 + 2.77\sigma_{phi}^{\,3})$<br>$d_N = d_w \exp(-1.441\sigma_{phi}^{\,2})$ | Empirical |
| Hutchinson et al. (1961) | $k = 2.53\times10^5 [\frac{d}{F\exp(0.6\sigma_{phi})}]^{2.75}$ | Empirical |
| Jorgensen (1988) | $k = 84105\frac{(\phi^{m+2})}{(1-\phi)^2}$ | Empirical |
| Katz and Thompson (1986) | $k = (\frac{1013}{226}) l_c^{\,2} \frac{\sigma}{\sigma_0} = (\frac{1013}{226}) l_c^{\,2} / F$<br>$= (\frac{1013}{226}) l_c^{\,2} (\phi)^m$ | Theoretical |
| Kenyon (1988) | $k = CT_{2gm}^{\,2}\phi^4$ | Empirical |
| Kozeny-Carman (1927,1956) | $k = \frac{1013\phi^3}{f\tau(1-\phi)^2 S_g^{\,2}}$, or<br>$k = \frac{1013000\phi^3 d^2}{180(1-\phi)^2}$, $(S_g = 6/d,\ f\tau = 5)$ | Theoretical |
| Krumbein and Monk (1943) | $k = 760000 d_w^{\,2} \exp(-1.31\sigma_{phi})$ | Empirical |

**Table A-1 Selected permeability models (continued)**

| | | |
|---|---|---|
| Pape, et al (1999) | Sandstone:<br>$k = 0.031\phi + 7.463\phi^2 + 0.191(10\phi)^{10}$<br>Shaly sandstone:<br>$k = 0.0062\phi + 1.493\phi^2 + 0.058(10\phi)^{10}$ | Semi-theoretical |
| Purcell (1949) | $k = 10.66(\sigma\cos\theta)^2 \phi f \int_0^1 \frac{ds_{nw}}{P_c^{\,2}}$ | Theoretical |
| Revil and Cathles III (1999) | Sandstone: $k_{sd} = \frac{10^9 \times d^2(\phi_{sd})^{3msd}}{24}$<br>Clayey sand: $k = k_{sd}[1 - \varphi_v(\frac{1-\phi_{sh}}{\phi_{sd}})]^{3mcs}$ | Theoretical |
| Sen, et al (1990) | $k = 0.794(\phi^m T_1)^{2.15}$<br>$k = 10^{6.59}(\phi^m V_p / S)^{2.08}$ | Empirical |
| Swanson (1981) | $k = 399(\frac{S_b}{P_c})_{\max}^{1.691}$ | Empirical |
| Thomeer (1983) | $k = 3.8068 F_g^{-1.3334}(S_{b\infty} / P_d)^{2.0}$ | Empirical |
| Timur (1968) | $k = 0.136\frac{(100\phi)^{4.4}}{(100S_{wir})^2}$ | Empirical |
| Morris and Biggs (1967) | $k = (250\frac{\phi^3}{S_{wir}})^2$ | Empirical |
| Zawisza (1993) | $k = 45584\phi^{3.15}(1 - S_{wir})^2$<br>$S_{wir} = V_{sh}^{\,0.61}(1 - 2.5\phi)^{3.18}$ | Empirical |

**Table A-2 Selected capillary pressure models**

| Authors | Equations | Note |
|---|---|---|
| Alger et al (1989) | $\phi(1-S_w) = a + b\phi + c\log k + d\log h$ | Empirical |
| Brooks and Corey (1964) | $S_e = (\frac{P_c}{P_d})^{-\lambda}$<br>$S_e = \frac{S_w - S_{wir}}{1 - S_{wir}}$ | Empirical |
| Guthrie and Greenberger (1955) | $S_w = a\log k + c$<br>$S_w = a_1\phi + a_2\log k + c$ | Empirical |
| Hawkins, et al (1993) | $\log P_c = -F_g / \ln(1-S_w) + \log P_d$<br>(Thomeer's equation)<br>$F_g = [\ln(5.21\frac{k^{0.1254}}{100\phi})]^2 / 2.303$<br>$P_d = 9.378/(k^{0.3406}\phi)$ | Empirical (based on Thomeer's model) |
| Kwon and Pickett (1975) | $P_c = A(k\ /\phi)^{-B}$ | Empirical |
| Leverett (1949) | $J(S_w) = \frac{0.2179 P_c}{\sigma\cos\theta}\sqrt{\frac{k}{\phi}}$ | Semi-empirical |
| Pittman (1992)* | $\log r_{10} = 0.459 + 0.5\log k - 0.385\log(100\phi)$<br>$\log r_{35} = 0.255 + 0.565\log k - 0.523\log(100\phi)$ | Empirical |
| Thomeer (1960) | $\frac{S_b}{S_{b\infty}} = e^{-Fg/\log(Pc/Pd)}$ | Theoretical |
| Winland (1980)** | $\log r_{35} = 0.732 + 0.588\log k - 0.864\log(100\phi)$ | Empirical |

* Not all equations are listed, only the two most widely used are listed here.

**Was first published by Kolodzie (1980)

# APPENDIX B

# ESTIMATES OF EFFECTIVE POROSITY

**Table B-1 Measured petrophysical data and calculated effective porosity (from Wu and Berg, 2003)**

| Sample Formation Name | Permeability (md) | Porosity (%) | d (μm)* | MPD* (μm) | Clay (%) | $Q_v$* (meq/ml) | $P_{dma}$* (psi) | Effective Porosity (%) |
|---|---|---|---|---|---|---|---|---|
| "Discrete Particle" Clays | | | | | | | | |
| Berea | 796 | 21.2 | 170 | 25.7 | 5 | 0.03 | 6.5 | 20.2 |
| Miocene "S" | 1173 | 22.9 | 145 | 31 | 5 | 0.03 | 6.2 | 21.9 |
| Paluxy | 1037 | 24.8 | 110 | 23.8 | 5 | 0.02 | 7.8 | 23.8 |
| Cotton Valley | 150 | 14.1 | 166 | 21.2 | 6 | 0.06 | 6.8 | 12.9 |
| Tar Springs | 420 | 19 | 146 | 19.2 | 3 | 0.03 | 8.2 | 18.4 |
| "Pore-Lining" Clays | | | | | | | | |
| Tusculoosa | 41 | 25.7 | 180 | 10.9 | 15 | 0.11 | 8.8 | 15.2 |
| Vicksburg | 7 | 18.3 | 253 | 5.6 | 11 | 0.14 | 14.5 | 10.6 |
| Hosston | 0.82 | 10.9 | 235 | 2.2 | 7 | 0.13 | 50 | 6 |
| Wilcox | 1.4 | 13.2 | 245 | 3.5 | 10 | 0.37 | 20.5 | 6.2 |
| Frio | 58 | 26.5 | 88 | 8 | 12 | 0.36 | 17.1 | 18.1 |
| "Pore-Bridging" Clays | | | | | | | | |
| Vicksburg | 0.09 | 19.1 | 162 | 0.54 | 20 | 0.15 | 47 | 1.1 |
| Hosston | 0.15 | 8.45 | 253 | 1.34 | 10 | 0.2 | 92 | – ** |
| Wilcox | 0.031 | 11.1 | 113 | 0.42 | 10 | 0.54 | 122 | 2.1 |
| Wilcox | 0.21 | 12.9 | 71 | 1.47 | 10 | 0.36 | 70 | 3.9 |

Source: Neasham, 1977, effective porosity values are calculated with equation 4-1

* d: meadian grain diameter (μm); MPD: Median pore throat diameter (μm); $Q_v$ : Cation Exchange Capability per unit pore volume ( meq/ml); $P_{dma}$: Air-Mercury Displacement Pressure (psi)

** a negative value is obtained. This may be caused by the measurement of porosity and clay content.

**Table B-2 Petrographic and X-Ray diffraction analysis of Yowlumne sandstone, Kern County, California**

| Well | Depth (ft) | *d* (mm) | Detrital composition (%) | | | | | *k* (md) | $\phi_t$ (%) | X-ray defraction (wt %) | | | $\phi_e$ (%) |
|---|---|---|---|---|---|---|---|---|---|---|---|---|---|
| | | | Qz | FSP | RF | Clay | Cement | | | Kaolinite | Illite | Verm+Ch+ Mon | |
| T54-4 | 11459.3 | 0.24 | 39 | 44 | | 11 | 6 | 138 | 16.8 | 75 | 9 | 16 | 13.13 |
| | 11467.2 | 0.25 | 46 | 34 | 1 | 14 | 5 | 74 | 19.2 | 80 | 11 | 9 | 14.79 |
| | 11506.5 | 0.48 | 52 | 34 | 3 | 6 | 5 | 90 | 19 | 69 | 13 | 18 | 16.77 |
| | 11525.8 | 0.42 | 47 | 39 | 6 | 5 | 3 | 53 | 18.7 | 68 | 14 | 18 | 16.81 |
| | 11567.5 | 0.31 | 49 | 33 | 3 | 11 | 4 | 191 | 21 | 78 | 3 | 19 | 17.62 |
| | 11588.1 | 0.37 | 48 | 38 | 2 | 8 | 4 | 108 | 19.4 | 77 | 10 | 13 | 16.79 |
| | 11601.5 | 0.33 | 51 | 35 | 4 | 9 | 1 | 37 | 16.9 | 77 | 11 | 12 | 13.94 |
| | 11626.5 | 0.22 | 46 | 38 | 3 | 5 | 8 | 1.5 | 15.3 | 35 | 19 | 46 | 12.54 |
| T27x-34 | 12263.5 | 0.29 | 46 | 41 | 4 | 5 | 4 | 25 | 17 | 40 | 26 | 34 | 14.29 |
| | 12284.5 | 0.33 | 42 | 41 | 6 | 7 | 5 | 42 | 17.5 | 61 | 17 | 22 | 14.57 |
| | 12286.5 | 0.37 | 44 | 42 | 6 | 5 | 3 | 6 | 15.7 | 34 | 42 | 24 | 12.68 |
| | 12317.5 | 0.39 | 40 | 43 | 8 | 6 | 2 | 152 | 17.8 | 77 | 10 | 13 | 15.84 |
| T55X-34 | 12981.5 | 0.23 | 68 | 13 | 3 | 13 | 2 | 0.8 | 11.5 | 38 | 31 | 31 | 4.2 |
| | 13004.5 | 0.45 | 70 | 17 | 2 | 6 | 4 | 3.9 | 13 | 78 | 5 | 17 | 11.13 |
| | 13116.5 | 0.47 | 62 | 25 | 2 | 6 | 4 | 5.4 | 13.8 | 82 | 10 | 8 | 11.98 |

Source: Pike (1981)

d = mean grain size, Qz = quartz, FSP = feldspar, RF = rock fragment, *k* = air permeability, $\phi_t$ = total porosity (Helium porosity), $\phi_e$ = effective porosity, Verm+Ch+Mon = Vermiculite + Chlorite + Montmorillonite

# APPENDIX C

# MEASURED PETROGRAPHIC ANALYSIS

**Table C-1 Summary of selected quartzose sandstones**

| Formation | Number of Samples | D50 (mm) | Detrital Composition | | Matrix (%) | Cement (%) | Core Measurement | |
|---|---|---|---|---|---|---|---|---|
| | | | Qz (%) | O (%) | | | *k* (md) | $\phi$ (%) |
| Muddy | 7 | 0.157 | 86 | 12 | 2 | 0 | 2595 | 30.8 |
| Muddy | 6 | 0.17 | 89 | 5 | 1 | 4 | 738 | 25.5 |
| Muddy | 4 | 0.16 | 84 | 12 | 4 | 0 | 102 | 16.7 |
| Yegua | 32 | 0.2 | 42 | 42 | 8 | 9 | 722 | 22.3 |
| Strawn | 14 | 0.12 | 70 | 12 | 9 | 9 | 109 | 22.1 |
| Frio 19B | 22 | 0.18 | 32 | 45 | 5 | 19 | 1298 | 23.3 |
| Stevens | 22 | 0.29 | 46 | 38 | 10 | 6 | 194 | 19.4 |
| Stevens | 34 | 0.29 | 47 | 39 | 9 | 6 | 75 | 18 |
| L.Miocene | 24 | 0.22 | 86 | 4 | 5 | 5 | 170 | 18.7 |
| Dakota | 24 | 0.17 | 76 | 7 | 5 | 12 | 142 | 14.7 |
| Terry | 9 | 0.14 | 30 | 48 | 6 | 16 | 3.5 | 14.5 |
| “J-2” | 16 | 0.23 | 88 | 5 | 4 | 2 | 22 | 12.9 |
| Frontier | 6 | 0.16 | 39 | 45 | 12 | 4 | 7.5 | 10.5 |
| Muddy | 11 | 0.2 | 73 | 12 | 7 | 8 | 2.9 | 11.8 |
| Woodbine | 10 | 0.19 | 72 | 8 | 9 | 11 | 0.17 | 8.8 |
| Marchand | 6 | 0.19 | 78 | 9 | 0 | 12 | 0.3 | 7 |
| Norphlet | 21 | 0.24 | 76 | 13 | 4 | 7 | 1.26 | 7.4 |
| Muddy | 4 | 0.25 | 91 | 4 | 1 | 4 | 134 | 16.4 |

D50: median grain diameter; Qz: quartz; O: other. Data collected and compiled by Dr. Robert R. Berg

**Table C-2 Summary of selected shaly sandstones**

| Formation | Number of Samples | D50 (mm) | Detrital Composition | | Matrix (%) | Cement (%) | Core Measurement | |
|---|---|---|---|---|---|---|---|---|
| | | | Qz (%) | O (%) | | | *k* (md) | $\phi$ (%) |
| Muddy | 4 | 0.1 | 37 | 5 | 42 | 17 | 200 | 24.1 |
| Wilcox | 5 | 0.12 | 57 | 20 | 16 | 7 | 959 | 31 |
| Wilcox | 3 | 0.06 | 51 | 22 | 24 | 3 | 85 | 23 |
| Wilcox | 9 | 0.11 | 53 | 6 | 29 | 12 | 3.5 | 20.3 |
| Frio | 12 | 0.09 | 46 | 21 | 24 | 9 | 5.7 | 19.4 |
| Wilcox | 14 | 0.17 | 56 | 21 | 13 | 11 | 4.4 | 18 |
| Vicksburg | 17 | 0.18 | 20 | 46 | 19 | 16 | 0.14 | 12.2 |
| Yegua | 9 | 0.12 | 41 | 30 | 21 | 9 | 37 | 24.5 |
| Wilcox | 28 | 0.11 | 35 | 37 | 20 | 8 | 0.75 | 15.2 |
| Muddy | 7 | 0.18 | 44 | 18 | 38 | 0 | 0.29 | 9.3 |

D50: median grain diameter; Qz: quartz; O: other. Data collected and compiled by Dr. Robert R. Berg

**Table C-3 Petrographic analysis, Dakota, Coyote Creek**

| Depth | $P_{90}$ (mm) | Detrital Composition | | | | MX+CMT (%) | Core Measurement | |
|---|---|---|---|---|---|---|---|---|
| | | Qz (%) | F (%) | RX (%) | O (%) | | *k* (md) | $\phi$ (%) |
| 6286 | 0.051 | 88 | 0 | 5 | 1 | 28 | 6.1 | 12.2 |
| 6290 | 0.056 | 86 | 1 | 9 | 2 | 25 | 32 | 13.2 |
| 6296 | 0.066 | 79 | 1 | 6 | 1 | 33 | 12 | 12 |
| 6303 | 0.066 | 77 | 1 | 10 | 1 | 32 | 41 | 13.5 |
| 6306 | 0.06 | 86 | 0 | 5 | 2 | 26 | 34 | 13.6 |
| 6313 | 0.053 | 90 | 1 | 4 | 1 | 15 | 7.4 | 11.6 |
| 6315 | 0.056 | 88 | 0 | 7 | 0 | 22 | 12 | 12.2 |
| 6319 | 0.057 | 71 | 0 | 5 | 0 | 26 | 31 | 13.2 |
| 6325 | 0.067 | 92 | 0 | 5 | 0 | 17 | 57 | 15.3 |
| 6463 | 0.063 | 74 | 0 | 14 | 9 | 15 | 7.8 | 11.2 |
| 6468 | 0.054 | 78 | 1 | 8 | 6 | 22 | 5.9 | 12.1 |
| 6477 | 0.088 | 77 | 2 | 11 | 5 | 18 | 37 | 15.1 |
| 6482 | 0.09 | 18 | 0 | 4 | 47 | 37 | 1.1 | 7.5 |
| 6487 | 0.085 | 77 | 0 | 13 | 6 | 18 | 43 | 15.7 |
| 6490 | 0.121 | 75 | 1 | 17 | 3 | 19 | 163 | 16.4 |
| 6495 | 0.176 | 82 | 2 | 8 | 4 | 14 | 242 | 16.7 |
| 6438 | 0.095 | 78 | 2 | 14 | 4 | 4 | 63 | 14.8 |
| 6445 | 0.113 | 82 | 1 | 14 | 2 | 4 | 396 | 17.8 |
| 6451 | 0.109 | 82 | 1 | 12 | 3 | 5 | 93 | 15.5 |
| 6457 | 0.083 | 89 | 1 | 5 | 2 | 6 | 261 | 16 |
| 6463 | 0.104 | 86 | 1 | 10 | 2 | 3 | 340 | 18.3 |
| 6468 | 0.126 | 84 | 1 | 10 | 3 | 5 | 145 | 16.7 |
| 6471 | 0.096 | 83 | 2 | 12 | 1 | 6 | 187 | 16.9 |
| 6486 | 0.116 | 75 | 1 | 19 | 2 | 7 | 910 | 19.4 |
| 6492 | 0.157 | 87 | 0 | 9 | 2 | 8 | 285 | 12.7 |

Source: David R. Sneed (1988)

$P_{90}$: ninetieth percentile of grain size distribution; Qz: monocrystalline quartz; F: feldspar; RX: rock fragment; O: other; MX+CMT: combined total percentage of matrix and cement; k: core permeability.

**Table C-4 Petrographic analysis, Dakota, Coyote Creek**

| Depth | $P_{90}$ (mm) | Detrital Composition | | | | MX+CMT (%) | Core Measurement | |
|---|---|---|---|---|---|---|---|---|
| | | Qz (%) | F (%) | RX (%) | O (%) | | *k* (md) | $\phi$ (%) |
| 6286 | 0.051 | 88 | 0 | 5 | 1 | 28 | 6.1 | 12.2 |
| 6290 | 0.056 | 86 | 1 | 9 | 2 | 25 | 32 | 13.2 |
| 6296 | 0.066 | 79 | 1 | 6 | 1 | 33 | 12 | 12 |
| 6303 | 0.066 | 77 | 1 | 10 | 1 | 32 | 41 | 13.5 |
| 6306 | 0.06 | 86 | 0 | 5 | 2 | 26 | 34 | 13.6 |
| 6313 | 0.053 | 90 | 1 | 4 | 1 | 15 | 7.4 | 11.6 |
| 6315 | 0.056 | 88 | 0 | 7 | 0 | 22 | 12 | 12.2 |
| 6319 | 0.057 | 71 | 0 | 5 | 0 | 26 | 31 | 13.2 |
| 6325 | 0.067 | 92 | 0 | 5 | 0 | 17 | 57 | 15.3 |
| 6463 | 0.063 | 74 | 0 | 14 | 9 | 15 | 7.8 | 11.2 |
| 6468 | 0.054 | 78 | 1 | 8 | 6 | 22 | 5.9 | 12.1 |
| 6477 | 0.088 | 77 | 2 | 11 | 5 | 18 | 37 | 15.1 |
| 6482 | 0.09 | 18 | 0 | 4 | 47 | 37 | 1.1 | 7.5 |
| 6487 | 0.085 | 77 | 0 | 13 | 6 | 18 | 43 | 15.7 |
| 6490 | 0.121 | 75 | 1 | 17 | 3 | 19 | 163 | 16.4 |
| 6495 | 0.176 | 82 | 2 | 8 | 4 | 14 | 242 | 16.7 |
| 6438 | 0.095 | 78 | 2 | 14 | 4 | 4 | 63 | 14.8 |
| 6445 | 0.113 | 82 | 1 | 14 | 2 | 4 | 396 | 17.8 |
| 6451 | 0.109 | 82 | 1 | 12 | 3 | 5 | 93 | 15.5 |
| 6457 | 0.083 | 89 | 1 | 5 | 2 | 6 | 261 | 16 |
| 6463 | 0.104 | 86 | 1 | 10 | 2 | 3 | 340 | 18.3 |
| 6468 | 0.126 | 84 | 1 | 10 | 3 | 5 | 145 | 16.7 |
| 6471 | 0.096 | 83 | 2 | 12 | 1 | 6 | 187 | 16.9 |
| 6486 | 0.116 | 75 | 1 | 19 | 2 | 7 | 910 | 19.4 |
| 6492 | 0.157 | 87 | 0 | 9 | 2 | 8 | 285 | 12.7 |

Source: David R. Sneed (1988)
$P_{90}$: ninetieth percentile of grain size distribution; Qz: monocrystalline quartz; F: feldspar; RX: rock fragment; O: other; MX+CMT: combined total percentage of matrix and cement; k: core permeability.

**Table C-5 Petrographic analysis, Yegua, Cities Service Dincans 1**

| Depth | $P_{90}$ (mm) | Detrital Composition | | | | MX+CMT (%) | Core Measurement | | Log Porosity (%) |
|---|---|---|---|---|---|---|---|---|---|
| | | Qz (%) | F (%) | RX (%) | O (%) | | *k* (md) | $\phi$ (%) | |
| 8219.3 | 0.085 | 57 | 19 | 21 | 3 | 20 | 1050 | 29.6 | 29 |
| 8233.0 | 0.042 | 54 | 16 | 26 | 5 | 13 | 58 | 21.6 | 29 |
| 8235.5 | 0.117 | 49 | 20 | 28 | 3 | 14 | 1400 | 25.2 | 28.5 |
| 8249.8 | 0.170 | 56 | 21 | 23 | 1 | 18 | 2800 | 28.8 | 23 |
| 8259.5 | 0.115 | 52 | 23 | 24 | 1 | 13 | 880 | 26.5 | 28 |
| 8345.3 | 0.094 | 56 | 18 | 23 | 2 | 12 | 1700 | 28.4 | 23 |
| 8360.5 | 0.121 | 45 | 21 | 33 | 1 | 21 | 3150 | 30.2 | 30 |
| 8371.4 | 0.116 | 45 | 24 | 29 | 2 | 30 | 3216 | 30.7 | 31 |
| 8408.0 | 0.040 | 46 | 16 | 34 | 4 | 16 | 274 | 29.4 | 28 |
| 8414.0 | 0.040 | 45 | 18 | 31 | 6 | 5 | 67 | 27.1 | 29.5 |
| 8433.0 | 0.095 | 51 | 19 | 28 | 2 | 14 | 1825 | 31.8 | 31 |
| 8442.0 | 0.113 | 49 | 20 | 28 | 3 | 20 | 2383 | 30.3 | 30 |
| 8465.8 | 0.053 | 47 | 21 | 27 | 5 | 11 | 553 | 31.4 | 28 |
| 8473.0 | 0.049 | 43 | 22 | 31 | 4 | 11 | 127 | 30 | 28 |
| 8479.0 | 0.037 | 40 | 18 | 39 | 3 | 15 | 60 | 25.3 | 29 |

Source: David R. Sneed (1988)
$P_{90}$: ninetieth percentile of grain size distribution; Qz: monocrystalline quartz; F: feldspar; RX: rock fragment; O: other; MX+CMT: combined total percentage of matrix and cement; k: core permeability.

**Table C-6 Petrographic analysis, J sandstone, Huckabay 1 Flader**

| Depth | $P_{90}$ (mm) | Detrital Composition | | | | MX+CMT (%) | Core measurement | | Log Porosity (%) |
|---|---|---|---|---|---|---|---|---|---|
| | | Qz (%) | F (%) | RX (%) | O (%) | | *k* (md) | $\phi$ (%) | |
| 6179 | 0.105 | 57 | 4 | 30 | 2 | 7 | 0.6 | 12.4 | 9.5 |
| 6194 | 0.095 | 56 | 4 | 35 | 1 | 9 | 3.7 | 11.5 | 11 |
| 6198 | 0.109 | 64 | 4 | 27 | 1 | 6 | 0.7 | 12.9 | 10.5 |
| 6200 | 0.101 | 68 | 3 | 25 | 1 | 5 | 3.5 | 12.9 | 11 |
| 6206.5 | 0.129 | 55 | 0 | 43 | 0 | 2 | 22 | 13.3 | 12 |
| 6207.5 | 0.139 | 50 | 4 | 45 | 1 | 2 | 12 | 11.3 | 12.5 |
| 6216.3 | 0.092 | 43 | 1 | 54 | 0 | 7 | 48 | 17.4 | 12 |
| 6218.8 | 0.102 | 33 | 1 | 60 | 1 | 6 | 8.5 | 12.5 | 14 |
| 6221 | 0.117 | 54 | 2 | 39 | 2 | 4 | 51 | 14.4 | 10 |
| 6222 | 0.118 | 58 | 0 | 34 | 1 | 11 | 43 | 15.4 | 12.5 |
| 6224 | 0.095 | 63 | 1 | 30 | 1 | 5 | 12 | 14.7 | 12 |
| 6226.8 | 0.196 | 68 | 2 | 28 | 2 | 2 | 85 | 14.7 | 14 |
| 6228.5 | 0.203 | 70 | 0 | 27 | 0 | 5 | 60 | 10.7 | 11 |
| 6252.2 | 0.105 | 56 | 1 | 41 | 1 | 2 | 4 | 14.5 | 14 |
| 6262 | 0.133 | 63 | 1 | 35 | 0 | 7 | 14 | 13.2 | 11 |

Source: David R. Sneed (1988)
$P_{90}$: ninetieth percentile of grain size distribution; Qz: monocrystalline quartz; F: feldspar; RX: rock fragment; O: other; MX+CMT: combined total percentage of matrix and cement; k: core permeability.

**Table C-7 Petrographic analysis, Stevens sandstone, Tenneco 66-11, Yowlumne field**

| Depth | $P_{90}$ (mm) | Detrital Composition (%) | | | | MX+CMT (%) | Core Measurement | | Log Porosity (%) |
|---|---|---|---|---|---|---|---|---|---|
| | | Qz | F | RX | O | | $k$ (md) | $\phi$ (%) | |
| 11155.5 | 0.057 | 54 | 23 | 4 | 4 | 16 | 36 | 14.8 | 17.5 |
| 11158.0 | 0.147 | 49 | 27 | 8 | 6 | 8 | 257 | 20.1 | 21.5 |
| 11159.0 | 0.085 | 58 | 26 | 7 | 4 | 11 | 275 | 18.4 | 18 |
| 11167.0 | 0.044 | 54 | 26 | 2 | 5 | 26 | 104 | 18.1 | 21.5 |
| 11168.0 | 0.085 | 57 | 30 | 7 | 3 | 7 | 160 | 20.8 | 21 |
| 11174.0 | 0.067 | 54 | 32 | 5 | 4 | 11 | 110 | 19.3 | 20.5 |
| 11175.0 | 0.109 | 55 | 28 | 6 | 5 | 9 | 164 | 19.4 | 21 |
| 11197.0 | 0.105 | 49 | 28 | 8 | 6 | 11 | 140 | 20.8 | 20 |
| 11199.5 | 0.058 | 52 | 32 | 5 | 4 | 12 | 109 | 18.4 | 18 |
| 11216.5 | 0.082 | 52 | 29 | 7 | 5 | 10 | 124 | 18.2 | 21.5 |
| 11217.5 | 0.082 | 48 | 31 | 6 | 6 | 17 | 204 | 18.9 | 18 |
| 11218.5 | 0.092 | 53 | 33 | 5 | 4 | 12 | 169 | 19.8 | 20.5 |
| 11221.8 | 0.113 | 48 | 31 | 6 | 8 | 9 | 349 | 20.1 | 21 |
| 11222.5 | 0.085 | 47 | 29 | 8 | 4 | 16 | 306 | 20.3 | 20 |
| 11231.5 | 0.095 | 54 | 28 | 9 | 5 | 10 | 174 | 19.7 | 21 |
| 11232.5 | 0.082 | 48 | 31 | 6 | 4 | 16 | 135 | 19.5 | 20 |
| 11234.5 | 0.095 | 52 | 26 | 6 | 5 | 19 | 106 | 19.5 | 20.5 |
| 11244.5 | 0.080 | 47 | 34 | 7 | 6 | 15 | 316 | 19.9 | 21 |
| 11245.5 | 0.067 | 50 | 31 | 5 | 8 | 12 | 299 | 21.2 | 22 |
| 11246.5 | 0.088 | 49 | 35 | 7 | 5 | 10 | 279 | 19 | 20 |

Source: David R. Sneed (1988)

**Table C-8 Petrographic analysis of Middle Jurassic Brent sandstones, North Sea**

| D50 (mm) | Standard Deviation (mm) | Detrital Composition(%) | | Matrix (%) | Cement (%) | Thin-section Porosity (%) | | Core Measurement | |
|---|---|---|---|---|---|---|---|---|---|
| | | Qz | O | | | Primary | Dissolution | k(md) | $\phi$ (%) |
| 0.136 | 0.056 | 74 | 5 | 3 | 18 | 20.3 | 5 | 285 | 22.7 |
| 0.124 | 0.042 | 56 | 5 | 4 | 35 | 7.3 | 1.7 | 0.2 | 9.2 |
| 0.153 | 0.059 | 63 | 6 | 9 | 22 | 6.7 | 1.3 | 0.06 | 9.9 |
| 0.235 | 0.12 | 68 | 5 | 8 | 19 | 18 | 6 | 772 | 22.2 |
| 0.166 | 0.066 | 73 | 5 | 10 | 13 | 18.7 | 4.7 | 161 | 21.9 |
| 0.168 | 0.054 | 57 | 9 | 15 | 18 | 13 | 7.3 | 7 | 20 |
| 0.231 | 0.085 | 68 | 9 | 6 | 18 | 15 | 4 | 168 | 19.5 |
| 0.242 | 0.106 | 60 | 11 | 6 | 24 | 12.3 | 4.3 | 101 | 17.1 |
| 0.157 | 0.067 | 53 | 13 | 9 | 25 | 11.3 | 2.7 | 7 | 16.7 |
| 0.277 | 0.071 | 67 | 9 | 6 | 19 | 18.3 | 4.7 | 2790 | 25.3 |
| 0.201 | 0.06 | 72 | 2 | 4 | 22 | 5.3 | 0 | 0.07 | 14.8 |
| 0.142 | 0.044 | 70 | 5 | 7 | 18 | 9 | 3 | 2.1 | 17.3 |
| 0.285 | 0.097 | 68 | 10 | 9 | 13 | 15 | 6.3 | 37.5 | 21.5 |
| 0.331 | 0.106 | 76 | 3 | 8 | 13 | 16.3 | 4 | 353 | 21.8 |
| 0.3 | 0.11 | 63 | 6 | 13 | 18 | 16 | 7.7 | 423 | 21.8 |
| 0.647 | 0.312 | 69 | 9 | 13 | 9 | 12.3 | 6.3 | 85.3 | 19.2 |

Data from Walderhaug (2000). Permeability from personal communication between Walderhaug and Berg.

# APPENDIX D

# MEASURED CAPILLARY PRESSURES

**Table D-1 Air-brine plate capillary pressures, San Francisco #14 well, Caballos Formation, San Francisco, Colombia**

| *No.* | $S_w$ at different pressures | | | | | | |
|---|---|---|---|---|---|---|---|
| | 1psi | 2psi | 5psi | 10psi | 35psi | 100psi | 200psi |
| 21B | 0.88 | 0.743 | 0.448 | 0.279 | 0.194 | 0.146 | 0.113 |
| 2B | 0.771 | 0.533 | 0.281 | 0.185 | 0.131 | 0.096 | 0.076 |
| 6B | 0.959 | 0.938 | 0.882 | 0.815 | 0.573 | 0.38 | 0.28 |
| 3B | 0.95 | 0.924 | 0.741 | 0.604 | 0.424 | 0.315 | 0.246 |
| 25B | 0.665 | 0.443 | 0.265 | 0.192 | 0.117 | 0.079 | 0.065 |
| 10B | 0.667 | 0.572 | 0.398 | 0.275 | 0.173 | 0.105 | 0.082 |
| 29B | 0.869 | 0.77 | 0.502 | 0.36 | 0.205 | 0.145 | 0.116 |
| 14B | 0.945 | 0.912 | 0.857 | 0.846 | 0.824 | 0.792 | 0.77 |
| 15B | 0.941 | 0.929 | 0.661 | 0.385 | 0.223 | 0.155 | 0.137 |
| 16B | 0.984 | 0.969 | 0.878 | 0.783 | 0.639 | 0.482 | 0.339 |

From Dr. John Calhoun, 2002, personal communication

**Table D-2 Air-water centrifuge capillary pressures, Duke Sand Formation, Desdemona Field, Eastland County, TX**

| *Well* | *No.* | $S_w$ at different pressures | | | | | | | | |
|---|---|---|---|---|---|---|---|---|---|---|
| | | 1psi | 2psi | 5psi | 10psi | 20psi | 40psi | 60psi | 90psi | 120psi |
| | 8A | 1 | 1 | 1 | 0.869 | 0.72 | 0.577 | 0.488 | 0.404 | 0.369 |
| | 9A | 1 | 1 | 1 | 1 | 0.862 | 0.694 | 0.577 | 0.477 | 0.44 |
| J.R. | 11A | 1 | 1 | 0.527 | 0.409 | 0.315 | 0.255 | 0.228 | 0.205 | 0.199 |
| Grimshaw | 12A | 1 | 1 | 0.788 | 0.637 | 0.488 | 0.364 | 0.33 | 0.315 | 0.31 |
| No.1 | 14A | 1 | 1 | 0.58 | 0.42 | 0.319 | 0.244 | 0.215 | 0.21 | 0.205 |
| | 20A | 1 | 1 | 1 | 0.754 | 0.577 | 0.43 | 0.394 | 0.369 | 0.365 |
| | 25A | 1 | 1 | 1 | 1 | 1 | 0.933 | 0.911 | 0.882 | 0.87 |

From Dr. John Calhoun, 2002, personal communication

**Table D-3 Air-water centrifuge capillary pressures**
**Duke Sand Formation, Desdemona Field, Erath and Eastland County, TX**

| *Well* | *No.* | $S_w$ at different pressures | | | | | | | |
|---|---|---|---|---|---|---|---|---|---|
| | | 1psi | 2psi | 5psi | 10psi | 25psi | 50psi | 100psi | 150psi |
| Grady | 2 | 0.518 | 0.357 | 0.207 | 0.158 | 0.134 | 0.115 | 0.106 | 0.093 |
| Thornton | 4 | 0.536 | 0.37 | 0.241 | 0.2 | 0.17 | 0.148 | 0.115 | 0.093 |
| No.1 | 9 | 0.662 | 0.543 | 0.379 | 0.32 | 0.238 | 0.197 | 0.14 | 0.106 |
| (Erath | 12 | 1 | 0.795 | 0.583 | 0.477 | 0.42 | 0.389 | 0.364 | 0.344 |
| County) | 18 | 1 | 1 | 1 | 0.9 | 0.788 | 0.656 | 0.566 | 0.521 |
| | 22 | 0.394 | 0.306 | 0.202 | 0.17 | 0.141 | 0.129 | 0.113 | 0.102 |
| Lee | 2 | 1 | 0.5 | 0.244 | 0.233 | 0.199 | 0.17 | 0.148 | 0.134 |
| Edwin | 4 | 1 | 0.391 | 0.289 | 0.247 | 0.207 | 0.177 | 0.158 | 0.143 |
| Terry | 6 | 1 | 0.42 | 0.331 | 0.295 | 0.238 | 0.202 | 0.182 | 0.162 |
| No.1 | 8 | 1 | 1 | 0.577 | 0.488 | 0.424 | 0.374 | 0.34 | 0.325 |
| (Erath | 12 | 1 | 0.518 | 0.319 | 0.241 | 0.189 | 0.18 | 0.165 | 0.153 |
| County) | 17 | 1 | 0.391 | 0.28 | 0.244 | 0.194 | 0.165 | 0.146 | 0.132 |
| L.E. | 1 | 1 | 1 | 0.35 | 0.297 | 0.215 | 0.182 | 0.167 | 0.162 |
| Clark | 2 | 1 | 1 | 0.33 | 0.283 | 0.223 | 0.187 | 0.177 | 0.172 |
| No.1 | 6 | 1 | 0.363 | 0.289 | 0.249 | 0.207 | 0.177 | 0.146 | 0.127 |
| (Eastland | 11 | 1 | 0.416 | 0.297 | 0.266 | 0.223 | 0.197 | 0.167 | 0.162 |
| County) | 13 | 1 | 0.35 | 0.225 | 0.215 | 0.184 | 0.155 | 0.134 | 0.129 |
| | 16 | 0.458 | 0.391 | 0.29 | 0.233 | 0.19 | 0.143 | 0.104 | 0.102 |
| W.T. | 2 | 1 | 1 | 1 | 0.976 | 0.9 | 0.781 | 0.649 | 0.6 |
| Yardley | 3 | 1 | 1 | 0.603 | 0.457 | 0.334 | 0.281 | 0.244 | 0.22 |
| No.1 | 5 | 0.48 | 0.391 | 0.3 | 0.248 | 0.202 | 0.183 | 0.159 | 0.14 |
| (Eastland | 6 | 0.424 | 0.385 | 0.313 | 0.236 | 0.174 | 0.148 | 0.13 | 0.12 |
| County) | 10 | 1 | 0.513 | 0.357 | 0.307 | 0.25 | 0.217 | 0.199 | 0.19 |
| | 4 | 1 | 0.813 | 0.449 | 0.301 | 0.249 | 0.225 | 0.195 | 0.178 |
| Era | 5 | 1 | 0.92 | 0.8 | 0.664 | 0.539 | 0.49 | 0.443 | 0.415 |
| Moorhead | 10 | 0.502 | 0.423 | 0.317 | 0.238 | 0.178 | 0.138 | 0.107 | 0.099 |
| No.1 | 13 | 0.404 | 0.288 | 0.209 | 0.185 | 0.151 | 0.131 | 0.116 | 0.109 |
| (Eastland | 15 | 0.616 | 0.429 | 0.297 | 0.25 | 0.191 | 0.166 | 0.144 | 0.134 |
| County) | 19 | 0.46 | 0.382 | 0.27 | 0.228 | 0.182 | 0.148 | 0.119 | 0.11 |

From Dr. John Calhoun, 2002, personal communication

**Table D-4 Air-brine centrifugal capillary pressures, Stevens sandstone, T67X-11 well, Yowlumne Field, Kern County, California**

| *No.* | $S_w$ at different pressures | | | | | | |
|---|---|---|---|---|---|---|---|
| | 1psi | 2psi | 4psi | 8psi | 15psi | 35psi | 450psi |
| 1 | 1 | 0.962 | 0.56 | 0.428 | 0.348 | 0.29 | 0.24 |
| 21 | 1 | 0.981 | 0.562 | 0.417 | 0.324 | 0.25 | 0.18 |
| 19 | 1 | 0.989 | 0.588 | 0.421 | 0.32 | 0.237 | 0.18 |
| 35 | 1 | 0.982 | 0.611 | 0.459 | 0.351 | 0.29 | 0.23 |
| 6 | 1 | 0.989 | 0.596 | 0.455 | 0.358 | 0.29 | 0.22 |
| 52 | 1 | 0.932 | 0.63 | 0.489 | 0.367 | 0.299 | 0.23 |
| 38 | 1 | 0.987 | 0.678 | 0.502 | 0.384 | 0.3 | 0.25 |
| 8 | 1 | 0.983 | 0.651 | 0.484 | 0.377 | 0.307 | 0.24 |
| 11 | 1 | 0.992 | 0.668 | 0.493 | 0.38 | 0.302 | 0.24 |
| 47 | 1 | 0.993 | 0.708 | 0.504 | 0.363 | 0.292 | 0.25 |

**Table D-5 Air-brine porous-plate capillary pressures, T27X-34 well, Yowlumne Field**

| *No.* | $S_w$ at different pressures | | | | | | |
|---|---|---|---|---|---|---|---|
| | 1psi | 2psi | 4psi | 8psi | 15psi | 35psi | 330psi |
| 12A | 1 | 1 | 0.897 | 0.59 | 0.468 | 0.359 | 0.237 |
| 37A | 1 | 1 | 0.645 | 0.498 | 0.382 | 0.299 | 0.199 |
| 41A | 1 | 0.975 | 0.657 | 0.476 | 0.356 | 0.279 | 0.184 |
| 70A | 1 | 1 | 0.676 | 0.525 | 0.401 | 0.322 | 0.209 |
| 73A | 1 | 0.935 | 0.565 | 0.45 | 0.359 | 0.276 | 0.179 |

**Table D-6 Air-brine centrifugal capillary pressures, T55X-34 well, Yowlumne Field**

| *No.* | $S_w$ at different pressures | | | | | |
|---|---|---|---|---|---|---|
| | 1psi | 2psi | 4psi | 8psi | 15psi | 35psi |
| 2A | 1 | 1 | 0.847 | 0.601 | 0.424 | 0.277 |
| 4B | 1 | 1 | 1 | 0.839 | 0.637 | 0.24 |
| 7A | 0.983 | 0.933 | 0.854 | 0.733 | 0.589 | 0.379 |
| 9B | 1 | 1 | 0.893 | 0.727 | 0.637 | 0.482 |
| 15A | 1 | 0.966 | 0.832 | 0.613 | 0.461 | 0.359 |
| 16B | 1 | 0.924 | 0.754 | 0.572 | 0.482 | 0.33 |
| 19A | 0.839 | 0.694 | 0.607 | 0.521 | 0.399 | 0.208 |
| 21A | 1 | 0.916 | 0.713 | 0.51 | 0.384 | 0.291 |
| 22B | 0.949 | 0.862 | 0.727 | 0.589 | 0.466 | 0.282 |
| 23B | 0.949 | 0.893 | 0.774 | 0.549 | 0.379 | 0.167 |

**Table D-7 Air-brine centrifugal capillary pressures, Stevens sandstone, T58-3 well, Paloma Field, Kern County, California.**

| *No.* | $S_w$ at different pressures | | | | | | |
|---|---|---|---|---|---|---|---|
| | 1psi | 2psi | 4psi | 8psi | 15psi | 35psi | 350psi |
| 1 | 1 | 1 | 1 | 1 | 0.95 | 0.728 | 0.57 |
| 2 | 1 | 1 | 1 | 1 | 0.998 | 0.786 | 0.577 |
| 3 | 1 | 1 | 1 | 1 | 1 | 1 | 0.75 |
| 7 | 1 | 1 | 1 | 0.905 | 0.694 | 0.546 | 0.377 |
| 8 | 1 | 1 | 1 | 0.973 | 0.82 | 0.643 | 0.418 |
| 9 | 1 | 1 | 1 | 0.985 | 0.862 | 0.658 | 0.453 |
| 10 | 1 | 1 | 1 | 1 | 1 | 0.925 | 0.655 |

**Table D-8 Air-Mercury Capillary Pressures, Shell Stegall 1A, Rosita field, Texas**

| No. / SHg (%) / Pc (psi) | 13849 | 13848 | 13847 | 14102 | 13864 | 14029 | 13863 |
|---|---|---|---|---|---|---|---|
| 10 | 1.85 | 1.3 | 1.2 | 3.33 | 0.57 | 1.29 | 1.2 |
| 12 | 1.85 | 1.3 | 1.2 | 3.33 | 0.57 | 1.29 | 1.2 |
| 15 | 1.85 | 1.3 | 1.2 | 3.33 | 1.14 | 1.94 | 1.2 |
| 30 | 1.85 | 1.3 | 1.2 | 3.33 | 1.14 | 1.94 | 1.2 |
| 45 | 1.85 | 1.3 | 1.81 | 3.33 | 1.14 | 1.94 | 1.2 |
| 60 | 1.85 | 1.3 | 1.81 | 3.33 | 1.14 | 1.94 | 1.2 |
| 75 | 1.85 | 1.3 | 2.41 | 4.17 | 1.14 | 1.94 | 1.8 |
| 105 | 2.47 | 1.3 | 2.41 | 4.17 | 1.14 | 1.94 | 1.8 |
| 165 | 2.47 | 1.95 | 2.41 | 5.83 | 1.7 | 1.94 | 1.8 |
| 225 | 2.47 | 1.95 | 2.41 | 10.00 | 1.11.74 | 1.94 | 1.8 |
| 315 | 2.47 | 1.95 | 2.41 | 29.17 | 2.84 | 2.58 | 2.99 |
| 450 | 3.09 | 2.6 | 3.01 | 40.00 | 8.52 | 11.61 | 8.38 |
| 615 | 15.43 | 11.04 | 13.86 | 46.67 | 30.11 | 28.39 | 24.55 |
| 750 | 31.48 | 27.92 | 37.95 | 50.00 | 43.75 | 37.42 | 38.92 |
| 930 | 43.21 | 40.91 | 46.39 | 52.50 | 55.68 | 49.68 | 50.90 |
| 1000 | 43.83 | 42.21 | 48.8 | 54.17 | 57.95 | 53.55 | 53.29 |

**Table D-8 Air-Mercury Capillary Pressures, Shell Stegall 1A, Rosita field, Texas (Continued)**

| No. / SHg(%) / Pc (psi) | 14092 | 14111 | 14110 | 14107 | 14105 | 13874 | 13876 |
|---|---|---|---|---|---|---|---|
| 10 | 2.02 | 2 | 2.59 | 3.23 | 1.85 | 2.89 | 1.54 |
| 12 | 2.02 | 2 | 2.59 | 3.23 | 1.85 | 2.89 | 1.54 |
| 15 | 2.02 | 2 | 3.45 | 3.23 | 1.85 | 2.89 | 1.54 |
| 30 | 2.02 | 2 | 3.45 | 3.23 | 1.85 | 2.89 | 1.54 |
| 45 | 2.02 | 2 | 3.45 | 3.23 | 2.78 | 2.89 | 3.08 |
| 60 | 2.02 | 3 | 3.45 | 3.23 | 2.78 | 2.89 | 3.08 |
| 75 | 2.02 | 3 | 3.45 | 3.23 | 2.78 | 2.89 | 3.08 |
| 105 | 2.02 | 3 | 4.31 | 3.23 | 3.7 | 2.89 | 3.08 |
| 165 | 2.02 | 4 | 4.31 | 4.03 | 4.63 | 3.47 | 3.85 |
| 225 | 3.03 | 5 | 5.17 | 7.26 | 7.41 | 4.05 | 3.85 |
| 315 | 4.04 | 13 | 7.76 | 20.16 | 18.52 | 8.67 | 5.38 |
| 450 | 10.10 | 31 | 21.55 | 30.65 | 32.41 | 19.65 | 16.92 |
| 615 | 22.22 | 40 | 29.31 | 37.90 | 38.89 | 32.95 | 32.31 |
| 750 | 32.32 | 43 | 33.62 | 41.94 | 41.67 | 40.46 | 40.00 |
| 930 | 39.39 | 47 | 37.93 | 45.97 | 45.37 | 48.55 | 48.46 |
| 1000 | 40.40 | 48 | 39.66 | 46.77 | 46.3 | 49.13 | 50.77 |

# APPENDIX E

## MEASURED AND CAPILLARY-PRESSURE DERIVED PETROPHYSICAL PROPERTIES

**Table E-1 Measured and capillary-pressure derived petrophysical properties, San Francisco #14 well, Caballos Formation, San Francisco, Colombia**

| *No.* | *Depth (ft)* | *k* (md) | $\phi$ | $P_d$ (psi) | $S_{wir}$ | $\beta$ | *Fg* | $\lambda$ |
|---|---|---|---|---|---|---|---|---|
| 21B | 2972 | 117 | 0.162 | 2 | 0.1 | 3 | 0.14 | 0.67 |
| 2B | 2973 | 377 | 0.134 | 1 | 0.07 | 3 | 0.12 | 0.71 |
| 6B | 3009 | 0.6 | 0.1 | 5 | 0.27 | 1 | 0.43 | 0.53 |
| 3B | 3018 | 7.57 | 0.126 | 2 | 0.24 | 2 | 0.36 | 0.56 |
| 25B | 3021 | 1150 | 0.16 | 1 | 0.06 | 3 | 0.11 | 0.73 |
| 10B | 3022 | 259 | 0.15 | 1 | 0.07 | 3 | 0.20 | 0.61 |
| 29B | 3035 | 66.5 | 0.139 | 2 | 0.12 | 2 | 0.15 | 0.68 |
| 14B | 3107 | 0.02 | 0.041 | — | — | — | — | — |
| 15B | 3112 | 5.01 | 0.101 | 2 | 0.13 | 2 | 0.25 | 0.78 |
| 16B | 3129 | 0.45 | 0.088 | 10 | 0.33 | 1 | 0.44 | 0.42 |

**Table E-2 Measured and capillary-pressure derived petrophysical properties, Duke Sands Formation, Desdemona Field, Eastland County, TX**

| *Well* | *No.* | *Depth (ft)* | *k* (md) | $\phi$ | $P_d$ (psi) | $S_{wir}$ | $\beta$ |
|---|---|---|---|---|---|---|---|
| J.R. | 8A | 2729 | 1.3 | 0.136 | 5 | 0.35 | 1 |
| Grimshaw | 9A | 2730 | 0.1 | 0.049 | 10 | 0.35 | 1 |
| No.1 | 11A | 2732 | 31 | 0.111 | 2 | 0.19 | 2 |
| | 12A | 2733 | 2.1 | 0.078 | 2 | 0.25 | 2 |
| | 14A | 2735 | 55 | 0.157 | 2 | 0.2 | 2 |
| | 20A | 2741 | 1.7 | 0.114 | 5 | 0.3 | 2 |
| | 25A | 2746 | 0.18 | 0.081 | 20 | 0.85 | 1 |
| W. T. | 2 | 2696 | 2.1 | 0.075 | 20 | 0.5 | 2 |
| Yardley | 3 | 2700 | 28 | 0.12 | 2 | 0.22 | 2 |
| No.1 | 5 | 2705 | 127 | 0.147 | 1 | 0.12 | 3 |
| | 6 | 2707 | 189 | 0.157 | 1 | 0.1 | 3 |
| | 10 | 2712 | 81 | 0.137 | 1 | 0.18 | 2 |
| Era | 4 | 2684 | 20 | 0.105 | 20 | 0.17 | 2 |
| Moorhead | 5 | 2692 | 4 | 0.083 | 2 | 0.38 | 2 |
| No.1 | 10 | 2698 | 176 | 0.163 | 1 | 0.09 | 3 |
| | 13 | 2703 | 603 | 0.155 | 1 | 0.1 | 3 |
| | 15 | 2706 | 124 | 0.148 | 1 | 0.12 | 3 |
| | 19 | 2708 | 333 | 0.177 | 1 | 0.1 | 3 |

**Table E-3 Measured core plug and capillary-pressure derived properties, Duke Sands Formation, Desdemona Field, Erath and Eastland County, TX**

| *Well* | *No.* | *Depth (ft)* | *k* (md) | $\phi$ | $P_d$ (psi) | $S_{wir}$ | $\beta$ |
|---|---|---|---|---|---|---|---|
| Grady | 2 | 2804 | 277 | 0.148 | 1 | 0.08 | 3 |
| Thornton | 4 | 2806 | 193 | 0.163 | 1 | 0.08 | 3 |
| No.1 | 9 | 2813 | 164 | 0.172 | 1 | 0.09 | 3 |
| (Erath | 12 | 2815 | 17 | 0.108 | 1 | 0.34 | 2 |
| County) | 18 | 2835 | 0.24 | 0.063 | 5 | 0.5 | 1 |
| | 22 | 2840 | 1400 | 0.167 | 1 | 0.1 | 3 |
| L.E. | 1 | 2680 | 22 | 0.087 | 2 | 0.15 | 2 |
| Clark | 2 | 2681 | 41 | 0.101 | 2 | 0.16 | 2 |
| No.1 | 6 | 2687 | 134 | 0.124 | 1 | 0.1 | 3 |
| (Eastland | 11 | 2694 | 169 | 0.18 | 1 | 0.15 | 3 |
| County) | 13 | 2695 | 331 | 0.187 | 1 | 0.12 | 3 |
| | 16 | 2698 | 77 | 0.136 | 1 | 0.1 | 2 |
| Lee | 2 | 2702 | 185 | 0.152 | 1 | 0.12 | 3 |
| Edwin | 4 | 2703 | 190 | 0.16 | 1 | 0.12 | 3 |
| Terry | 6 | 2704 | 303 | 0.179 | 1 | 0.15 | 3 |
| No.1 | 8 | 2705 | 26 | 0.126 | 2 | 0.32 | 2 |
| (Erath | 12 | 2708 | 212 | 0.131 | 3 | 0.14 | 3 |
| County) | 17 | 2714 | 228 | 0.146 | 1 | 0.12 | 3 |

*k* and $\phi$ are from Dr. John Calhoun (2002, personal communication), other properties are derived.

**Table E-4 Measured and capillary-pressure derived petrophysical properties, Stevens sandstone, Yowlumne and Paloma Fields, Kern County, California**

| *Well* | *No.* | *k* (md) | Porosity | $P_d$ (psi) | $S_{wir}$ | F | m | Fg | $\lambda$ | $\beta$ |
|---|---|---|---|---|---|---|---|---|---|---|
| T67X- | 1 | 139 | 0.195 | 2 | 0.2 | 13.6 | 1.6 | 0.1 | 0.72 | 3 |
| 11 | 21 | 113 | 0.198 | 2 | 0.15 | 16.5 | 1.73 | 0.14 | 0.78 | 3 |
| | 19 | 98 | 0.191 | 2 | 0.17 | 17.2 | 1.72 | 0.12 | 0.5 | 3 |
| | 35 | 87 | 0.191 | 2 | 0.2 | 16.8 | 1.7 | 0.15 | 0.65 | 3 |
| | 26 | 85 | 0.178 | 2 | 0.2 | 16.2 | 1.61 | 0.16 | 0.65 | 3 |
| | 52 | 75 | 0.174 | 2 | 0.2 | 20.7 | 1.73 | 0.15 | 0.77 | 3 |
| | 38 | 63 | 0.177 | 2 | 0.22 | 13.7 | 1.51 | 0.14 | 0.67 | 3 |
| | 8 | 63 | 0.169 | 2 | 0.21 | 18 | 1.63 | 0.16 | 0.65 | 3 |
| | 11 | 61 | 0.183 | 2 | 0.21 | 16.3 | 1.64 | 0.17 | 0.59 | 3 |
| | 47 | 59 | 0.185 | 2 | 0.23 | 16.5 | 1.66 | 0.12 | 0.68 | 3 |

**Table E-4 Measured and capillary-pressure derived petrophysical properties, Stevens sandstone, Yowlumne and Paloma Fields, Kern County, California (cont.)**

| *Well* | *No.* | *k* (md) | Porosity | $P_d$ (psi) | $S_{wir}$ | F | m | Fg | λ | β |
|---|---|---|---|---|---|---|---|---|---|---|
| | 2A | 12 | 0.148 | 4 | 0.25 | 18.8 | 1.54 | 0.186 | 0.98 | 2 |
| | 4B | 2.5 | 0.099 | 4 | 0.2 | 29.9 | 1.47 | 0.491 | 0.42 | 1 |
| | 7A | 4.5 | 0.122 | 2 | 0.3 | 22.5 | 1.48 | 0.47 | 0.38 | 1 |
| | 9B | 3.7 | 0.129 | 2 | 0.45 | 22.2 | 1.51 | 0.45 | 0.47 | 1 |
| T55X- | 15A | 16 | 0.16 | 3 | 0.32 | 16.8 | 1.54 | 0.24 | 0.78 | 2 |
| 34 | 16B | 11 | 0.138 | 2 | 0.3 | 22.2 | 1.57 | 0.37 | 0.59 | 2 |
| | 19A | 41 | 0.17 | 2 | 0.15 | 18.4 | 1.64 | 0.28 | 0.38 | 2 |
| | 21A | 21 | 0.177 | 2 | 0.26 | 16.8 | 1.63 | 0.24 | 0.73 | 2 |
| | 22B | 27 | 0.132 | 2 | 0.2 | 18 | 1.43 | 0.3 | 0.51 | 2 |
| | 23B | 12 | 0.173 | 3 | 0.1 | 23.7 | 1.8 | 0.34 | 0.52 | 2 |
| | 12A | 11 | 0.136 | 3.5 | 0.2 | 29.9 | 1.7 | 0.2 | 0.75 | 2 |
| T27X- | 37A | 50 | 0.172 | 2 | 0.17 | 22.2 | 1.76 | 0.192 | 0.71 | 2 |
| 34 | 41A | 50 | 0.186 | 2 | 0.15 | 18.6 | 1.74 | 0.178 | 0.73 | 2 |
| | 70A | 56 | 0.171 | 2 | 0.17 | 20.7 | 1.72 | 0.23 | 0.66 | 2 |
| | 73A | 92 | 0.175 | 2 | 0.15 | 20.3 | 1.73 | 0.19 | 0.67 | 3 |
| | 1 | 2.3 | 0.145 | 8 | 0.56 | 28.7 | 1.74 | — | — | 2 |
| | 2 | 1.3 | 0.12 | 15 | 0.56 | 36 | 1.69 | — | — | 2 |
| T58- | 7 | 5.2 | 0.169 | 8 | 0.37 | 24.3 | 1.79 | — | — | 2 |
| 3 | 8 | 2.8 | 0.162 | 8 | 0.4 | 26.9 | 1.81 | — | — | 2 |
| | 9 | 1.4 | 0.15 | 10 | 0.43 | 32 | 1.83 | — | — | 2 |
| | 10 | 0.52 | 0.147 | 15 | 0.65 | 36.1 | 1.87 | — | — | 1 |

Capillary pressures (air-water) were measured with centrifugal method.

**Table E-5 Measured and capillary-pressure (air-mercury) derived petrophysical properties Shell Stegall 1A, Rosita field, Texas**

| *No.* | *k* (md) | Porosity | $P_d$ (psi) | $S_{wir}$ | β | Note |
|---|---|---|---|---|---|---|
| 13849 | 0.09 | 0.162 | 450 | 0.4 | 1 | Sheared zone |
| 13848 | 0.07 | 0.154 | 450 | 0.4 | 1 | Sheared zone |
| 13847 | 0.09 | 0.166 | 450 | 0.4 | 1 | Sheared zone |
| 14102 | 0.15 | 0.12 | 200 | 0.4 | 1 | Normal zone |
| 13864 | 0.12 | 0.176 | 450 | 0.3 | 1 | Sheared zone |
| 14029 | 0.11 | 0.155 | 315 | 0.35 | 1 | Contorted zone |
| 13863 | 0.11 | 0.167 | 400 | 0.3 | 1 | Contorted zone |
| 14092 | 0.08 | 0.099 | 315 | 0.5 | 1 | Normal zone |
| 14111 | 0.19 | 0.1 | 225 | 0.5 | 1 | Normal zone |
| 14110 | 0.09 | 0.116 | 315 | 0.55 | 1 | Normal zone |
| 14107 | 0.19 | 0.124 | 200 | 0.4 | 1 | Normal zone |
| 14105 | 0.18 | 0.108 | 200 | 0.45 | 1 | Normal zone |
| 13874 | 0.15 | 0.173 | 225 | 0.4 | 1 | Normal zone |
| 13876 | 0.12 | 0.13 | 315 | 0.4 | 1 | Normal zone |

# APPENDIX F

# RELATIVE PERMEABILITIES

**Table F-1 Relative permeabilities, Stevens sandstone, 27X-34, Yowlumne Field, Kern County, California**

| No. 1 | | | No.3 | | |
|---|---|---|---|---|---|
| $S_w$ | $k_{rw}$ | $k_{ro}$ | $S_w$ | $k_{rw}$ | $k_{ro}$ |
| 0.161 | | 1 | 0.193 | | 1 |
| 0.43 | 0.098 | 0.077 | 0.463 | 0.081 | 0.036 |
| 0.447 | 0.102 | 0.064 | 0.474 | 0.086 | 0.032 |
| 0.467 | 0.106 | 0.048 | 0.485 | 0.089 | 0.027 |
| 0.481 | 0.109 | 0.038 | 0.496 | 0.092 | 0.023 |
| 0.49 | 0.11 | 0.032 | 0.506 | 0.1 | 0.021 |
| 0.496 | 0.111 | 0.028 | 0.515 | 0.104 | 0.018 |
| 0.513 | 0.114 | 0.018 | 0.526 | 0.114 | 0.016 |
| 0.525 | 0.118 | 0.014 | 0.544 | 0.13 | 0.013 |
| 0.543 | 0.13 | 0.01 | 0.57 | 0.153 | 0.0092 |
| 0.564 | 0.142 | 0.0064 | 0.59 | 0.171 | 0.007 |
| 0.574 | 0.154 | 0.005 | 0.605 | 0.174 | 0.0063 |
| 0.584 | 0.165 | 0.0039 | 0.628 | 0.2 | 0.0048 |
| 0.594 | 0.175 | 0.0027 | 0.681 | 0.257 | 0.0012 |
| 0.611 | 0.213 | 0.0011 | 0.702 | 0.268 | |
| 0.623 | 0.242 | 0.00014 | | | |
| 0.626 | 0.263 | | | | |

**Table F-1 Relative permeabilities, Stevens sandstone, 27X-34, Yowlumne Field, Kern County, California (cont.)**

| No. 5 | | | No.10 | | |
|---|---|---|---|---|---|
| $S_w$ | $k_{rw}$ | $k_{ro}$ | $S_w$ | $k_{rw}$ | $k_{ro}$ |
| 0.156 | | 1 | 0.336 | | 1 |
| 0.536 | 0.038 | 0.0081 | 0.477 | 0.063 | 0.123 |
| 0.542 | 0.039 | 0.0071 | 0.491 | 0.07 | 0.111 |
| 0.555 | 0.044 | 0.005 | 0.511 | 0.079 | 0.093 |
| 0.572 | 0.048 | 0.0033 | 0.526 | 0.086 | 0.08 |
| 0.582 | 0.051 | 0.0026 | 0.562 | 0.105 | 0.051 |
| 0.592 | 0.052 | 0.002 | 0.59 | 0.124 | 0.032 |
| 0.611 | 0.054 | 0.0011 | 0.613 | 0.143 | 0.02 |
| 0.644 | 0.055 | 0.00026 | 0.634 | 0.163 | 0.012 |
| 0.656 | 0.387 | | 0.646 | 0.175 | 0.0082 |
| | | | 0.656 | 0.185 | 0.0057 |
| | | | 0.662 | 0.193 | 0.0043 |
| | | | 0.668 | 0.206 | 0.0034 |
| | | | 0.675 | 0.217 | 0.0024 |
| | | | 0.683 | 0.227 | 0.0013 |
| | | | 0.688 | 0.246 | 0.00082 |
| | | | 0.698 | 0.343 | |

$k_{rw}$ : water permeability relative to oil permeability at initial water saturation
$k_{ro}$: oil permeability relative to oil permeability at initial water saturation

**Table F-2 Summary of the properties of the four sample**

| No. | $k_a$ | $\phi$ | $S_{wi}$ | $k_o$ |
|---|---|---|---|---|
| 1 | 45 | 0.162 | 0.161 | 30 |
| 3 | 7.1 | 0.146 | 0.193 | 4.1 |
| 5 | 59 | 0.186 | 0.156 | 31 |
| 10 | 60 | 0.177 | 0.336 | 21 |

$k_a$: air permeability (md)
$\phi$ : porosity
$S_{wi}$ : initial water saturation (fractional)
$k_o$ : oil permeability at initial water saturation

# VITA


| | |
|---|---|
| NAME | Tao Wu |
| E-Mail | wutao_2002@yahoo.com |
| ADDRESS | c/o Shao YongFu<br>Beijing Cancer Hospital, Panjiayuan Nanli #17<br>Chaoyang District, Beijing, 100021<br>People's Republic of China |


EDUCATION

| | |
|---|---|
| December 2004 | Texas A&M University, College Station, Texas<br>Ph.D., Geology |
| June 1995 | China University of Geosciences, Beijing, P. R. China<br>M.S., Geology |
| June 1992 | Jianghan Petroleum Institute, Jinzhou, P. R. China<br>B.S., Geology |

PROFESSIONAL EXPERIENCE

| | |
|---|---|
| Summer 2004 | Intern, ExxonMobil Upstream Research Company<br>Houston, Texas |
| 2002 – 2004 | Graduate Teaching Assistant<br>Department of Geology & Geophysics<br>Texas A&M University, College Station, Texas |
| 2000 – 2002 | Graduate Research Assistant<br>Ocean Drilling Program<br>Texas A&M University, College Station, Texas |
| 1995 – 2000 | Lecturer<br>China University of Geosciences, Beijing, P. R. China |

PROFESSIONAL MEMBERSHIP

| | |
|---|---|
| 2000 – present | American Association of Petroleum Geologists<br>Society of Exploration Geophysicists<br>Society of Petroleum Engineers |

AWARDS RECEIVED

| | |
|---|---|
| 2002 | AAPG Grants-in-Aid, AAPG Foundation |